EFFICIENT ANALYSIS OF OSCILLATORS WITH MULTIPLE TIME DIMENSIONS

by
Lei (Lana) Zhu

A Thesis
Presented to Lakehead University
in Partial Fulfillment of the Requirement for the Degree of
Master of Applied Science
in
Control Engineering

Thunder Bay, Ontario, Canada

November 2005

Reproduced with permission of the copyright owner. Further reproduction prohibited without permission.

Library and Archives Canada

Published Heritage Branch

395 Wellington Street
Ottawa ON K1A 0N4
Canada

Bibliothèque et Archives Canada

Direction du Patrimoine de l'édition

395, rue Wellington
Ottawa ON K1A 0N4
Canada

Your file Votre référence
ISBN: 978-0-494-15652-0
Our file Notre référence
ISBN: 978-0-494-15652-0

NOTICE:
The author has granted a non-exclusive license allowing Library and Archives Canada to reproduce, publish, archive, preserve, conserve, communicate to the public by telecommunication or on the Internet, loan, distribute and sell theses worldwide, for commercial or non-commercial purposes, in microform, paper, electronic and/or any other formats.

The author retains copyright ownership and moral rights in this thesis. Neither the thesis nor substantial extracts from it may be printed or otherwise reproduced without the author's permission.

AVIS:
L'auteur a accordé une licence non exclusive permettant à la Bibliothèque et Archives Canada de reproduire, publier, archiver, sauvegarder, conserver, transmettre au public par télécommunication ou par l'Internet, prêter, distribuer et vendre des thèses partout dans le monde, à des fins commerciales ou autres, sur support microforme, papier, électronique et/ou autres formats.

L'auteur conserve la propriété du droit d'auteur et des droits moraux qui protège cette thèse. Ni la thèse ni des extraits substantiels de celle-ci ne doivent être imprimés ou autrement reproduits sans son autorisation.

In compliance with the Canadian Privacy Act some supporting forms may have been removed from this thesis.

While these forms may be included in the document page count, their removal does not represent any loss of content from the thesis.

Conformément à la loi canadienne sur la protection de la vie privée, quelques formulaires secondaires ont été enlevés de cette thèse.

Bien que ces formulaires aient inclus dans la pagination, il n'y aura aucun contenu manquant.

Canada

Reproduced with permission of the copyright owner. Further reproduction prohibited without permission.

Abstract

LEI(LANA) ZHU. Efficient Analysis of Oscillators with Multiple Time Dimensions (Under the Supervision of Dr. Carlos E. Christoffersen).

Harmonic Balance (HB) analysis is an established technique for the analysis of nonlinear circuits. In this thesis, we present a method to find the transient and steady-state behavior of oscillators based on a harmonic balance implementation which proves to be faster than traditional time domain simulations. It is derived from the warped multi-time partial differential equation (WaMPDE) approach developed in recent years. This approach efficiently separates the frequency modulation (FM) and amplitude modulation (AM) in oscillators. A review of Multi-time Partial Differential Equation (MPDE) and WaMPDE is presented along with the motivation and interest in warped multiple time axes. The first proposed method shows how to obtain initial boundary conditions for a WaMPDE system consistently with arbitrary physical initial conditions in the system of ordinary differential equations in transient analysis. The second proposed method improves steady-state analysis since it does not require a good initial guess of the oscillation frequency and exploits the frequency-domain latency of circuits by using a different number of harmonics in each state variable. The WaMPDE approach is used to simultaneously bring the circuit state to the region of convergence of the HB analysis and determine the optimum number of harmonics required at each node in the circuit. In both transient and steady-state, an adaptive time step control technique is employed in one of the time axes and this considerably reduces the computational effort. Simulation results of different applications are described to demonstrate the performance of the proposed method. Finally, the proposed methods are validated with experimental results.

Reproduced with permission of the copyright owner. Further reproduction prohibited without permission.

Biographical Summary

Lei(Lana) Zhu was born in Nanjing, China on July 22, 1973. She received the Electrical Engineering degree at the Southeast University in China in August 1998. From 1994 to 2001 she was a junior design engineer and later a design engineer in Electrical Engineering Design Department of Nanjing Power Supply Bureau, China. During this time, she designed over 40 communication projects for transformer substations with the aid of AutoCAD and developed a fiber communication network in Nanjing Power Systems.

In November 2001 she immigrated to Canada and enrolled in the master program of Control Engineering of Lakehead University in September 2003. Her research interest includes circuits analysis and simulation in multiple time axes, oscillator design, phase-locked-loops, and general communication circuits. She is also a student member of the Institute of Electrical and Electronics Engineers (IEEE).

Reproduced with permission of the copyright owner. Further reproduction prohibited without permission.

Acknowledgments

I have had the privilege of learning from Dr. Carlos E. Christoffersen during my graduate studies at Lakehead University. I want to express my deep appreciation to his generous support and patient guidance. It was my great pleasure to study in his research group.

I also want to thank Dr. Krishnamoorthy Natarajan for his co-supervising my thesis work. Thanks are also due to Dr. Abdelhamid Tayebi and Dr. Xiaoping Liu for their enthusiastic instruction during my course study; to Mr. Manfred Klein for his kind and generous help during my experiment.

Appreciations also go to all the graduate students. They give me lots of help in Matlab, LaTex and course understanding.

Finally, I would like to thank my husband and my daughter, Kris Qin and Sophie Qin, for their endless love and encouragement.

Lei (Lana) Zhu

lzhu1@lakeheadu.ca
http://flash.lakeheadu.ca/~ lzhu1

Reproduced with permission of the copyright owner. Further reproduction prohibited without permission.

Contents

Reproduced with permission of the copyright owner. Further reproduction prohibited without permission.

Reproduced with permission of the copyright owner. Further reproduction prohibited without permission.

Reproduced with permission of the copyright owner. Further reproduction prohibited without permission.

List of Figures

Reproduced with permission of the copyright owner. Further reproduction prohibited without permission.

Reproduced with permission of the copyright owner. Further reproduction prohibited without permission.

Reproduced with permission of the copyright owner. Further reproduction prohibited without permission.

Reproduced with permission of the copyright owner. Further reproduction prohibited without permission.

List of Tables

Reproduced with permission of the copyright owner. Further reproduction prohibited without permission.

List of Symbols

t_1 – Fast time.
t_2 – Slow time.
τ_1 – Warped time.
τ_2 – Real time.
$\omega(\tau_2)$ – Local angular frequency.
$u(t)$ – Voltage in time domain.
$u(\tau_1, \tau_2)$ – Voltage in warped multi-time domain.
$X(k)$ – The Fourier coefficient of the k_{th} harmonic.
$x(t)$ – State variable.
G – Conductance matrix.
C – Linear charge matrix.
$Q(u(t))$ – Nonlinear charge vector.
$I(u(t))$ – Nonlinear device current vector.
$S(t)$ – Supply sources vector.
ϵ – Local truncation error.
I_s – Diode or transistor saturation current.
BF – Forward beta.
BR – Reverse beta.
V_T – Thermal voltage.
i_S – Excitation current.
C_j – Diode junction capacitance.
$CJ0$ – Zero-biased junction capacitance.
VJ – Diode built-in potential.
μ – Diode grading coefficient.
N – Emission coefficient factor.
J – Jacobian matrix.
$\Im$ – Imaginary part.
$\Re$ – Real part.
$F()$ – Error function.
HB – Harmonic Balance.
DFT – Direct Fourier transform.

Reproduced with permission of the copyright owner. Further reproduction prohibited without permission.

Chapter 1

Introduction

1.1 Motivations and Objectives of This Study

The analysis of either the transient or the steady-state response of oscillators has been always a hot topic in circuit simulations since it is usually difficult in dealing with the different changing rates of circuit behaviors and the unknown oscillation frequency. For transient analysis, the traditional time-domain method using a time-marching approach to solve a system of ordinary differential equations (ODEs) is popular to determine the transient directly. However, in some cases the transient takes a long time to converge to the steady-state, resulting in an extremely expensive computational cost. For steady-state analysis, Harmonic Balance (HB) has been the dominant approach in recent years. Though HB is one of the most important frequency domain techniques, it still has some limitations. In particular, regular HB needs a good initial guess to converge to the desired solution. If a good initial guess of the solution is not provided HB analysis of oscillators may converge to an unstable equilibrium point or it may not converge at all. In oscillator analysis, it is especially difficult to get a good initial guess of the oscillator frequency. Another problem of the regular HB is that the number of harmonics is usually the same for all state variables and this number is always fixed during the simulation. If one state variable in the circuit presents a strong nonlinearity, lots of harmonics are needed for that particular node while other nodes do not need so many harmonics. The simulation process may be time-consuming. All these limitations restrict harmonic balance to be used universally in circuit analysis.

In this thesis work we made some developments to improve the ability of oscillator analysis, searching a fast and accurate route to discover both the transient and the steady-state solutions.

Reproduced with permission of the copyright owner. Further reproduction prohibited without permission.

Since the fast oscillator frequency and the relatively much slower transient variation in the response of most of the oscillators, multiple time axes are employed to separate the circuit behavior, providing a possible way to quickly compute the circuit response. A variation of that method [1] is known as Warped Multi-time Partial Differential Equation (WaMPDE) which is efficiently dealing with the frequency modulation in oscillators in multiple time domains. The system of ODEs is replaced by a system of partial differential equations with one of the time axes focusing on oscillations and the other on the transient envelope. Based on WaMPDE, we present two robust and fast approaches, transient approach and steady-state approach, for precisely capturing the transient and steady-state response of oscillators in multiple time domain, respectively. They both save considerable computational efforts compared with the traditional time domain analysis.

1. Transient Analysis

   Here we address the problem of finding the WaMPDE boundary conditions corresponding to a set of physical initial conditions. The key of this new approach is to build and solve a system of equations where the unknowns are the boundary conditions of the WaMPDE that match the ODE result. The method starts by running a regular time-marching simulation of the oscillator for a short time until some oscillations are produced. The analysis is transformed from ODE to WaMPDE when frequency variation slows down. The ODE solution determines both the initial guess of the local frequency and an approximate mapping between multiple time scales. Once the correct boundary conditions are found, the WaMPDE method is used to quickly find the transient and steady-state behavior of oscillators. A new system called boundary condition system is established considering the mapping of multi-time axes and the ODE solution with boundary conditions as unknowns. After solving this system it is possible to obtain the state variables as functions of two time scales in the subsequent WaMPDE analysis. This procedure transforms a portion of the ODE solution into the WaMPDE boundary condition with accuracy. To reduce the computational cost resulting from the large amount of time steps during the WaMPDE simulation, an adaptive algorithm is employed to pre-determine the optimum time step size in each line depending on the local truncation error. With accurate boundary conditions and optimum time steps, the transient response is achieved in a precise and quick way.

Reproduced with permission of the copyright owner. Further reproduction prohibited without permission.

2. Steady-state Analysis

   The steady-state approach is based on a new adaptive harmonic balance technique derived from WaMPDE. To reduce the computational cost resulting from large amount of harmonics required in some strong nonlinear variables, an adaptive HB is used to determine the number of harmonics for each state variable separately. The number of harmonics used in the calculation is always very close to the minimum required for the desired accuracy. This technique provides the following features: first, the oscillator frequency is traceable; second, smaller computational effort is required compared with the time-consuming transient analysis; and third, a good initial guess of the solution is not necessary. An adaptive time step control algorithm and an adaptive tolerance are also used to reduce the computational effort.

1.2 Thesis Overview

A review of the MPDE and WaMPDE concept is presented in Chapter 2. Chapter 3 illustrates the procedure of finding the WaMPDE boundary conditions in transient analysis and provides a case study. Chapter 4 develops the harmonic balance formulation in multiple time axes to analyze the steady-state with the same case mentioned in Chapter 3. Simulation results of other two different oscillators are discussed and compared with experimental results in Chapter 5. In the last chapter we summarize the conclusion and propose the direction of the future work.

1.3 Publications

1. Lei (Lana) Zhu and Carlos E. Christoffersen, "Fast Transient Analysis of Oscillators Using Multiple Time Scales with Accurate Initial Conditions," 2005 IEEE Canadian Conference on Electrical and Computer Engineering Digest, Saskatoon, May 2005, pp.700-703.

2. Lei (Lana) Zhu and Carlos E. Christoffersen, "Adaptive Harmonic Balance Analysis of Oscillators Using Multiple Time Scales," Proceedings of the 3rd International IEEE Northeast Workshop on Circuits & Systems, Quebec City, June 2005, pp.187-190.

Reproduced with permission of the copyright owner. Further reproduction prohibited without permission.

Chapter 2

Literature Review

2.1 Introduction

Over the past several years Harmonic Balance (HB) has been under extensive research to improve limitations mentioned in Chapter 1. For example in [2] HB equations are modified by including the Kurokawa condition to eliminate the DC solution. In [3] a voltage source probe at the fundamental frequency that is an open circuit at all other frequencies is inserted to avoid the DC solution. By means of an iterative process the amplitude and frequency of the probe are adjusted until there is no current through the probe. At this point the autonomous solution is found. A similar probe concept with the addition of a continuation method has been proposed more recently [4] to improve convergence. However, the research work is still going on to explore a method which achieves the minimum number of harmonics required for the desired accuracy for each state variable to save the computational effort. Another point of view is the expensive computational cost resulted from the long transient. Several techniques have been proposed to skip the transient and find the steady state directly. We mention here just a few. For example [5] provides a method to find the steady-state of high-Q oscillators using the transient analysis in SPICE. In [6], a Newton algorithm is used to find the periodic response and the period of oscillators quickly in lightly damped systems. However, the complete transient solution is still not accessible in these methods.

The concept of multiple time was firstly mentioned a few decades ago although its value in a general context has been recognized recently. In [7] Roychowdhury presented a new mathematical formulation and numerical method to efficiently represent signals with widely separated rates

Reproduced with permission of the copyright owner. Further reproduction prohibited without permission.

of variation, transforming the ordinary differential equation descriptions of a system into partial differential ones. In [1] the multiple-time scale analytical formulation for oscillatory dynamical systems is presented. Here, we review the approach that Roychowdhury presented to deal with two different type of signals: amplitude modulation (AM) signals with Multi-time Partial Differential Equation (MPDE) and frequency modulation (FM) signals with Warped Multi-time Partial Differential Equations (WaMPDE).

2.2 MPDE

MPDE means Multi-time Partial Differential Equation. It uses at least two time axes to represent variables in some circuits which contain parts that vary at two or more widely separated rates. Such signal happens in many physical systems, for example, communication circuits, switched circuits, electronic autonomous circuits, *etc.* Those kinds of systems are difficult to analyze by using traditional numerical integration algorithms since the circuit behavior is varied in different rates. In MPDE, the derivatives in the system of ODEs are replaced by:

$$\frac{dx(t)}{dt} = \frac{\partial \hat{x}(t_1, t_2)}{\partial t_1} + \frac{\partial \hat{x}(t_1, t_2)}{\partial t_2}.$$

The circuit behavior is separated in two different time axes: fast time (t_1) and slow time (t_2). MPDE largely improves the computational effort. Consider a simple quasi-periodic oscillating wave with amplitude controlled by a slow sinusoidal signal [1],

$$y(t) = \sin(\frac{2\pi}{T_1}t)\sin(\frac{2\pi}{T_2}t), \tag{2.1}$$

with $T_1 = 0.02s$ and $T_2 = 1s$. This is an amplitude modulation signal shown in Fig. 2.1.

If T_2 is much larger than T_1 (which is common in AM signals), it will take a long time and many undulations to observe a whole period. By separating $y(t)$ in slow (envelope) and fast (oscillation) dynamics, we transform the original signal to the multiple time representation,

$$\hat{y}(t_1, t_2) = \sin(\frac{2\pi}{T_1}t_1)\sin(\frac{2\pi}{T_2}t_2), \tag{2.2}$$

with much fewer sampling points shown in Fig. 2.2.

It is clear that the behavior of $\hat{y}(t_1, t_2)$ does not have as many undulations as $y(t)$. Moreover, the signal can be characterized by relatively few points which do not depend on the relative value of T_1 and T_2. For example, 20 points were used in each sinusoid to generate Fig. 2.1, hence

Reproduced with permission of the copyright owner. Further reproduction prohibited without permission.

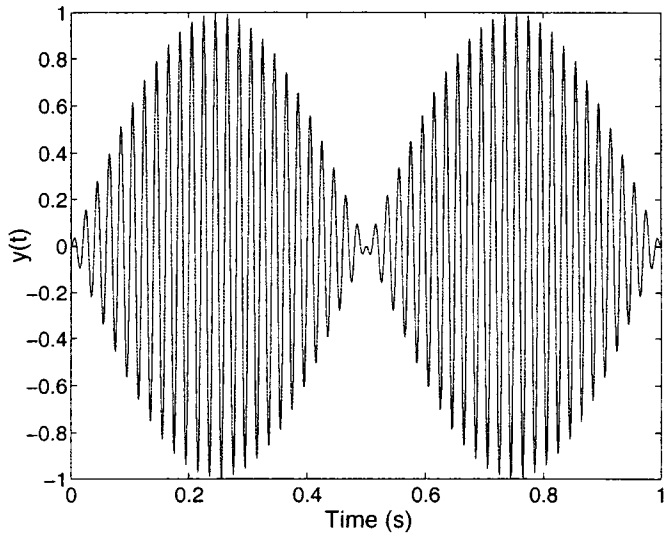

Figure 2.1: Example of an AM signal $y(t)$.

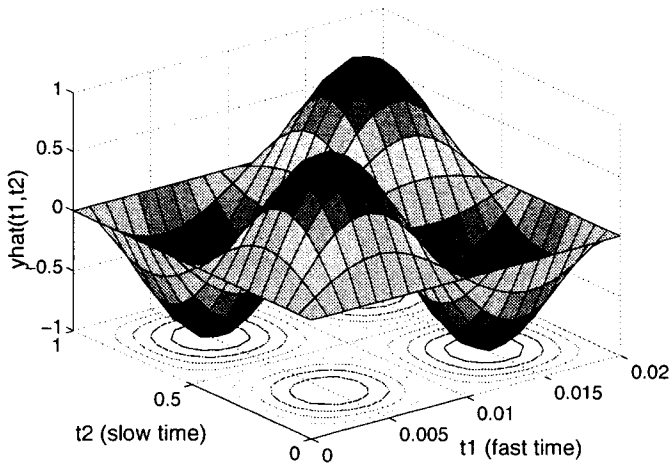

Figure 2.2: MPDE representation of $y(t)$.

Reproduced with permission of the copyright owner. Further reproduction prohibited without permission.

the total number was 1000. Fig. 2.2 was plotted with 400 points on a uniform of 20×20 grid, two times less than in Fig. 2.1. In some applications where rates are more widely separated, the saving will be much more evident. It is also easy to recapture $y(t)$ from $\hat{y}(t_1, t_2)$ by simply setting $t_1 = t_2 = t$. The advantage of this approach is that it results in large improvements in simulation speed compared with regular time simulation. That is the main reason why we use multiple time scales.

It is obvious that MPDE is a perfect technique to solve amplitude modulation signals, especially when the separation factor n ($n = \frac{T_2}{T_1}$) is a large number. However, it is not efficient when applied in a frequency modulation (FM) signal which commonly happens in autonomous systems, such as oscillators. MPDE can not handle the changing frequency well. So we introduce another concept (WaMPDE) to deal with the FM problems.

2.3 WaMPDE

WaMPDE means Warped Multi-time Partial Differential Equation. The local frequency is a function of time in a FM signal. WaMPDE makes this frequency undulation uniform by warping one of the time scales in MPDE. As a result the local frequency is normalized to a constant value and the warped time becomes a function of time. The multi-time partial differential equation can be represented as:

$$\frac{dx(t)}{dt} = \omega(\tau_2)\frac{\partial \hat{x}(\tau_1, \tau_2)}{\partial \tau_1} + \frac{\partial \hat{x}(\tau_1, \tau_2)}{\partial \tau_2}.$$

Also separating the circuit behavior in two different time axes: the warped time τ_1 and the slow time τ_2. The warped function $\omega(\tau_2)$ is chosen to be an unknown function *a priori*, consistent with the smooth phase condition along the real time axis. It also reveals the inherent and time-varying local frequency of oscillators. That is one of the advantages of the WaMPDE approach. The result of WaMPDE is a multi-time partial-differential equation in warped and unwarped time scales, together with a warped function describing the relation of the two time axes [1].

Consider a simple two-tone quasi-periodic FM signal in Fig. 2.3.

$$x(t) = \cos(\varphi(t)) = \cos((2\pi f_0 t) + k\cos(2\pi f_2 t)), \tag{2.3}$$

with $f_0 = 1\text{MHz}$, $f_2 = 20\text{kHz}$ and $k = 8\pi$. The local frequency or called instantaneous frequency

Reproduced with permission of the copyright owner. Further reproduction prohibited without permission.

is modulated by a slow sinusoidal signal,

$$f(t) = \frac{1}{2\pi} \times \frac{\partial \varphi(t)}{\partial t} = f_0 - k f_2 \sin(2\pi f_2 t).$$

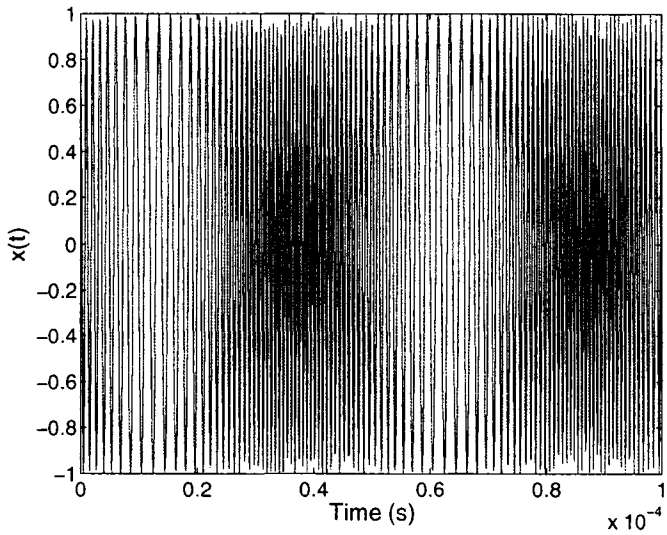

Figure 2.3: Example of a FM signal $x(t)$.

The waveform seems quite dense and not easy to analyze in Fig. 2.3. Following the same MPDE approach as for Eq. 2.1, we define the multi-time form as

$$\hat{x}(t_1, t_2) = \cos((2\pi f_0 t_1) + k\cos(2\pi f_2 t_2)), \tag{2.4}$$

with two time axes used directly to present the oscillation and the modulation, respectively. The bivariate waveform shown in Fig. 2.4 is not a simple surface but including many undulations which is not easy to sample along the t_2 axis. It is evident that FM-type signals cannot be handled efficiently by MPDE since the multiple representation is quite difficult to analyze.

We use WaMPDE to resolve Eq. 2.4, also separating the oscillation period and transient variation in multiple time axes. To surpass the fast undulations, we use a warped time scale τ_1 instead of t_1 to normalize the local frequency and keep another time scale τ_2 as the real time axis:

$$\hat{x}_2(\tau_1, \tau_2) = \cos(\tau_1), \tag{2.5}$$

Reproduced with permission of the copyright owner. Further reproduction prohibited without permission.

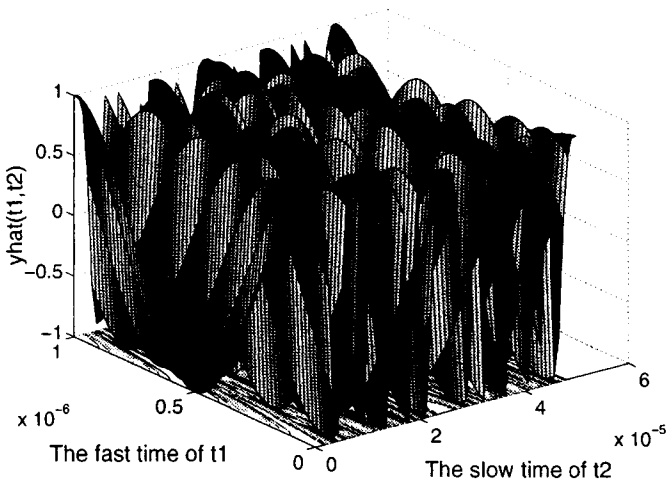

Figure 2.4: MPDE representation of $x(t)$.

with $x(t) = \hat{x}_2(\phi(t), t)$ and

$$\tau_1 = \phi(\tau_2) = 2\pi f_0 \tau_2 + k\cos(2\pi f_2 \tau_2).$$

The warped time becomes a function of time. The result of $\hat{x}_2(\tau_1, \tau_2)$ is a multi-time expression in warped and unwarped time scales shown in Fig. 2.5.

There are much less undulation than Fig. 2.4 and the signals can be sampled with relatively few points since the rescaled time axis stretches and squeezes the real time axis differently at different times to even out the period of the fast undulation. A mapping between warped time (τ_1) and real time (τ_2) function which is a curved path is also established in Fig. 2.6.

The solution of WaMPDE is not unique. For example, if we set

$$\hat{x}_3(\tau_1, \tau_2) = \cos(\tau_1 + 2\pi f_2 \tau_2) \tag{2.6}$$

with $x(t) = \hat{x}_3(\phi(t), t)$ and

$$\tau_1 = \phi(\tau_2) = 2\pi f_0 \tau_2 + k\cos(2\pi f_2 \tau_2) - 2\pi f_2 \tau_2.$$

We also get another WaMPDE representation. The WaMPDE result is plotted in Fig. 2.7, as well as the warped function represented in Fig. 2.8.

Reproduced with permission of the copyright owner. Further reproduction prohibited without permission.

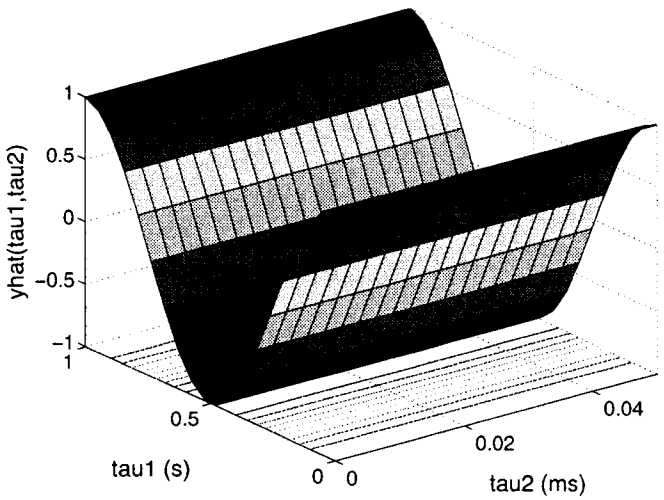

Figure 2.5: The first WaMPDE representation of $x(t)$.

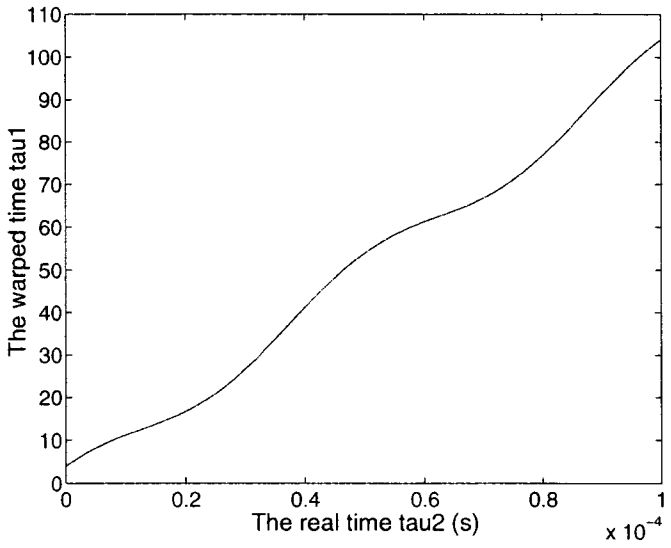

Figure 2.6: The relation between τ_1 and τ_2.

Reproduced with permission of the copyright owner. Further reproduction prohibited without permission.

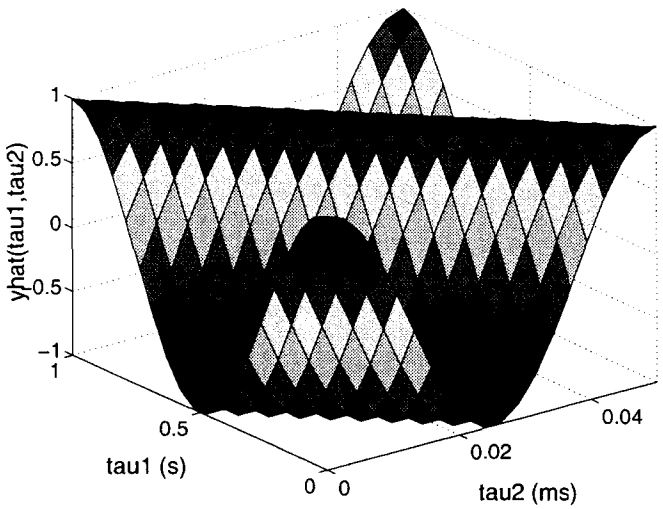

Figure 2.7: The second WaMPDE representation of $x(t)$.

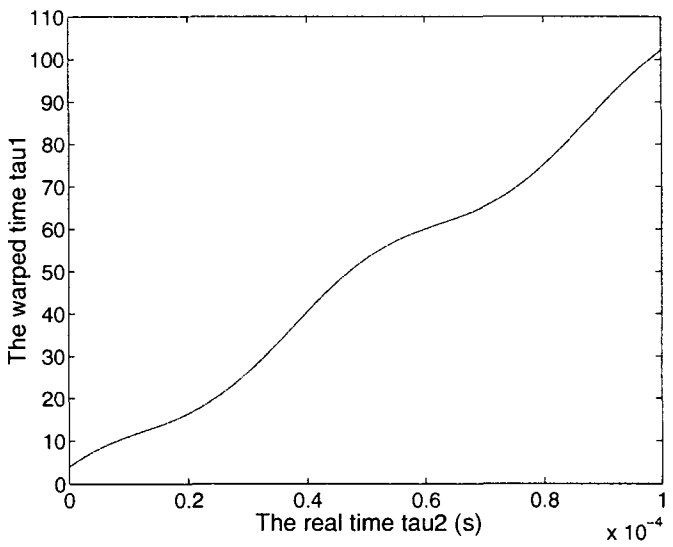

Figure 2.8: The relation between τ_1 and τ_2.

Reproduced with permission of the copyright owner. Further reproduction prohibited without permission.

Although we select different τ_1, the multi-time representation is still smooth and retains the same property of being easy to sample. The warped function which also describes the local frequency is similar to Fig. 2.6. It seems that WaMPDE is efficient and effective to solve FM problems when the two frequencies vary at widely separated rates. It is also easy to recover the initial signal by simply setting:

$$\begin{cases} \tau_2 = t \\ \tau_1 = \phi(\tau_2) = \phi(t) \end{cases}.$$

2.4 Comparison of MPDE and WaMPDE

Since MPDE and WaMPDE are all multi-time partial differential equations some similarities remain between two formulations. Also they have their own characteristics.

Firstly, we point out differences. The differences between MPDE and WaMPDE are:

1. In MPDE method, two time scales t_1 and t_2, all represent the real time t, though they are split into slow and fast dynamics; while in WaMPDE the warped time τ_1 which is a function of the real time τ_2 has no meaning of real time.

2. WaMPDE requires a mapping between warped time and real time to represent the relation of two time axes while MPDE does not. The (t_1, t_2) plane in MPDE is a straight-line whereas the (τ_1, τ_2) plane in WaMPDE is a curved path.

3. MPDE only deals with oscillatory systems with constant frequency. WaMPDE is used to analyze free-running oscillatory systems with time-varying oscillation frequency, no matter whether it is known or not.

4. In MPDE derivatives with respect to time are substituted as follows:

$$\frac{dx(t)}{dt} = \frac{\partial \hat{x}(t_1, t_2)}{\partial t_1} + \frac{\partial \hat{x}(t_1, t_2)}{\partial t_2}$$

while WaMPDE:

$$\frac{dx(t)}{dt} = \omega(\tau_2)\frac{\partial \hat{x}(\tau_1, \tau_2)}{\partial \tau_1} + \frac{\partial \hat{x}(\tau_1, \tau_2)}{\partial \tau_2}$$

with warped function $\omega(\tau_2)$ and $\tau_1 = \phi(\tau_2)$.

Reproduced with permission of the copyright owner. Further reproduction prohibited without permission.

The similarities between MPDE and WaMPDE are the following.

1. They are appropriate to represent signals varying at two or more widely separated rates.
2. They all preserve the rectangular shape of the domain box.
3. The original signal is easy to recover.
4. The computational time is usually much faster than the regular time domain simulation when the system is in two or more widely separated rates of variations.
5. MPDE is a special case of WaMPDE form by simply setting: $\tau_1 = \phi(\tau_2) = t$.

2.5 Boundary Conditions in WaMPDEs

To solve the WaMPDEs, it is necessary to first specify boundary conditions (BCs) which are imposed on differential equations to fit the solution in a particular situation. BCs describe the behavior at the edges of the simulation region and different BCs lead to different quasi-periodic and envelope-modulated solutions. A system of nonlinear algebraic equations can be solved numerically with BCs by applying time-domain or frequency-domain methods. These methods will be described in the next chapter. In this section, we focus on how to obtain the BCs in WaMPDEs. It is not easy since we need a whole line in $(\tau_1, 0)$ plane, and this issue is not explored with detail in the literature.

Here we discuss some possibilities of getting the BCs in WaMPDEs. The first thing is to rewrite the circuit's equations in terms of multivariate functions, in effect transforming the ODEs into WaMPDEs. Therefore, initial condtion which is usually a discrete point $(t = 0)$ in ODEs is required to transform to a continuous line in WaMPDE $(\tau_1, 0)$. The procedure to obtain the BCs of WaMPDE is illustrated as follows. First, the initial value $x(0)$ of ODEs corresponds to $\hat{x}(0, 0)$ in WaMPDEs. Secondly, we can use one full period of the ODE solution or the interpolation of two periods of the ODE solution as a BC for $(\tau_1, 0)$ line and the periodic condition along τ_1 is:

$$\hat{x}(0, \tau_2) = \hat{x}(2\pi, \tau_2)$$

Then this appropriate BC leads to periodic solutions in the τ_1 time axis and envelope-modulated solutions in the τ_2 time axis.

In steady-state analysis, we consider periodic BCs:

Reproduced with permission of the copyright owner. Further reproduction prohibited without permission.

$$\begin{cases} \hat{x}(0,\tau_2) = \hat{x}(2\pi,\tau_2) \\ \hat{x}(\tau_1,0) = \hat{x}(\tau_1,\tau_2) \end{cases}.$$

2.6 Oscillator Theory

Oscillators are those kinds of circuits which have periodic output signals but without periodic input signals [8]. They are widely used in electrical and communication engineering systems. In this section we will review the general structure of oscillators along with the condition of oscillations and indicate the importance of this thesis work.

Electronic oscillator circuits are always feedback networks whose purpose is to control the frequency of oscillations. Fig. 2.9 shows the necessary components of an oscillator. It contains an amplifier with frequency-dependent forward loop gain $G(j\omega)$ and a frequency-dependent feedback network with feedback gain $H(j\omega)$.

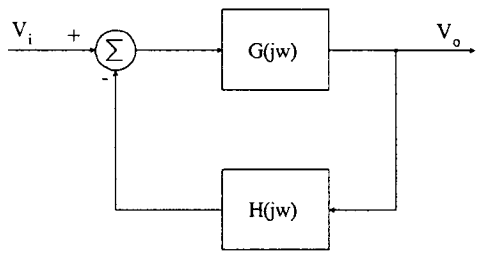

Figure 2.9: Block diagram of an oscillator.

The output voltage is given by

$$V_o = \frac{V_i G(j\omega)}{1 + G(j\omega)H(j\omega)}$$

To sustain oscillations, the circuit must obey the Nyquist criterion [8] at the oscillation frequency ω_0:

$$G(j\omega_0)H(j\omega_0) = -1.$$

Those are two conditions to occur oscillations: the magnitude of the open-loop transfer function is equal to 1 and the phase shift is 180 degree.

There are several types of oscillators, such as LC-tuned bipolar oscillator, Colpitts oscillator, voltage-controlled oscillators (VCO). VCOs are usually designed using the Clapp-Gouriet

Reproduced with permission of the copyright owner. Further reproduction prohibited without permission.

configuration shown in Fig. 2.10 which splits the oscillator into two parts: tuning elements with positive resistance to determine the oscillation frequency and the transistor with negative resistance to compensate for all the losses. The diode D_1 to tune the oscillator frequency is added in series with the inductor L_1. The varicap is connected to a DC tuning voltage V_{dc}. A negative resistor r_i in series with the tuned circuit is a must to maintain oscillations .

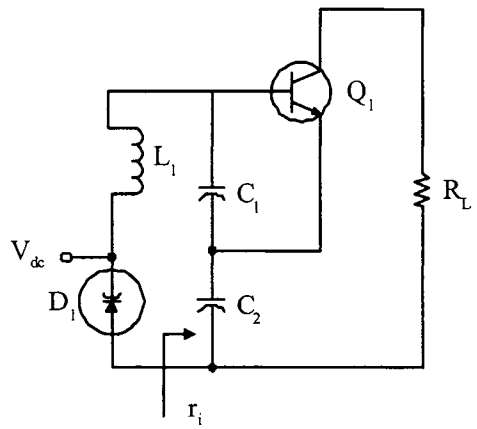

Figure 2.10: A sketch figure of VCO with a negative resistance r_i.

For oscillation to occur the negative resistance must be equal or larger than the positive resistance [8]. There is also a limit to the values of capacitances C_1 and C_2 at a certain oscillating frequency. The condition for sustained oscillation is:

$$r_i = -\frac{g_m}{\omega^2 C_1 C_2}, \tag{2.7}$$

with input impedance r_i, transistor's mutual conductance g_m and the oscillation frequency ω. Thus the internal resistance of the inductor is satisfied with:

$$r \leq r_i. \tag{2.8}$$

If a large operating frequency range is to be achieved, C_1 and C_2 must be made large and the inductor must have a high Q so that the internal resistance r is small. The oscillation occurs at a local frequency ω which is given by

Reproduced with permission of the copyright owner. Further reproduction prohibited without permission.

$$\omega = \sqrt{\frac{1}{L_1}(\frac{1}{C_1} + \frac{1}{C_2} + \frac{1}{C_D})} \tag{2.9}$$

where C_D is the varicap junction capacitance.

In most cases the simulation is the only way to find the oscillation amplitude. Therefore, the simulation of the steady-state and the transient response of oscillators are always significant aspects in circuit analysis. Because of the extremely long simulation time in some oscillators, robust and fast approaches for capturing both the steady-state and transient response become a must. However, it is often difficult to analyze the response of a general autonomous system in a satisfactory manner. A variation of that method is known as WaMPDE which has already been reviewed in the previous section. In this thesis work we develop two fast and accurate approaches to solve the steady-state and transient behavior of oscillators respectively in frequency domain based on WaMPDE. References [1, 9, 10, 11] are a few examples as well as those mentioned in Chapter 1 [2, 3, 4]. Other relevant developments are the exploitation of frequency-domain latency in HB [12, 13] and the use of fast transients to find the steady-state regime [10, 14]. The techniques in [12, 13] take advantage of the fact that in most circuits the number of harmonics necessary to represent each variable (voltage, current) is not the same. By using a different number of harmonics in each variable or compressing the transient behavior, a significant reduction in the computational effort is achieved. In order to accelerate the finding of the steady-state regime, the transient behavior of the circuit is artificially reduced in [14]. In [10], an envelope-transient analysis is used to improve the convergence of the shooting method. From the next chapter, we will propose two new approaches trying to capture the steady-state and transient response of oscillators in a fast and precise manner.

Reproduced with permission of the copyright owner. Further reproduction prohibited without permission.

Chapter 3

Transient Analysis

Transient analysis of oscillators is one important area in circuit analysis although it usually requires a long simulation time as mentioned in Chapter 1. In [7], multiple time axes are employed to separate the fast and slow variations in the response of oscillators, giving a possible way to quickly compute the transient. The System of ODEs is replaced by a system of partial differential equations. If an accurate transient analysis is required, the initial conditions in the ODEs must be precisely mapped into boundary conditions in WaMPDE. At the beginning of this work the boundary conditions in the WaMPDE are approximated using the values of one period of the ODE solution or the interpolation of two periods of the ODE solution to map the result to the WaMPDE domain as mentioned in Chapter 2. However these simple methods to find the boundary conditions are not accurate enough to produce results consistent with the ODE result. This problem has not been treated so far. In this thesis work we present a method to accurately perform this mapping and thus allow the transient analysis of oscillators with any initial guesses. In this chapter we will first analyze an ideal VCO circuit to further illustrate the efficiency of WaMPDE formulation and the importance of boundary conditions in WaMPDE. Secondly the motivation of the new approach will be pointed out and the transient method will be proposed in detail. A case study of a LC-tuned bipolar oscillator is used to demonstrate the performance of the new method in the last section.

3.1 Motivation: The Analysis of A Simple VCO Circuit Using WaMPDE

In this section, we simulate a simple circuit using numerical techniques derived from the WaMPDE to explore the voltage and current representations in multi-time domains. The circuit

Reproduced with permission of the copyright owner. Further reproduction prohibited without permission.

is an ideal VCO with $C = 1/(2\pi)$ pF, $C_m = 1/(4\pi)$ pF, and $L = 1/(2\pi)$ μH shown in Fig. 3.1 [1].

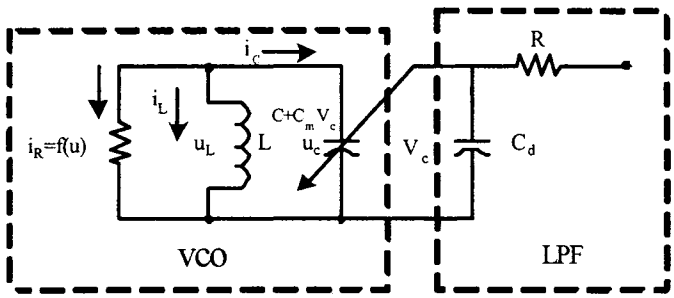

Figure 3.1: An ideal VCO circuit.

This VCO consists of a nonlinear resistor followed by a LC tank in parallel (resonator). The frequency is determined by the inductor L and the capacitors: C and C_m. Part of the tank capacitance is varied by a separate control voltage V_c, which allows the frequency control.

The nonlinear resistor is represented by:

$$i_R = f(u) = (G_0 - G_\infty)V_k \tanh(\frac{u}{V_k}) + G_\infty u.$$

where $G_0 = -0.1$, $G_\infty = 0.25$, and $V_k = 1$. The capacitor voltage u_c and the inductor current i_L are a series of fast resonance sinusoids whose frequency and amplitude are modulated at a much slower rate. In general, it is hard to solve both the frequency modulation and amplitude modulation in oscillatory system with traditional time domain method. Here we solve them in warped multiple time domains. Since the nominal oscillation rate of oscillators is very fast, it separate the comparatively slow part — FM and AM from the original signal. The oscillator behavior is discretized in two time axes: the warped time axis τ_1 (fast) and the real time axis τ_2 (slow). Then we build up the nonlinear equations and solve them with Newton-Raphson Method [15]. The warped function represents the changing local frequency of VCO and is an unknown function. Therefore, it was considered as one of the unknowns in the nonlinear equations.

3.1.1 ODE Analysis

The control voltage V_c is varied with two different periods:

$$V_c = 1.5\cos(\frac{2\pi}{T})t, \tag{3.1}$$

Reproduced with permission of the copyright owner. Further reproduction prohibited without permission.

$T_1 = 3 \times 10^{-5}s$ for fast variation shown in Fig. 3.2 and $T_2 = 1 \times 10^{-3}s$ for slow variation.

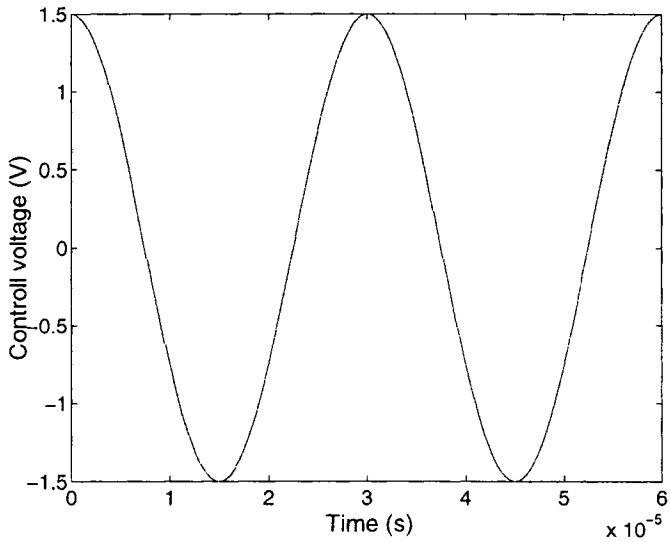

Figure 3.2: The fast varying control voltage.

Since the control voltage is 1.5V when $t = 0$, the initial local frequency of VCO is:

$$f_0 = \frac{1}{2\pi\sqrt{L(C + C_m V_{c0})}} = 0.75MHz$$

The local frequency as a function of time is given in:

$$f_{LQ} = \frac{1}{2\pi\sqrt{L(C + C_m V_c)}} = \frac{1}{\sqrt{1 + 0.75\cos\omega_c t}} \tag{3.2}$$

which is controlled by the control voltage and varies by a factor of almost 3 shown in Fig. 3.3.

Based on KCL, the current relation in this oscillator is:

$$i_R + i_L + i_C = 0, \tag{3.3}$$

with

$$\begin{cases} i_L = \frac{1}{L}\int u_L dt \\ i_C = \frac{dQ}{dt} = \frac{d[(C+C_m V_c)u_c]}{dt} = \frac{d[(C+C_m V_c)u_c]}{dt} = (C + C_m V_c)\frac{du_c}{dt} + C_m \frac{dV_c}{dt} u_c \end{cases}.$$

Based on KVL, the voltage relation is defined as:

Reproduced with permission of the copyright owner. Further reproduction prohibited without permission.

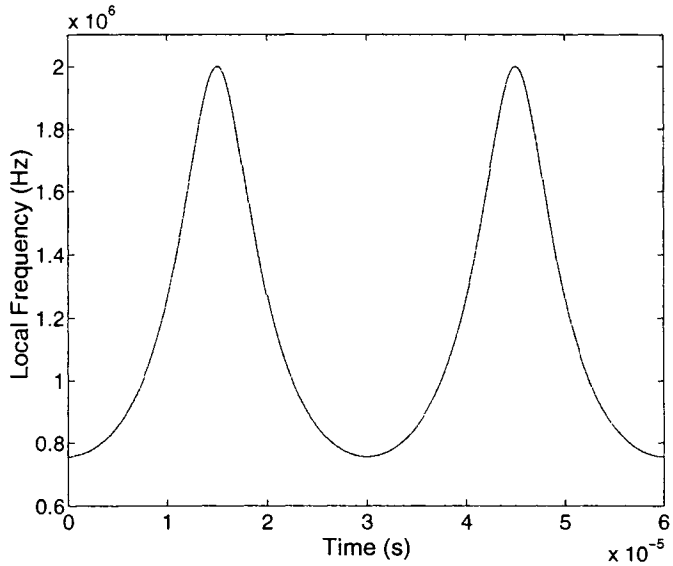

Figure 3.3: The local frequency.

$$u_L = u_c = u_R = u, \tag{3.4}$$

with

$$\begin{cases} u_c - L\frac{di_L}{dt} = 0 \\ i_L + (C + C_m V_c)\frac{du_c}{dt} + C_m \frac{dV_c}{dt} u_c - f(u_c) = 0 \end{cases},$$

with two state variables: capacitor voltage u_c and inductor current i_L. The initial condition is set to be $u_{c0} = 0$ and $i_{L0} = -1A$. We obtain the waveform of the capacitor voltage in Fig. 3.4 under the fast varying control voltage with explicit Runge-Kutta method by using the command *ode*45 in Matlab [16].

The frequency modulation and the amplitude modulation are clear in transient of the state variable. The simulation is started again under the slow varying control voltage and the result is shown in Fig. 3.5.

It is obvious that the control voltage modifies not only the local frequency, but also the amplitude and shape of the oscillator waveform [1]. Since it takes long computational time to generate Fig. 3.5 (about 200 seconds), and the fact that the oscillation and the envelope transient are two widely separated rates of variations, we use WaMPDE to separate those two variations

Reproduced with permission of the copyright owner. Further reproduction prohibited without permission.

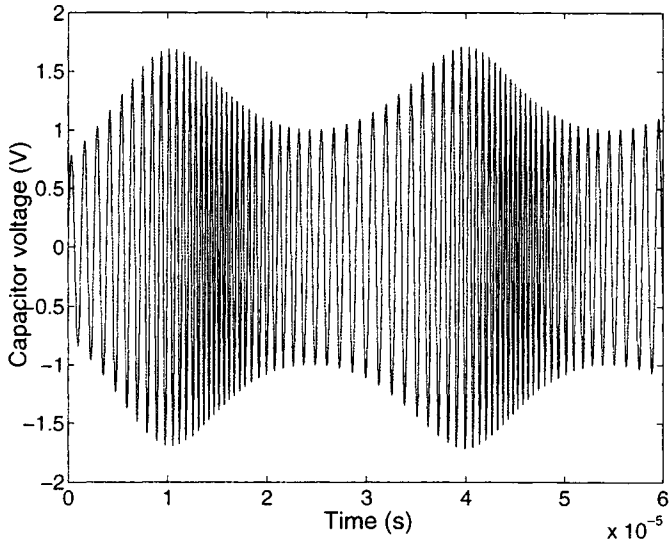

Figure 3.4: Capacitor voltage under fast varying control voltage.

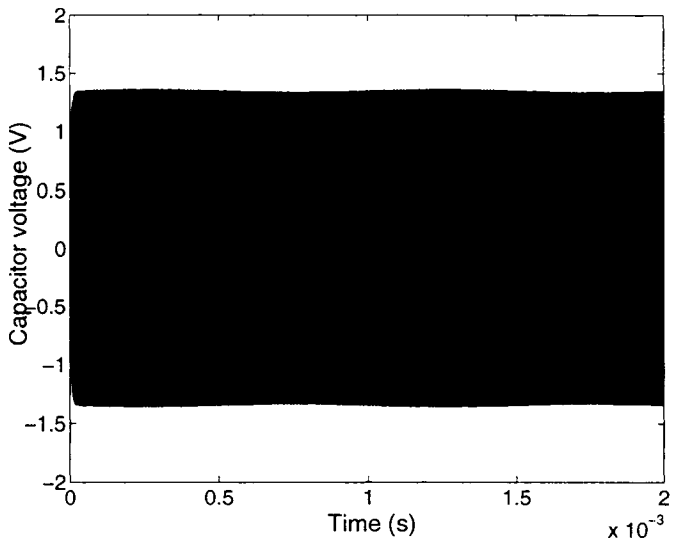

Figure 3.5: Capacitor voltage under slow varying control voltage.

Reproduced with permission of the copyright owner. Further reproduction prohibited without permission.

in order to reduce the simulation time.

3.1.2 3-D WaMPDE Analysis

The VCO is analyzed by using numerical techniques derived from WaMPDE. The procedure of WaMPDE analysis is illustrated as follows. Firstly, locate initial guesses on multiple time grids (τ_1, τ_2). The relation between τ_1 and τ_2 is defined by:

$$\tau_1 = \int_0^t \omega(\tau_2) d\tau_2, \tag{3.5}$$

where $\omega(\tau_2)$ is the unknown local frequency of the oscillator which is a function of real time τ_2. Secondly, build up the nonlinear equations. The ordinary differential equations (Eq. 3.3 and 3.4) are replaced by the partial differential equations in multi-time domain:

$$F_1(\tau_1, \tau_2) = u_c - L\left(\omega(\tau_2)\frac{\partial i_L}{\partial \tau_1} + \frac{\partial i_L}{\partial \tau_2}\right) = 0, \tag{3.6}$$

$$F_2(\tau_1, \tau_2) = i_L + (C + C_m V_c(\tau_2))(\omega(\tau_2)\frac{\partial u_c}{\partial \tau_1} + \frac{\partial u_c}{\partial \tau_2}) + C_m \frac{\partial V_c}{\partial \tau_2} u_c + f(u_c) = 0. \tag{3.7}$$

The warped function $\omega(\tau_2)$ is an additional unknown that must be calculated for each value of τ_2. The phase of one of the variables is then fixed to restore the number of unknowns to be equal to the number of equations. This is achieved by setting the phase of one of the variables to an arbitrary value to reduce one unknown,

$$F_3(\tau_1, \tau_2) = u_c(0, \tau_2) = 0. \tag{3.8}$$

So we solve those nonlinear equations with the Newton-Raphson Method (see the Appendix A) for each value of τ_2:

$$\begin{cases} x = \begin{bmatrix} u_c & i_L & \omega \end{bmatrix} \\ \\ F = \begin{bmatrix} F_1 & F_2 & F_3 \end{bmatrix} \end{cases}$$

The multi-time expression of the capacitor voltage is achieved by using some numerical techniques. Three methods, Finite Time-domain Method (FDTD), Harmonic Balance (HB), and Base Function Method (BF) are discussed in the following part to achieve numerical solutions of the WaMPDE expression.

Reproduced with permission of the copyright owner. Further reproduction prohibited without permission.

Finite Difference Time-domain Method (FDTD)

Finite Difference Time-domain Method (FDTD) is a straightforward way to numerically solve time-domain differential equations that describe a nonlinear system [17]. The solution of the ODEs is discretized in warped and real time axes. The unknowns are values along τ_1 axis which is periodic for each value of τ_2. The key work is to obtain a formula to compute $u_c\left(\tau_{1(n)}, \tau_{2(m)}\right)$ as a function of previous points. The time step of each grid is defined as

$$\begin{cases} h_1 = \tau_{1(n)} - \tau_{1(n-1)} \\ h_2 = \tau_{2(m)} - \tau_{2(m-1)} \end{cases}.$$

Those differentiation operators can be replaced by an approximate expression, such as Backward Euler (BE) Rule, Central-difference formula, Five-Point formula, or Trapezoidal Rule according to the desired accuracy [15]. Here we use Five-point formula to represent the differentiation operators along τ_1 time axis:

$$\frac{\partial x(\tau_1, \tau_2)}{\partial \tau_1} = \frac{x(\tau_1 - 2h_1, \tau_2) - 8x(\tau_1 + h_1, \tau_2) + 8x(\tau_1 - h_1, \tau_2) - x(\tau_1 + 2h_1, \tau_2)}{12h_1},$$

and Backward Euler Rule to represent the differentiation operators along τ_2 time axis:

$$\frac{\partial x(\tau_1, \tau_2)}{\partial \tau_2} = \frac{x(\tau_1, \tau_2) - x(\tau_1, \tau_2 - h_2)}{h_2}.$$

The nonlinear equations are discretized along two time axes and solved with Newton-Raphson Method. The WaMPDE expression of the capacitor voltage under fast varying control voltage is shown in Fig. 3.6, together with the warped function $\omega(\tau_2)$ in Fig. 3.7. The initial guesses are set to be $u_{c0} = 0$ and $i_{L0} = -1A$, the same as the ODE analysis. The boundary condition of the capacitor voltage is manually set to be a sinusoidal wave along τ_1 with an amplitude 1 V.

Compared with the traditional time domain analysis, the multi-time expression also represents the frequency modulation and amplitude modulation, but the waveform is much easier and clearer to analyze. The warped function relates to the inherent property of the nonlinear circuit since the Fig. 3.7 is simular to the local frequency shown in the Fig. 3.3.

The WaMPDE expression of the capacitor voltage under slow varying control voltage is shown in Fig. 3.8. As expected, the amplitude of the oscillation changes very little for the capacitor voltage which is consistent with ODE result. It also validates that the control voltage controls

Reproduced with permission of the copyright owner. Further reproduction prohibited without permission.

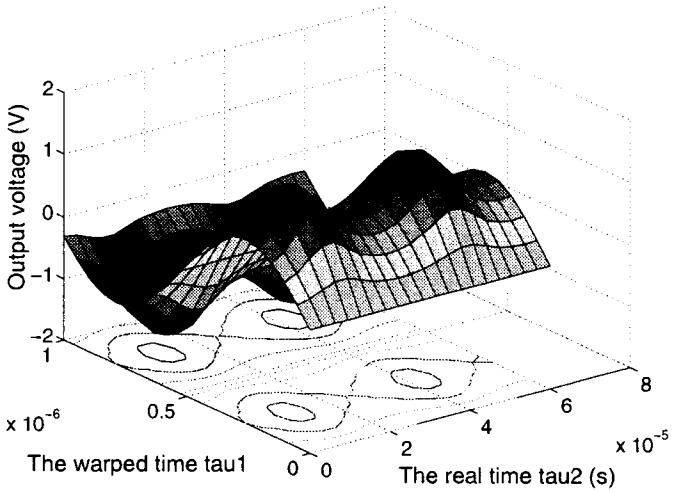

Figure 3.6: WaMPDE representation of capacitor voltage in fast varying control voltage (FDTD).

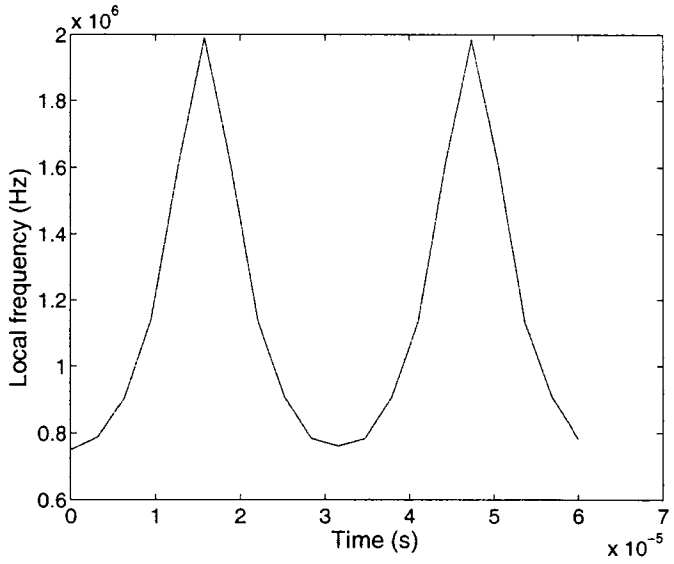

Figure 3.7: Warped Function (FDTD).

Reproduced with permission of the copyright owner. Further reproduction prohibited without permission.

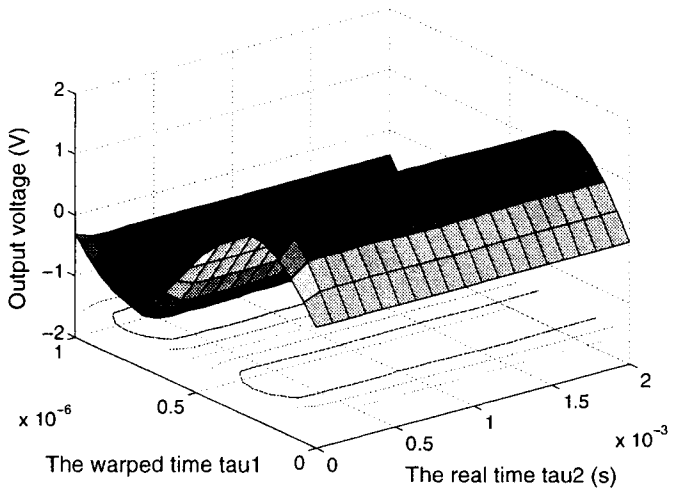

Figure 3.8: WaMPDE representation of capacitor voltage in slow varying control voltage (FDTD).

both the amplitude and the shape of the oscillator waveform. The computational time is almost one sixtieth of the traditional time-domain analysis.

Employing some small error numerical differentiations, such as Five-Point Rule, is a good way to improve the accuracy of the result. Decreasing h_1 or h_2 also improves the accuracy of the simulation. We use fast varying control voltage as example. Fig. 3.9 shows the result for 50 points in each side.

Excellent accuracy was achieved in Fig. 3.9. However, the computational effort required to compute the solution is increased since a greater number of steps are required to cover a constant time interval. The smaller the time steps, the longer the computational time.

Harmonic Balance Analysis (HB)

Harmonic balance is one of the most popular frequency-domain techniques to study the steady-state response of nonlinear systems. It is based on a Fourier-series expansion of state equations. When used on circuits behaving only with few harmonics, harmonic balance is significantly more efficient than traditional time-domain method since the number of Fourier coefficients may be smaller to achieve the same accuracy represented in the time domain.

In WaMPDE, the solution along the warped time axis is solved in the frequency domain. The

Reproduced with permission of the copyright owner. Further reproduction prohibited without permission.

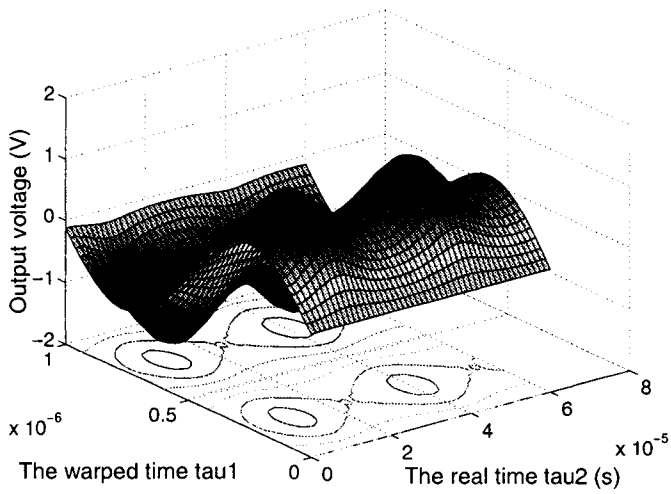

Figure 3.9: Capacitor voltage with 50 points in τ_1 and τ_2.

unknowns are the Fourier Coefficients along τ_1 corresponding to each value of τ_2. The imaginary part of the fundamental frequency of one of the state variables is set to be zero as the forcing function to solve the warped function $\omega(\tau_2)$. The key work of Harmonic Balance is to express the state variable x as a Fourier series:

$$x(\tau_1, \tau_2) = \Re\left\{\sum_{k=0}^{\infty} X(k) e^{jk\tau_1}\right\}, \tag{3.9}$$

where $X(k)$ is the Fourier coefficient of the k_{th} harmonic. The higher the k, the smaller the absolute values of $X(k)$. Large number of harmonics improves the accuracy but slows the computational speed. The number of the harmonics considered has a major impact on the accuracy of this method. This method is particularly appropriate for this VCO circuit due to the sinusoidal characteristic along the warped time axis. Only three harmonics were considered in the τ_1 time axis, and 20 points were sampled along the τ_2 time axis. The computational time is much faster than the time domain method and the results shown in Fig. 3.10 and Fig. 3.11 are exactly the same as FDTD.

Here we give some brief discussions about the transient behavior of this VCO circuit. Very small initial guess ($u_{c0} = 0$ and $i_{L0} = -0.01A$) is employed to observe the transient response. In Fig. 3.12 VCO enlarges its amplitude till it gets steady-state which is exact the same as the

Reproduced with permission of the copyright owner. Further reproduction prohibited without permission.

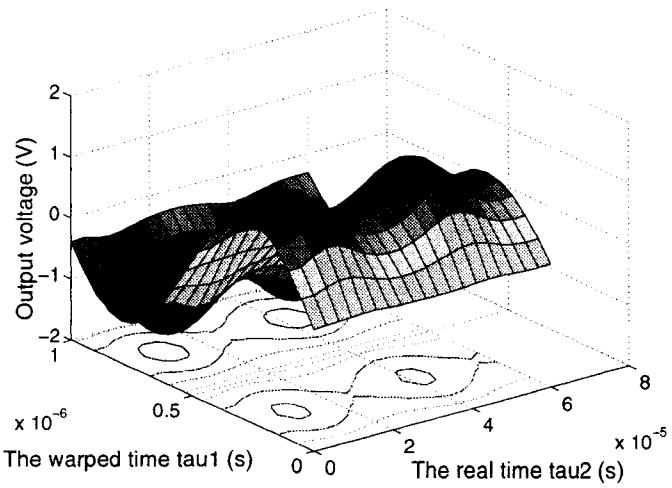

Figure 3.10: WaMPDE representation of capacitor voltage in fast varying control voltage (HB).

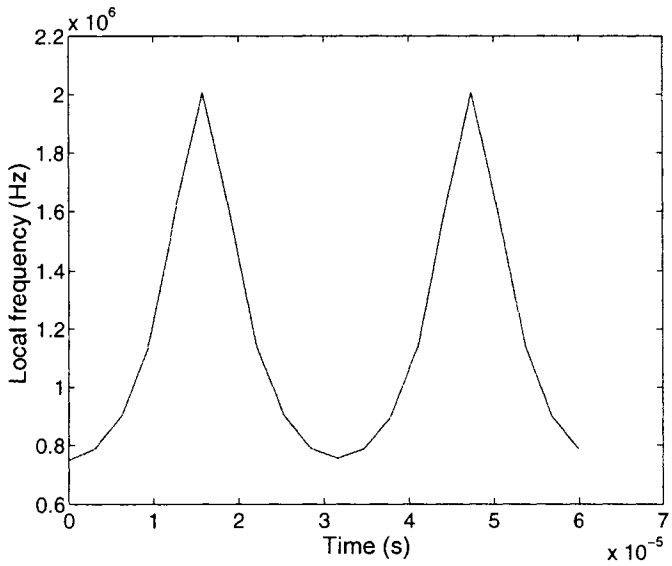

Figure 3.11: The local frequency (HB).

Reproduced with permission of the copyright owner. Further reproduction prohibited without permission.

previous analysis. The detail of achieving transient or steady-state solution will be addressed in the subsequent chapter.

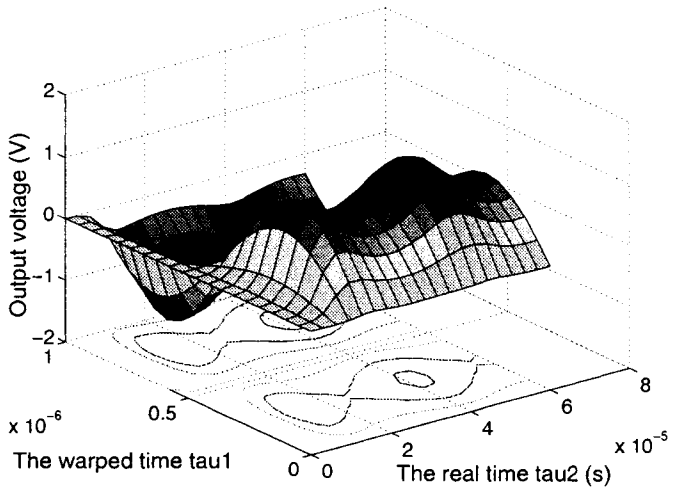

Figure 3.12: WaMPDE representation of capacitor voltage with small initial guesses.

Base Function Method

Base function is a novel technique to obtain the periodic steady-state response of nonlinear circuits [18]. Compared with harmonic balance, it has the potential to use fewer parameters to represent state variables in nonlinear circuits. Each state variable $x(t)$ is expressed by a linear combination of basis functions. We use this technique to find the solution along the warped time axis τ_1, such as

$$x(\tau_1) = \hat{x}(\tau_1, a) =$$

$$\sum_{i=0}^{n-1} [a_{2i+1}\varphi_{2i+1}(\tau_1) + a_{2i+2}\varphi_{2i+2}(\tau_1) + a_{2i+3}\varphi_{2i+3}(\tau_1) + a_{2i+4}\varphi_{2i+4}(\tau_1)]$$

with function values a_{2i+1}, a_{2i+3}, function derivatives a_{2i+2}, a_{2i+4}, and base functions $\varphi(\tau_1)$. Only three points in one period are considered due to the sinusoidal characteristic in this VCO circuit. The unknowns are values and derivatives at each chosen point. The capacitor voltage when $\tau_1 = 0$ is fixed as the forcing function. The results are similar to previous analysis with a much smaller computational effort. If the periodical solution consists of many harmonics, this method

Reproduced with permission of the copyright owner. Further reproduction prohibited without permission.

performs much better than HB since the unknown quantities for HB are largely increased. The WaMPDE results by using base function method are shown in Fig. 3.13 and Fig. 3.14.

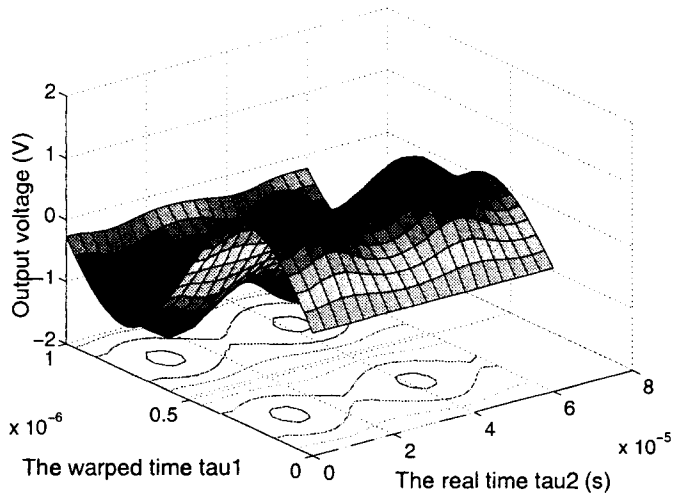

Figure 3.13: WaMPDE representation of capacitor voltage in fast varying control voltage (BF).

We mentioned before that the forcing function is not unique. Different warped functions result in different multi-time expressions of the selected node voltage or branch current. Here, we fix the inductor current when $\tau_1 = 0$ as the forcing function. The WaMPDE results are shown in Fig. 3.15.

The multi-time expression is different from what we discussed above. But the single time expression should be the same if we transform the waveform from multiple time domain to single time domain. This is discussed in the next section.

3.1.3 2-D WaMPDE Analysis

The WaMPDE method gives a possible way to largely reduce the computational effort in some nonlinear circuits. In this section we discuss a procedure to switch the waveform from the multiple time domain to the traditional time domain. It is easy to implement since the relation of τ_1 and τ_2 has been already defined in Eq. 3.5. The mapping between two time axes is the integral of the local frequency (see Fig. 3.7) which is a curved path shown in Fig. 3.16. The warped time τ_1 represents the phase accumulation. The oscillation period was divided by the normalized period 2π (*i.e.*, $\omega = 1$) along τ_1.

Reproduced with permission of the copyright owner. Further reproduction prohibited without permission.

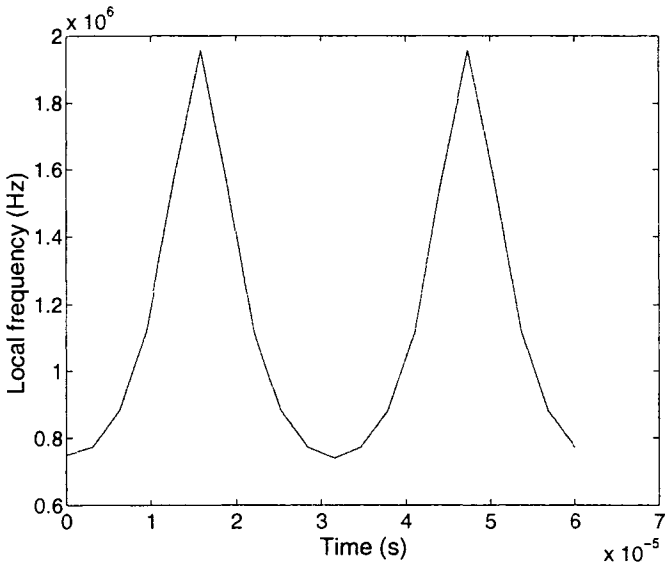

Figure 3.14: The local frequency (BF).

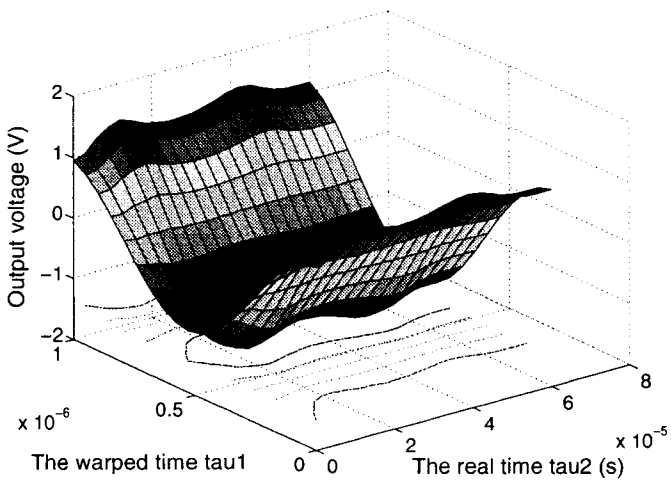

Figure 3.15: WaMPDE representation of capacitor voltage in different warped function.

Reproduced with permission of the copyright owner. Further reproduction prohibited without permission.

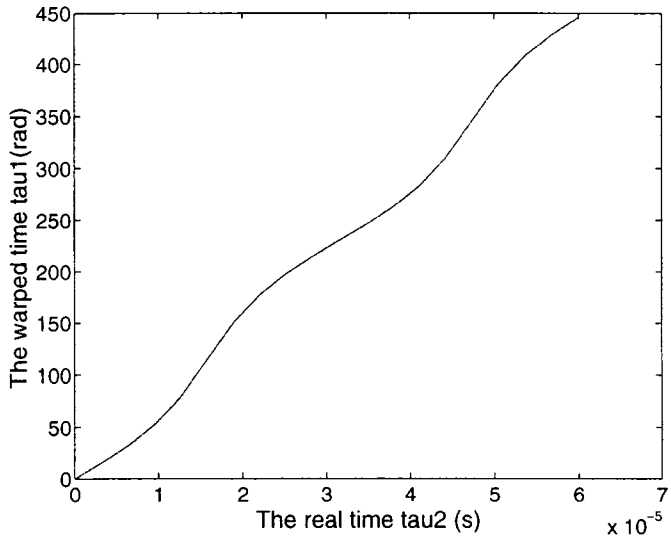

Figure 3.16: The relation of two time axes.

Linear interpolation is used to find the middle value between two known points since the time interval was very small. It allows the prediction of an unknown value if any two particular values on the same scale are known and the rate of change is assumed constant [19]. The formula for linear interpolation is

$$d = d_1 + \frac{g - g_1}{g_2 - g_1}(d_2 - d_1)$$

with desired value (g, d) and two closest approximations (g_1, d_1) and (g_2, d_2). The transformation is applicable in either fast or slow varying control voltage. As presented in Fig. 3.17 and Fig. 3.18, the waveforms present frequency and amplitude modulation, similar to the ODE result. It also proves that WaMPDE is accurate and efficient to solve the FM and AM in nonlinear circuits.

A small section (a few cycles around $5us$) of the 2-D WaMPDE output which is derived from FDTD, HB or Base function method, is compared with the ODE result with the different number of points along τ_2 shown in Fig. 3.19. It shows that the greater the number of points, the smaller the phase error between WaMPDE and ODE result.

We also summarized the comparison of these three methods in table 3.1 and the computational time of traditional time domain method in table 3.2. It is obvious that a long simulation time is needed in traditional time domain method especially under the slow varying control voltage. WaMPDE exhibits its strong ability of saving the computational effort. This is one of the

Reproduced with permission of the copyright owner. Further reproduction prohibited without permission.

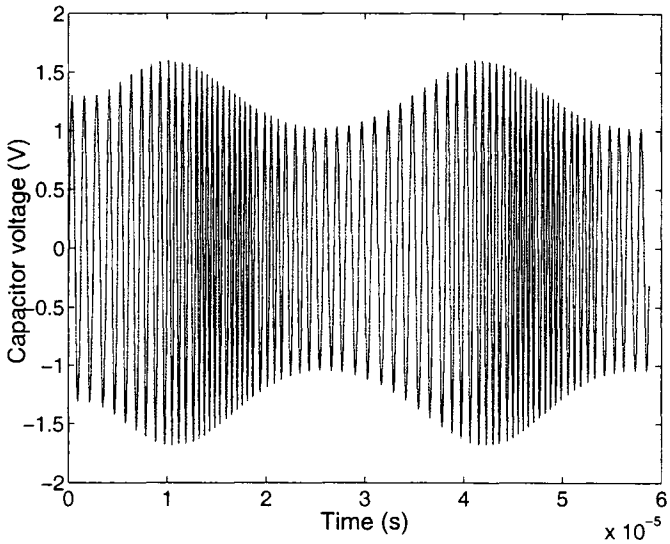

Figure 3.17: 2-D WaMPDE representation of capacitor voltage in fast varying control voltage.

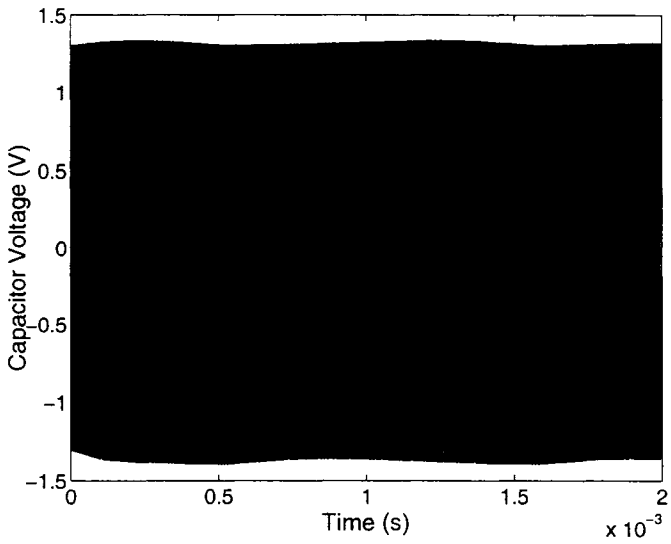

Figure 3.18: 2-D WaMPDE representation of capacitor voltage in slow varying control voltage.

Reproduced with permission of the copyright owner. Further reproduction prohibited without permission.

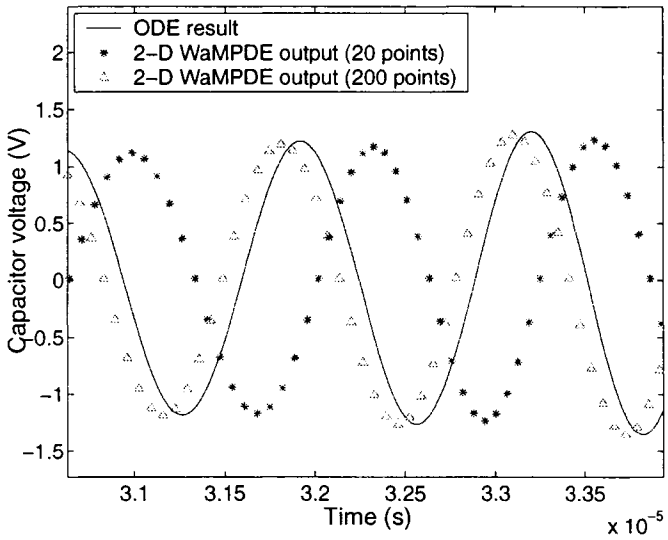

Figure 3.19: Comparison of ODE result with 2-D WaMPDE.

most significant advantages of this formulation. Compared with three methods, HB and Base function method perform better than FDTD since this VCO circuit has a sinusoidal characteristic. In general, HB is the best choice if the circuit only contains a few harmonics. Base function method is more efficient if the solution has many harmonics. Therefore, the choice of the method depends on different system and different requirements.

WaMPDE-based numerical method is a novel approach to efficiently present frequency and amplitude modulations in oscillators. The multi-time expression is easy to obtain either in the time domain or in the frequency domain. Considerable computational cost is saved compared with the traditional time domain method. The multi-time expression also reveals the direction to get the local frequency of oscillators. Three methods — Finite Difference Time-domain method, Harmonic balance, and Base functions method, are all successful in achieving correct WaMPDE multivariable representations. All those advantages makes WaMPDE powerful in circuit simulation. But there is a large phase error between univariate solution and the traditional time domain simulation due to the inaccurate boundary conditions. In the coming section we will present a new approach to obtain the accurate Boundary Conditions (BCs), trying to capture the transient response of oscillators precisely in multiple time domains.

Reproduced with permission of the copyright owner. Further reproduction prohibited without permission.

FDTD	τ_2=20	τ_2=40	τ_2=80	τ_2=160
τ_1 (points)	20	20	30	30
Computational Time (s)	2.687	4.437	16.953	34.406
Amplitude Error (%)	1.343	1.552	1.078	1.143
Phase Error (rad)	3.687	1.704	0.846	0.144
HB	τ_2=20	τ_2=40	τ_2=80	τ_2=160
τ_1 (harmonics)	3	5	5	7
Computational Time (s)	0.594	2.844	3.860	7.485
Amplitude Error (%)	2.730	0.498	0.315	0.105
Phase Error (rad)	4.437	1.591	0.818	0.344
BF	τ_2=20	τ_2=40	τ_2=80	τ_2=160
τ_1 (intervals)	3	4	5	6
Computational Time (s)	0.516	0.906	2.672	6.469
Amplitude Error (%)	4.376	2.781	1.171	0.047
Phase Error (rad)	0.712	0.198	0.103	0.006

Table 3.1: Comparison between three methods achieving WaMPDE.

ODE (Tolerance:1e-8)	Fast Varying CV	Slow Varying CV
Computational Time (s)	2.375	198.844

Table 3.2: Computational time of the ODE result.

Reproduced with permission of the copyright owner. Further reproduction prohibited without permission.

3.2 The Proposed Method

3.2.1 General Equation Formulation

Let the circuit be described by its nodal equations:

$$Gu(t) + C\frac{du(t)}{dt} + \frac{dQ(u(t))}{dt} + I(u(t)) = S(t), \tag{3.10}$$

here $u(t)$ is the vector of nodal voltages and selected branch currents; G is a matrix of conductances, such as resistors; C is the matrix representing the linear charge terms, such as inductors or capacitors; $Q(u(t))$ and $I(u(t))$ are vector functions corresponding to the nonlinear devices, such as voltage controlled capacitors or nonlinear resistors; and $S(t)$ is a vector that represents the power supply sources.

In the proposed method, whatever dealing with the steady-state or the transient behavior, the periodic solution in the warped time τ_1 is solved using the Harmonic balance technique (frequency domain) and the solution in the τ_2 direction is solved using a time marching technique (time domain). This arrangement is usually known as one of the envelope transient analysis. Each element of the $u(t)$ vector is now represented by a function of two time variables $u_n(\tau_1, \tau_2)$ (n denotes the node index) and is represented by a set of time-varying phasors,

$$u_n(\tau_1, \tau_2) = \Re\left\{\sum_{k=0}^{K} U_n^k(\tau_2) e^{jk\tau_1}\right\}, \tag{3.11}$$

where k is the harmonic number and the period in the warped time scale (τ_1) is normalized to 2π (*i.e.*, $\omega = 1$). Eq. (3.11) is now formulated in each frequency by using Fourier coefficients:

$$(G + C\Omega_k)U^k + C\frac{\partial U^k}{\partial \tau_2} + \Omega_k Q^k + \frac{\partial Q^k}{\partial \tau_2} + I^k - S^k = 0, \tag{3.12}$$

here, $\Omega_k = jk\omega_0(\tau_2)$. The $Q^k(U^k)$, $I^k(U^k)$ and S^k vectors are all functions of τ_2. I^k and Q^k are normally evaluated using the discrete Fourier transform (DFT). Eq. (3.12) is discretized in the τ_2 direction using the Backward Euler (BE) Rule or the Trapezoidal Rule. The resulting algebraic nonlinear system is then solved with the Newton-Raphson method for each value of τ_2.

As mentioned in Chapter 2, the fundamental frequency $\omega_0(\tau_2)$ is an additional unknown that must be calculated for each value of τ_2. The phase of one of the variables must then be fixed to restore the number of unknowns to be equal to the number of equations. That is usually achieved by setting the imaginary part of one of the variables to be a fixed value. For example,

Reproduced with permission of the copyright owner. Further reproduction prohibited without permission.

we can set the imaginary part of the fundamental frequency to be a fixed value a,

$$\Im(U_n^1) = a. \tag{3.13}$$

3.2.2 Transient Analysis with WaMPDE

As stated in Chapter 1, finding accurate initial conditions is essential in transient analysis. In WaMPDE, the boundary conditions along τ_1 when $\tau_2 = 0$ are required to be precise. Firstly, we show a comparison between ODE result and WaMPDE with boundary conditions from DC bias point in Fig. 3.20 to illustrate the importance of boundary conditions in envelope-transient analysis.

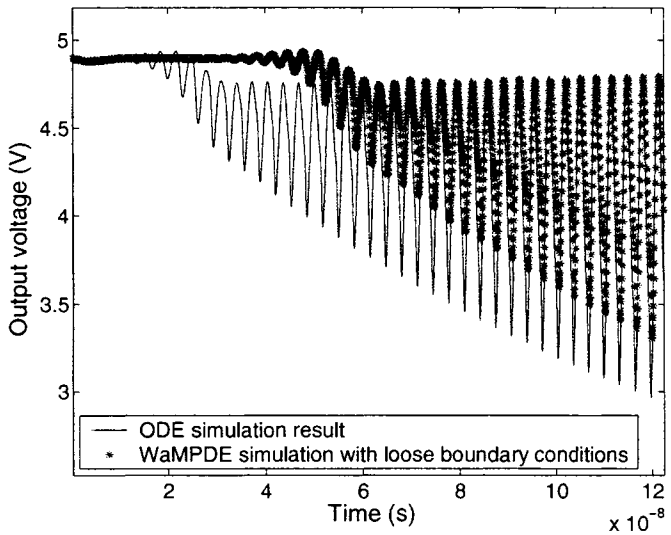

Figure 3.20: The comparison of ODE and WaMPDE with boundary conditions from DC bias point.

From Fig. 3.20 there is a large difference between two waveforms. That means the boundary conditions of WaMPDE can not be arbitrarily set. The boundary conditions along τ_1 for the initial value of τ_2 depend on the initial response of the oscillator and the mapping function $\tau_1(\tau_2)$. A simple approach is to obtain the boundary conditions of WaMPDE from one period of the ODE result or from the interpolation of two periods as shown in Fig. 3.21. Those calculations can give inaccurate results (note that the mapping function $\tau_1(\tau_2)$ is not known *a priori*).

In this thesis we provide a new approach to obtain precise boundary conditions to improve the accuracy of the WaMPDE method. Fig. 3.22 shows the procedure of obtaining precise boundary

Reproduced with permission of the copyright owner. Further reproduction prohibited without permission.

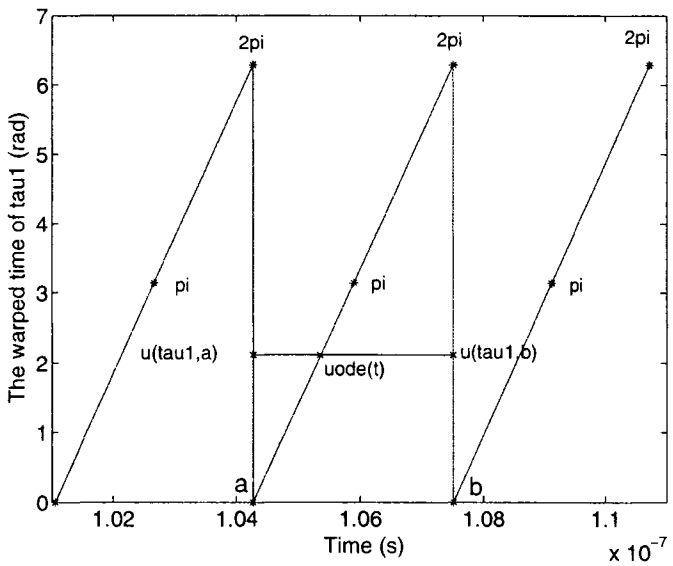

Figure 3.21: Relation between τ_1 and τ_2.

conditions.

The approach is summarized as follows. Firstly, run the ODE until some oscillations are produced. Secondly, filter one of the state variables from the ODE result to determine an initial guess of the local frequency. A band-pass filter is used to remove the DC component and harmonics higher than the fundamental frequency. A mapping between τ_1 and τ_2 (like the one shown in Fig. 3.21) is created according to the zero-crossing points in the filtered waveform since there is only the component of the fundamental frequency left. For example, the first zero-crossing point can be set to represent the phase zero; the second one represents the phase π; the third one represents the phase 2π, and so on. We use a straight line to connect these points in the (τ_1, τ_2) plane under the condition of the slowly changing frequency in circuits. This mapping continues for two or three periods. Linear or polynomial interpolation is used to calculate the state variables at two fixed values of τ_2 (a or b) corresponding to two vertical lines shown in Fig. 3.21: (τ_1, a) and (τ_1, b). Thirdly, build up the boundary condition equation:

$$u_{ode}(t) - [u(\tau_1, a) + \frac{u(\tau_1, b) - u(\tau_1, a)}{b - a}(t - a)] = 0. \tag{3.14}$$

Here $t \subset (a, b)$ and $\tau_2 = t$. After discretization, the vector corresponding to $u(\tau_1, b)$ is calculated using the WaMPDE method with $u(\tau_1, a)$ as boundary conditions. Eq. (3.12) and Eq. (3.14) form

Reproduced with permission of the copyright owner. Further reproduction prohibited without permission.

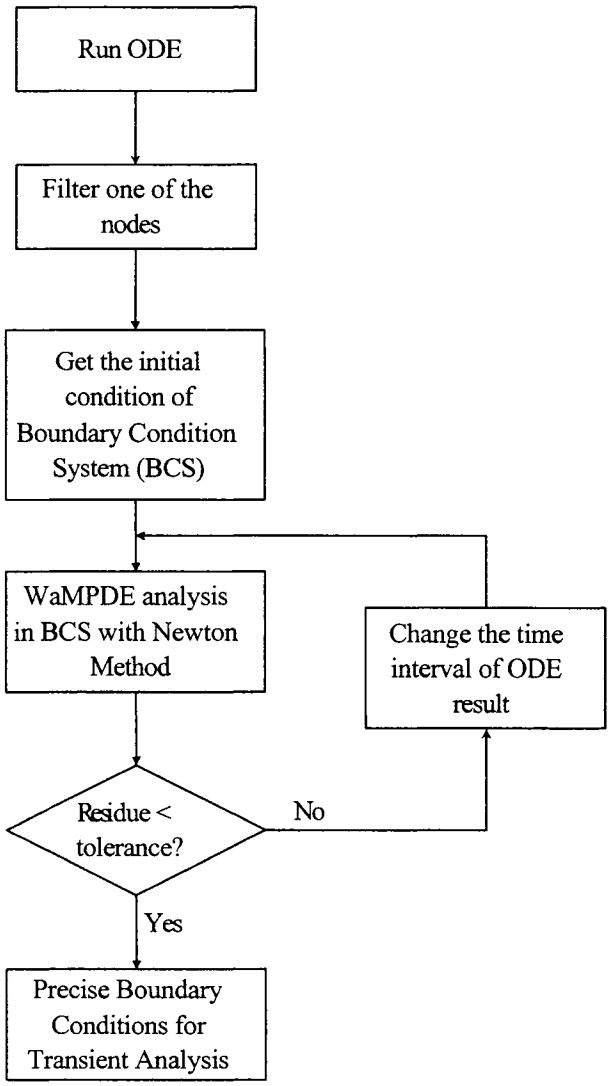

Figure 3.22: The procedure of getting precise boundary conditions.

Reproduced with permission of the copyright owner. Further reproduction prohibited without permission.

a system of equations that is solved with the Newton-Raphson method. The system is called Boundary Condition System (BCS). The unknowns are $u(\tau_1, a)$, $u(\tau_1, b)$ and the local frequency $\omega_0(0)$. The local frequency $\omega_0(0)$ is an additional unknown that must be calculated when τ_2 equals to WaMPDE starting time. The phase of one of the variables is then fixed to restore the number of unknowns to be equal to the number of equations. That is achieved by setting the imaginary part of one of the variables to be equal to reduce one unknown, such as:

$$\Im(U_n^1(a)) = \Im(U_n^1(b)).$$

The b value is automatically changed along with the local frequency in each Newton iteration. As a result the time interval of u_{ode} is adaptively adjusted to improve the accuracy of the final solution.

Fourthly, continue the transient analysis using the WaMPDE method starting with the boundary conditions found before. It is mentioned here that we can restore ODE from WaMPDE at any time. That is easy to implement since the mapping between the two time axes has already been obtained in Eq. (3.5). As shown in Eq. (3.12), the periodic solution in the warped time τ_1 is solved by the HB technique. The unknowns are changed to Fourier coefficients of each node voltage for each value of τ_2.

Since the focus is on the transient it is very important to estimate the local truncation error of each time step. The local truncation error is calculated by the difference between the result of numerical integration method and the extrapolation approximation,

$$\epsilon = max(U_n^k - U_n^{predict}).$$

ϵ is compared with some maximum allowable value $\epsilon_{\max}$ to evaluate the accuracy of the transient. The result will be rejected if ϵ is larger than $\epsilon_{\max}$. Adaptive time step control algorithm is used in order to minimize the number of time steps. The flow chart of adaptive time steps in transient analysis is shown in Fig. 3.23.

The time-step along τ_2 is adaptively changed by the local truncation error which predetermines the next optimum step size [20],

$$h_{new} = h_{old}(\frac{\epsilon_{\max}}{\epsilon})^{\frac{1}{m}},$$

where $m = 2$ in linear interpolation and $m = 3$ in quadratic interpolation. This results in

Reproduced with permission of the copyright owner. Further reproduction prohibited without permission.

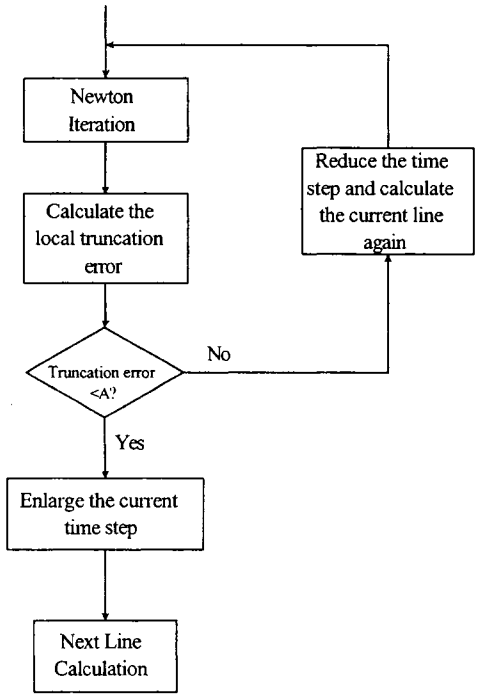

Figure 3.23: The flow chart of adaptive time steps.

WaMPDE expression with fewer time steps and therefore substantially reduces the computational cost and improves the accuracy in the transient simulation.

3.3 Simulation Result and Discussion

The transient analysis of a LC-tuned oscillator employing the proposed method is presented in this section. This example illustrates the main features of the proposed method: precise boundary conditions and faster computational time by using WaMPDE and an adaptive time step algorithm. Fig. 3.24 shows the schematic of a LC-tuned bipolar oscillator, which was one of the autonomous circuit examples in [10]. In this circuit $C_1 = C_2 = 33$ pF, $C_3 = 3.17$ pF, $C_c = 560$ pF, $L_1 = 100$ nH, $R_f = 680\ \Omega$, $Rb = 100$ kΩ, $R_c = 1.2$ kΩ and $V_{dd} = 10$ V.

In traditional time domain simulation, we solve the oscillator system with ordinary differential equations in time domain. In the proposed method with WaMPDE, we solve the oscillator system in multiple time domain with Newton-Raphson method. In order to describe the oscillator with the nodal equations, we replace the transistor part with the model shown in Fig. 3.25, the

Reproduced with permission of the copyright owner. Further reproduction prohibited without permission.

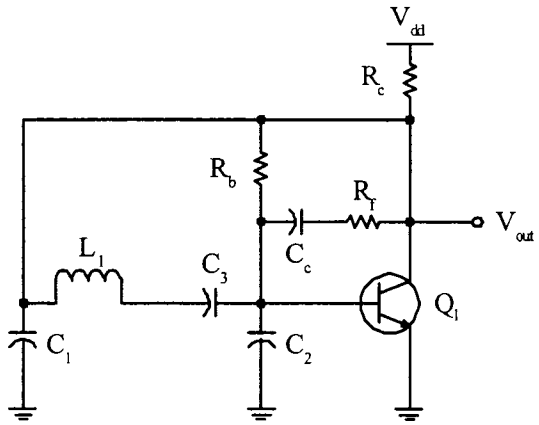

Figure 3.24: The schematic of the LC-tuned bipolar oscillator.

inductor with a capacitor gyrator model shown in Fig. 3.26, and the Thevenin source with a Norton source in Fig. 3.27. Then we substitute Fig. 3.24 with those models and define the node numbers in Fig. 3.28.

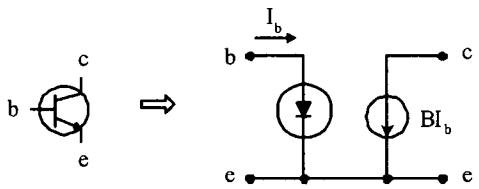

Figure 3.25: Large signal model of the transistor.

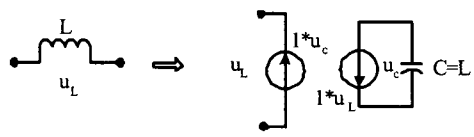

Figure 3.26: Gyrator model of the inductor.

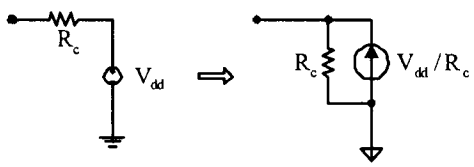

Figure 3.27: Model of the DC source.

Then we write nodal equations for all the nodes in the circuit followed by Eq. (3.10)

$$Gu(t) + C\frac{du(t)}{dt} + I(u(t)) = S(t),$$

Reproduced with permission of the copyright owner. Further reproduction prohibited without permission.

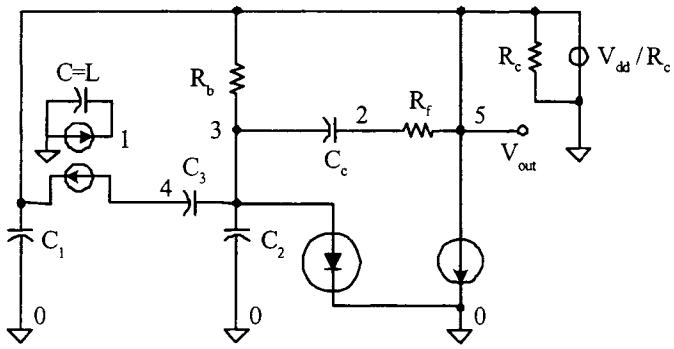

Figure 3.28: The equivalent circuit of the LC-tuned bipolar oscillator.

with each matrix defined by:

$$G = \begin{bmatrix} 0 & 0 & 0 & 1 & -1 \\ 0 & G_f & 0 & 0 & -G_f \\ 0 & 0 & G_b & 0 & -G_b \\ -1 & 0 & 0 & 0 & 0 \\ 1 & -G_f & -G_b & 0 & G_c + G_f + G_b \end{bmatrix} \quad C = \begin{bmatrix} L & 0 & 0 & 0 & 0 \\ 0 & C_c & -C_c & 0 & 0 \\ 0 & -C_c & C_c + C_2 + C_3 & -C_3 & 0 \\ 0 & 0 & -C_3 & C_3 & 0 \\ 0 & 0 & 0 & 0 & C_1 \end{bmatrix}$$

$$I(u) = \begin{bmatrix} 0 \\ 0 \\ I_b \\ 0 \\ I_c \end{bmatrix} \quad S = \begin{bmatrix} 0 \\ 0 \\ 0 \\ 0 \\ \frac{V_{dd}}{R_c} \end{bmatrix}$$

with $G_f = \frac{1}{R_f}$, $G_b = \frac{1}{R_b}$, $G_c = \frac{1}{R_c}$, $I_b = \frac{I_s}{BF}(e^{\frac{V_{BE}}{V_T}} - 1)$ and $I_c = BF \times I_b$. In these equations, $I_s(0.01pA)$, $BF(100)$,and $V_T(26mV)$ are DC parameters of the bipolar model. I_s represents the saturation current. BF is the forward beta and V_T designates the thermal voltage. The DC bias points of this oscillator are calculated as follows.

$$\begin{cases} U_1 = 0V \\ U_2 = 4.9V \\ U_3 = 0.7V \\ U_4 = 4.9V \\ U_5 = 4.9V \end{cases}.$$

Reproduced with permission of the copyright owner. Further reproduction prohibited without permission.

This oscillator exhibits a very slow initial transient. The amplitude of the output voltage slowly goes up and the oscillator takes long time to reach steady-state. Part of the transient using the regular time domain simulation is presented in Fig. 3.29, which takes 894 seconds in a $10\mu s$ time intervel. In this section, we solve the transient in multiple time domain, trying to improve the simulation accuracy and speed. The boundary condition of each node is solved by the proposed method. In this case, the inductor current was chosen to be the reference variable to decide the WaMPDE beginning time and the initial local frequency. The ODE result of this selected node is filtered in this case by a Butterworth filter for extracting zero-crossing points. A mapping of multiple times is also established by zero-crossing points (Fig. 3.21). Since the local frequency varies very slowly, we assume the straight line between each pair of these zero-crossing points. The proposed method also provides a robust route to switch WaMPDE and ODE simulation freely. Two different WaMPDE starting time are chosen to demonstrate the new approach in the following part.

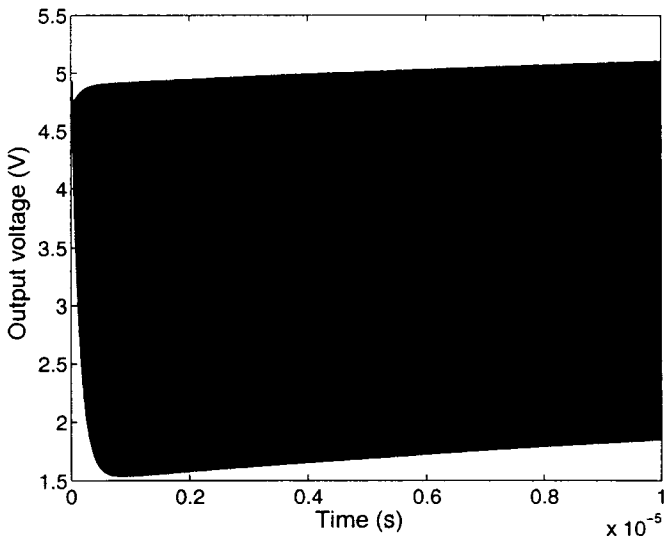

Figure 3.29: Transient response.

Case 1

Firstly, the ODE simulation is switched to the WaMPDE simulation at $0.1\mu s$ when the oscillation has already built up in regular time domain simulation. The initial number of the harmonics

Reproduced with permission of the copyright owner. Further reproduction prohibited without permission.

is defined to be 14 and the simulation stop time is set to be 1.05 ms according to the steady-state simulation result. Only 5 Newton iterations are needed at the beginning to get precise initial conditions which achieve a tolerance of 10^{-12}. The transient simulation simply starts from the specified initial conditions to achieve the steady-state stage. Adaptive HB increases or reduces the harmonic number in each value of τ_2 just as needed for each variable.The multi-time expression of the output voltage as a function of τ_1 and τ_2 is shown in Fig. 3.30.

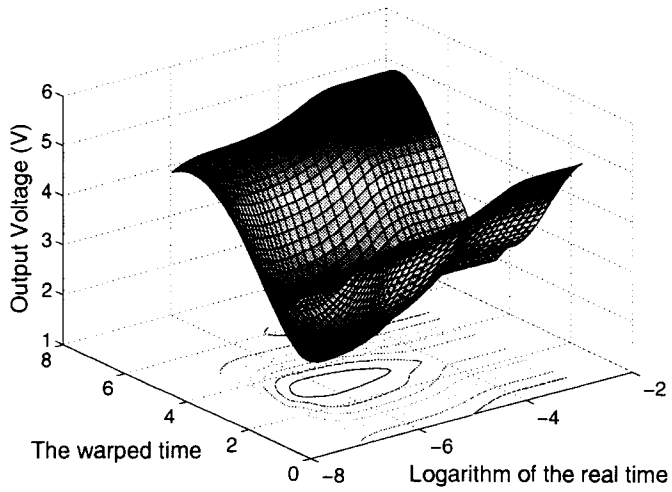

Figure 3.30: Bi-dimensional representation of the output voltage.

The oscillation and the transient variation are decoupled in two different time scales. The envelope transient slowly goes up and finally becomes constant along the τ_2 time axis which is consistent with Fig. 3.29, but the computational time is 45 seconds in a 1.19 ms time intervel, orders of magnitude faster than traditional transient analysis. The adaptive time step size is increased along the τ_2 time axis and presented in Fig. 3.31. The oscillator frequency determined by the warped function $\omega_0(\tau_2)$ is also represented in Fig. 3.31. It shows that the local frequency is different only at the beginning of the simulation and it will become constant when the oscillator achieves to the steady-state stage.

Since it is not difficult to transform from multi-time WaMPDE simulation to single time WaMPDE result, we provide the comparison of the waveforms obtained using the WaMPDE with the proposed boundary conditions and a regular time domain simulation. Very good agreement

Reproduced with permission of the copyright owner. Further reproduction prohibited without permission.

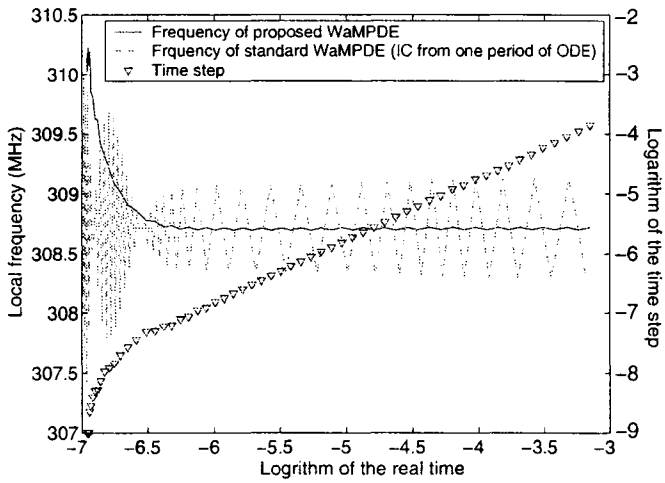

Figure 3.31: Adaptive time step and the fundamental frequency.

has been achieved shown in Fig. 3.32. The relative amplitude error and absolute phase error of the first harmonic in WaMPDE and ODE simulations are presented in Fig. 3.33. Both the amplitude error and the phase error are very small. This indicates that the two waveforms match each other very well and the proposed method is successful in detecting the transient behavior.

We mentioned in the previous section that some simplified methods are considered at the beginning of this work to obtain the boundary conditions. Here the results of WaMPDE simulations using the boundary conditions obtained from those simple approaches are shown in Fig. 3.31 and Fig. 3.34. The local frequency presents drastic oscillations and the agreement of the waveforms is not as good as the proposed WaMPDE, in this case due to a phase shift created by inaccurate boundary conditions. The initial local frequency is 310.141 MHz, which is a little bit larger than the value given by the ODE simulation. After performing many simulations it seems that a spike at the beginning of the WaMPDE simulation is inevitable but it does not influence the final solution since the agreement in all other variables is still very good.

Case 2

Secondly we switch the ODE simulation to the WaMPDE simulation at a time of $0.02\mu s$. Since the oscillations are just building up and the regular time domain simulation is in a fast variation, it is very difficult to obtain good boundary conditions in simplified methods, such as one period of

Reproduced with permission of the copyright owner. Further reproduction prohibited without permission.

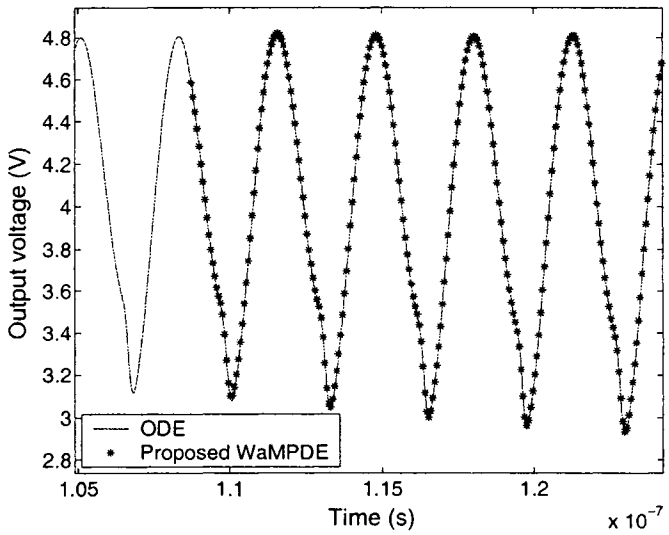

Figure 3.32: Proposed WaMPDE solution compared to ODE solution.

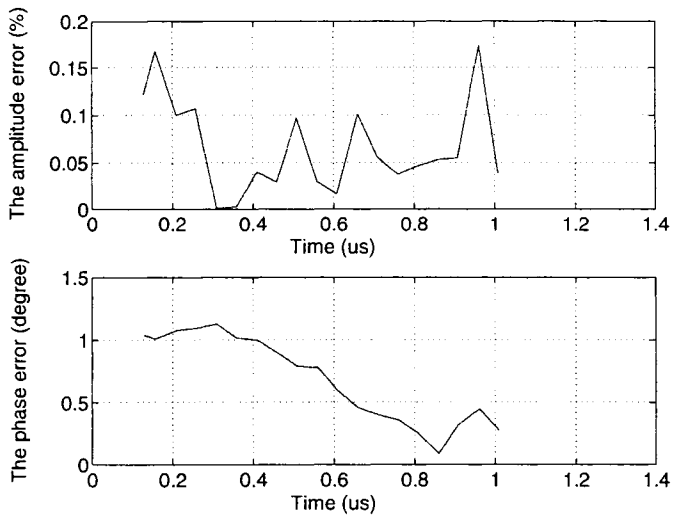

Figure 3.33: Relative error in the magnitude of the first harmonic.

Reproduced with permission of the copyright owner. Further reproduction prohibited without permission.

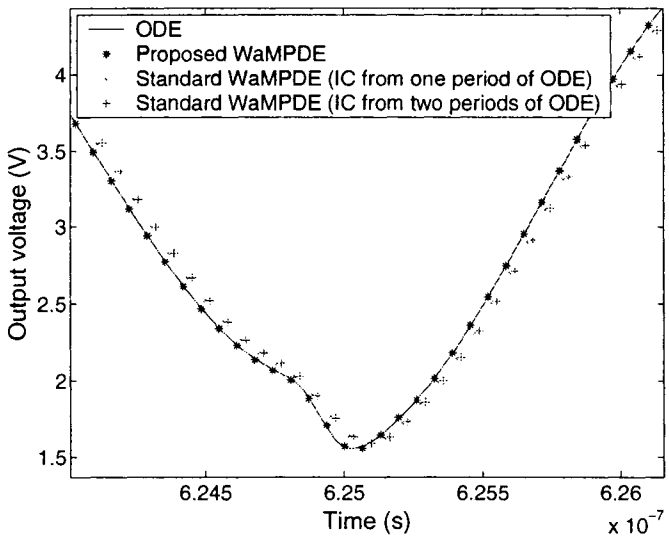

Figure 3.34: WaMPDE solutions compared to ODE solution.

ODE result or the interpolation of two ODE periods, but the proposed method still can find the boundary conditions of the WaMPDE with some accuracy (compared with the previous part). The bi-dimensional plot of the output voltage as a function of τ_1 and τ_2 is shown in Fig. 3.35. The computational time is still much faster than traditional transient analysis.

Fig. 3.36 shows the oscillator frequency obtained from both the proposed method and the simplified method, together with the adaptive time step along the τ_2 time axis. The oscillator frequency obtained from the new method is much smoother and quickly converges to the correct value though the initial value is a little bit larger.

Fig. 3.37 shows the comparison of WaMPDE with proposed boundary conditions and a traditional time domain simulation. The error function of the first harmonic in WaMPDE and ODE simulations is presented in Fig. 3.38. For the amplitude error, we can see that at the beginning of the part, there is a little bit large difference (less than 4%) since the oscillation is just built up. For the phase error, it also not as good as the performance in case 1. Though the match of two waveforms is not as good as the previous analysis due to the fast variation at the beginning of the ODE result, the proposed method still performs much better compared with the WaMPDE simulation with boundary conditions from the simple approach in Fig. 3.39 and the result is almost consistent with the time domain simulation.

Reproduced with permission of the copyright owner. Further reproduction prohibited without permission.

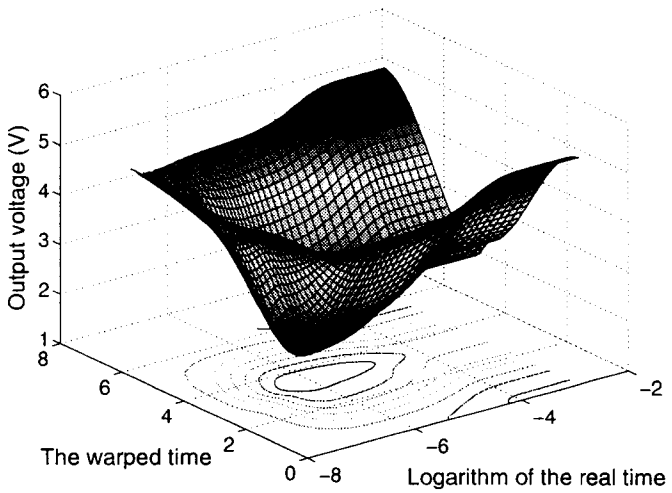

Figure 3.35: Bi-dimensional representation of output voltage.

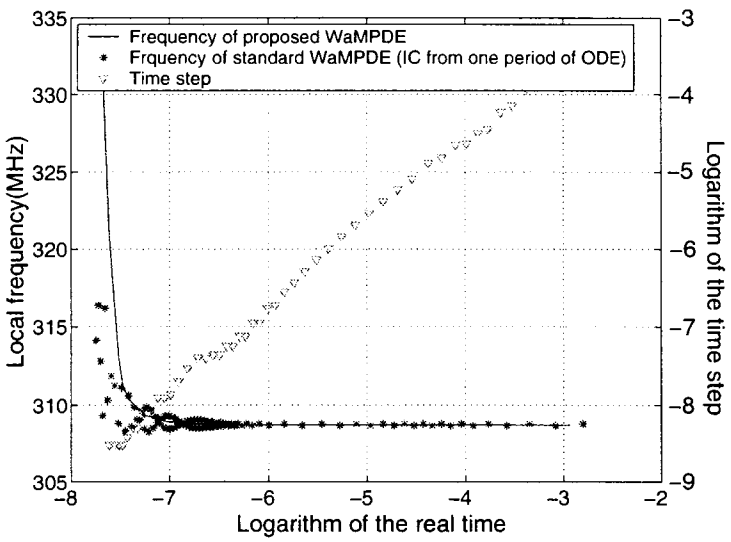

Figure 3.36: Adaptive time step and the fundamental frequency.

Reproduced with permission of the copyright owner. Further reproduction prohibited without permission.

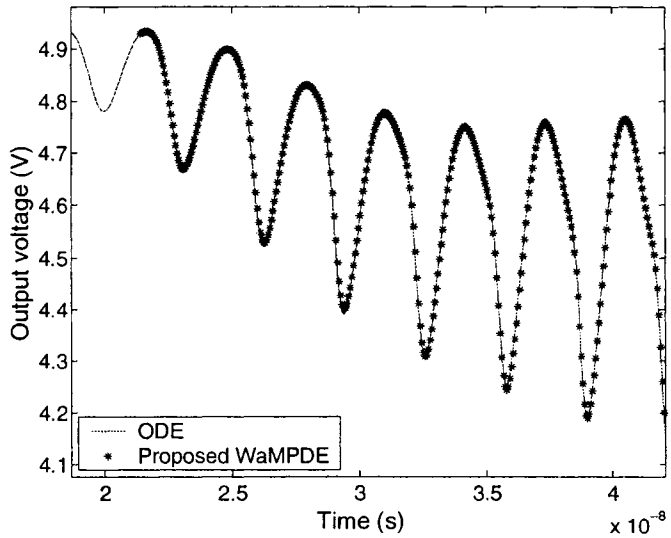

Figure 3.37: Proposed WaMPDE solution compared to ODE solution.

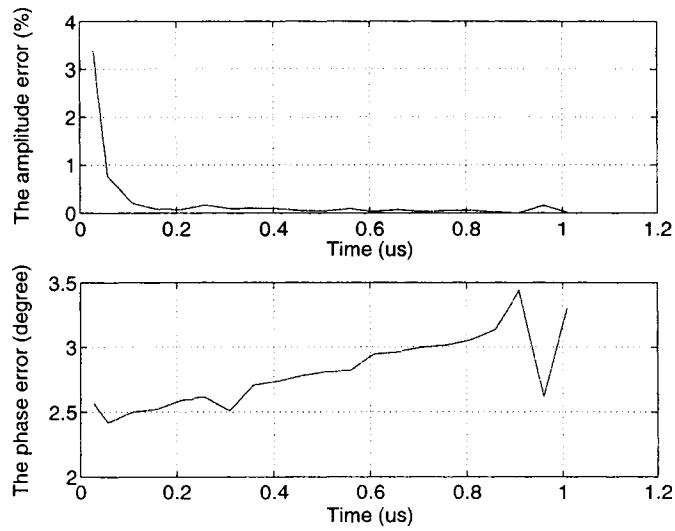

Figure 3.38: Relative error in the magnitude of the first harmonic.

Reproduced with permission of the copyright owner. Further reproduction prohibited without permission.

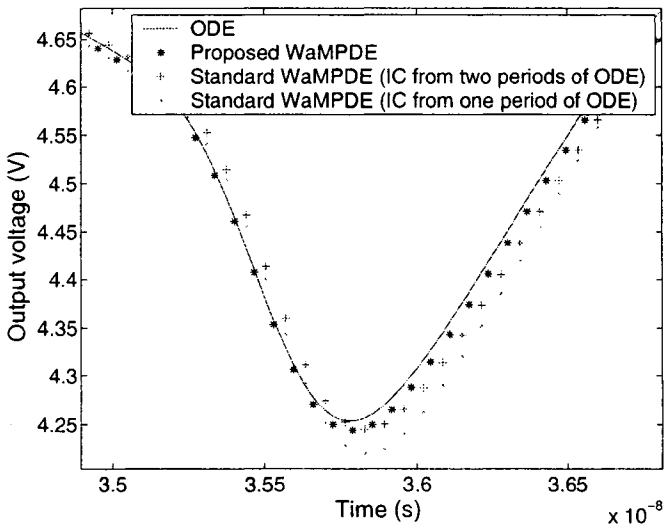

Figure 3.39: WaMPDE solutions compared to ODE solution.

The simulation of the LC-tuned bipolar oscillator demonstrates the efficiency of the proposed method dealing with transient analysis in oscillators. Boundary condition system improves the accuracy of the WaMPDE simulation in transient analysis.

Reproduced with permission of the copyright owner. Further reproduction prohibited without permission.

Chapter 4

Steady-state Analysis

4.1 Introduction

As mentioned in Chapter 1, regular HB is very sensitive to the initial guess. In this chapter a robust and fast approach for capturing the steady-state response of oscillators in frequency domain is presented. This approach based on a new adaptive HB technique which is derived from WaMPDE. Unlike previous implementations mentioned in Chapter 2, the number of harmonics used in the calculation is always very close to the minimum required for the desired accuracy. The proposed method is developed in the next section. We also presents a case study of the same oscillator mentioned in Chapter 3 to demonstrate the new approach.

4.2 The Proposed Method

The main idea of the proposed method is to use WaMPDE to find a good initial guess for regular HB analysis. There are two steps. First, we reach a point in τ_2 close to the steady-state in the minimum possible number of Newton iterations. It is assumed that the solution is very close to the steady-state when the local frequency function has become constant and the difference between two periodic solutions along τ_1 becomes small. At this point the envelope transient is stopped and we begin the second step: a regular oscillator HB analysis with the last multivariable solution as the initial guess. Since this initial guess is very close to the steady-state only a few additional Newton iterations are needed.

The simulation is started with an initial condition equal to the DC bias point. An excitation

Reproduced with permission of the copyright owner. Further reproduction prohibited without permission.

current,

$$i_S(\tau_1, \tau_2) = \begin{cases} I_0 cos(\tau_1) & \text{if } \tau_2 \leq t_a \\ 0 & \text{otherwise} \end{cases},$$

is injected from the ground node into one of the nodes where oscillations are expected. Here, I_0 is a small real number (normally a few μA) and t_a is set equal to the initial time-step size along τ_2 (h). The purpose of i_S is to start oscillations by moving the system away from the equilibrium point. The system will then naturally tend to reach the desired oscillatory steady-state. The key of the work presented here is first to reach a point in τ_2 close to the steady state in the minimum possible number of Newton iterations and then use the state at that point as the initial guess of a regular autonomous HB analysis. Since the focus is on the steady-state it is not necessary to calculate the transient evolution with great precision as long as it converges close to the actual steady-state of the circuit.

In order to minimize the number of iterations required to get close to the steady-state the following considerations are taken. First, the Backward Euler Rule is used. It is known that this integration method introduces numerical damping [21]. The effect of this is that any oscillations along the τ_2 (not along the τ_1 scale) scale are damped [21] and this is beneficial since it allows the use of a longer time step. Second, the tolerance of the Newton method is adaptively controlled during the transient evolution to prevent it from being unnecessarily small. This has the effect of reducing the number of Newton iterations that are necessary at each value of τ_2. The Newton tolerance (tol) is set to

$$tol = \max\left\{0.1\%\ U_{max}^k, 10^{-7}\right\},$$

where U_{max}^k is the amplitude of the largest oscillation in the circuit at the previous value of τ_2. Third, an adaptive time step algorithm is employed. The algorithm chooses the size of the time step along τ_2 (h) based on the number of Newton iterations required to achieve the desired tolerance. Since we focus on steady-state analysis, no truncation error checking is necessary in this case and so the number of necessary time steps is reduced. The flow chart of adaptive time steps is shown in Fig. 4.1.

Here, A represents the enlarge factor of the time step, such as 1.5; a and b are threshold values to either enlarge or reduce the current time step. If the number of Newton iterations is larger than a, such as 10, we reduce the time step; if it is smaller than b, such as 4, we enlarge

Reproduced with permission of the copyright owner. Further reproduction prohibited without permission.

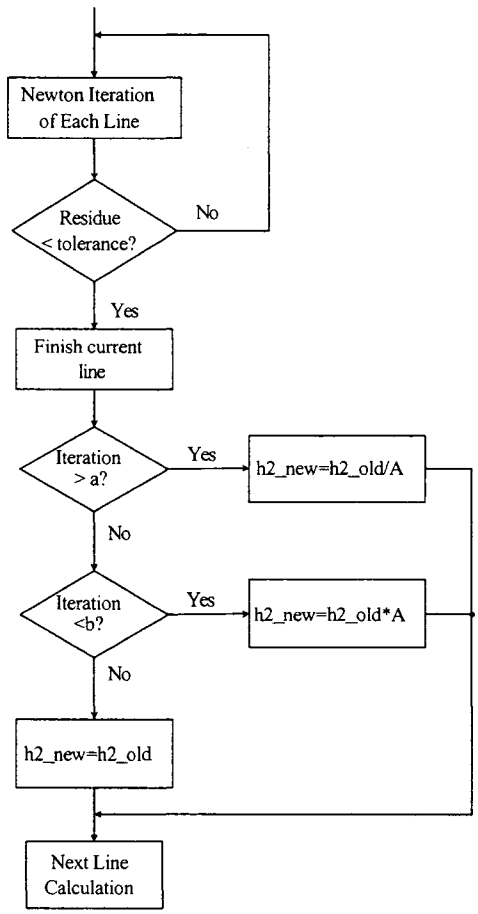

Figure 4.1: The flow chart of adaptive time steps.

the time step. Otherwise we keep it unchanged for the next line calculation.

It is assumed that the solution is very close to the steady state when the local frequency function has become constant and the difference between two periodic solutions along τ_2 becomes small,

$$\left\| \frac{U_n(\tau_2 + h) - U_n(\tau_2)}{U_n(\tau_2 + h)} \right\| < \epsilon_1,$$

where ϵ_1 is a small relative tolerance. If $U_n(\tau_2 + h)$ is very close to zero an absolute tolerance ϵ_2 is used:

$$\|U_n(\tau_2 + h) - U_n(\tau_2)\| < \epsilon_2.$$

At this point the envelope transient is stopped and a regular oscillator Harmonic balance

Reproduced with permission of the copyright owner. Further reproduction prohibited without permission.

analysis is started using the last solution along τ_2 as the initial guess. A small tolerance is used this time to achieve the desired accuracy (typically on the order of 10^{-9}). Note that the regular oscillator HB analysis is obtained by setting all derivatives with respect to τ_2 to be zero in Eq. (3.12). There is no need for probes [3, 4] or any other special provisions since the initial guess is very close to the steady-state solution. Normally only a few additional Newton iterations are needed.

Another provision to improve the efficiency of the simulation is to adaptively control the number of harmonics for each state variable u_n independently. At $\tau_2 = 0$, only a few harmonics have to be considered because the oscillations are small and sinusoidal. In our proposed method, only three harmonics (five unknowns) are considered initially. At the end of the calculation for each value of τ_2, the values of the last two harmonics are considered. If they are greater or smaller than some threshold values then the number of harmonics for that variable is increased or decreased by one, otherwise it is left unchanged for the next time step. The flow chart of the adaptive harmonic balance is shown in Fig. 4.2. A_i and B_i represent the magnitude of the last two harmonics for the i_{th} state variable.

One advantage of this approach is that the number of harmonics is increased just as needed, *i.e.* there is no need to perform an initial calculation with many harmonics to later decide the ones that must be removed. It is then important to start with a small oscillation value at $\tau_2 = 0$. Each row of Eq. (3.12) (nodal equation at one frequency) is considered as a number of frequencies equal to the number of harmonics of the corresponding nodal voltage. Each nodal equation is adaptively adjusted by the harmonic number in each corresponding node. In this way the number of equations is always kept equal to the number of unknowns and the computational effort is largely reduced.

4.3 Simulation Result and Discussion

We still use the case discussed in Chapter 3 to demonstrate the proposed method. The transient simulation using the regular time domain simulation has been already shown in Fig. 3.29. Here we use WaMPDE to solve the steady-state response. The simulation begins with DC bias points. The excitation current (i_S) was injected to the base node and I_0 was set to be $10\mu A$. Only a few time steps along τ_2 are necessary since the oscillations and the transient variations are decoupled in two different time scales. The stop time along τ_2 is 1.0326 ms. The bi-dimensional

Reproduced with permission of the copyright owner. Further reproduction prohibited without permission.

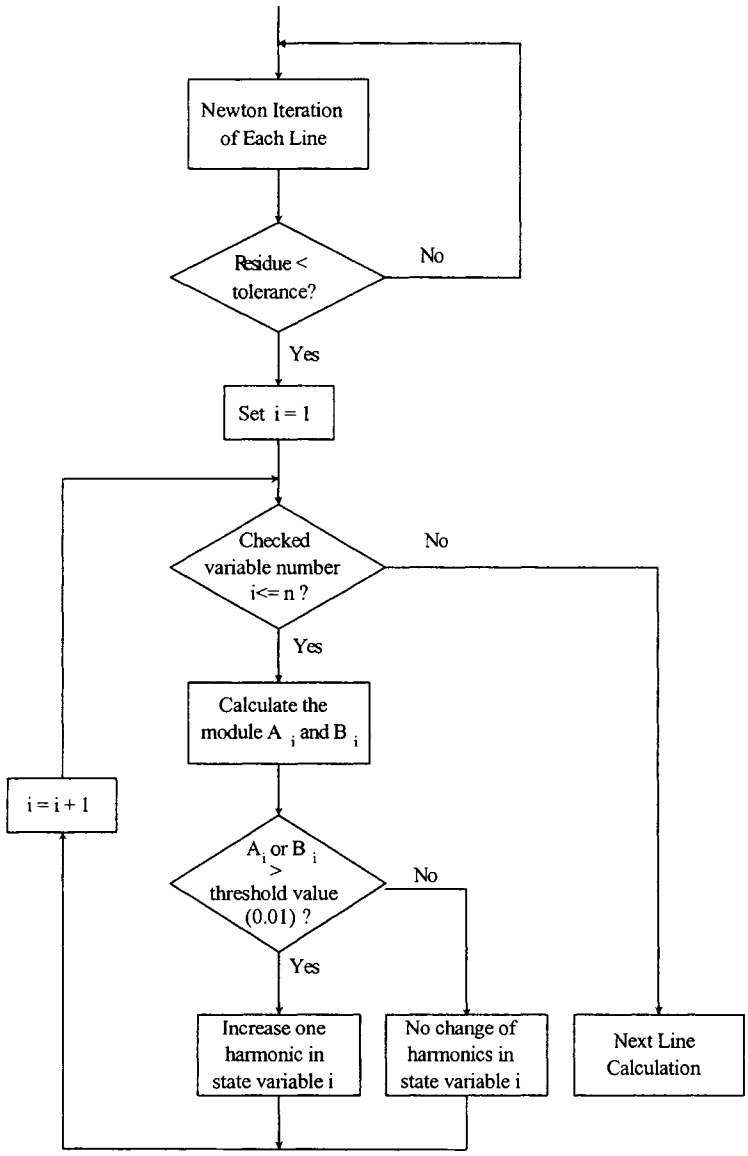

Figure 4.2: The flow chart of the adaptive harmonic balance.

Reproduced with permission of the copyright owner. Further reproduction prohibited without permission.

plot of the output voltage as a function of τ_1 and τ_2 is shown in Fig. 4.3. A logarithm scale was used along τ_2 to improve the visibility of the samples along that axis. Note that the initial time step is chosen very short but the adaptive algorithm quickly increases its size and thus only a few points are necessary to cover the entire simulation interval.

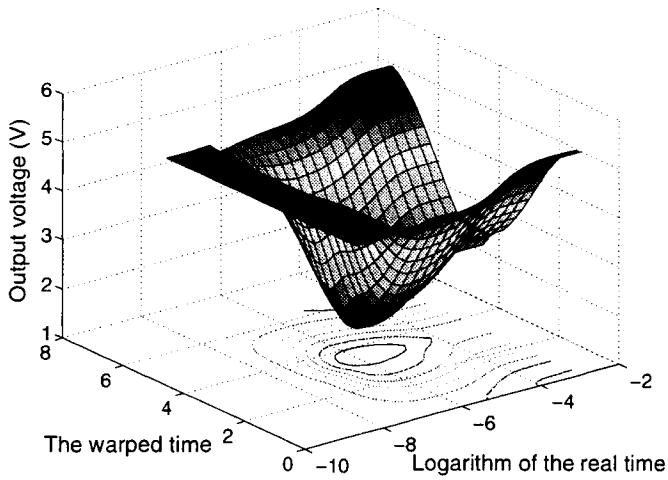

Figure 4.3: Bi-dimensional representation of the output voltage.

The adaptive control of the time step along τ_2 keeps the number of Newton iterations small for each value of τ_2 (typically 2–4, see Fig. 4.5). The oscillator frequency determined by the warped function $\omega_0(\tau_2)$ shown in Fig. 4.4 is 308.87 MHz. Fig. 4.4 demonstrates the robustness of the proposed method. Different initial frequencies far away from the solution quickly converge to the correct value and become constant in the asymptotic steady-state stage.

Fig. 4.5 shows the Jacobian matrix size and the number of Newton iterations at each time step (line number). It can be observed that few iterations are necessary at each time step. As mentioned before this is due to the adaptive time step and adaptive tolerance control algorithms. The Jacobian matrix size increases as the number of harmonics increases. If a fixed number of harmonics is considered the size of the Jacobian matrix is 116×116. It is obvious that the new approach drastically reduces the size of the Jacobian matrix for small values of τ_2 and saves considerable computational effort. The use of variable number of harmonics in this case increases the computational speed by a factor of six. It is mentioned here that we use the increment of

Reproduced with permission of the copyright owner. Further reproduction prohibited without permission.

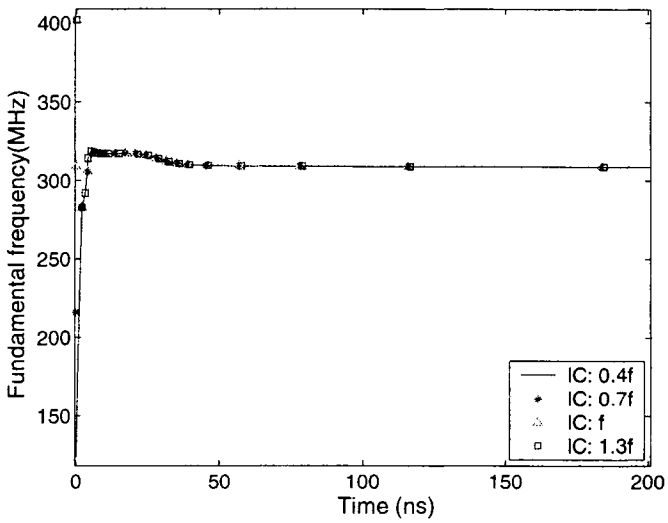

Figure 4.4: Fundamental frequency as a function of τ_2.

10^{-6} in Newton Method to calculate the Jacobian Matrix. If the increment is reduced to 10^{-7} or 10^{-9}, the accurate of Jacobian Matrix will improve 0.5% or 2.28%. Though the Jacobian Matrix contains some errors with 10^{-6}, the answer is still acceptable since the final multi-time solution converges to the correct value.

The adaptive time step and the adaptive tolerance were shown in Fig. 4.6. They are all increased along the τ_2 time axis. The use of the adaptive tolerance in this case saves the computational time by a factor of two. The tolerance of the regular HB analysis following the multi-time simulation was set to be 10^{-10}. Only 3 Newton iterations are necessary to obtain the steady-state solution with the initial guess provided by the multi-time simulation.

In Fig. 4.7 the steady state is shown together with the final multi-time result. The match is so close that it is hard to tell them apart, which demonstrates the adaptive HB is quite efficient to detect the steady-state behavior.

The simulation of the LC-tuned bipolar oscillator demonstrates the efficiency of the proposed method dealing with the steady-state analysis in oscillators. WaMPDE with adaptive scheme largely saves computational effort and both the oscillation frequency and the steady-state solution are obtained in a fast and accurate way.

Reproduced with permission of the copyright owner. Further reproduction prohibited without permission.

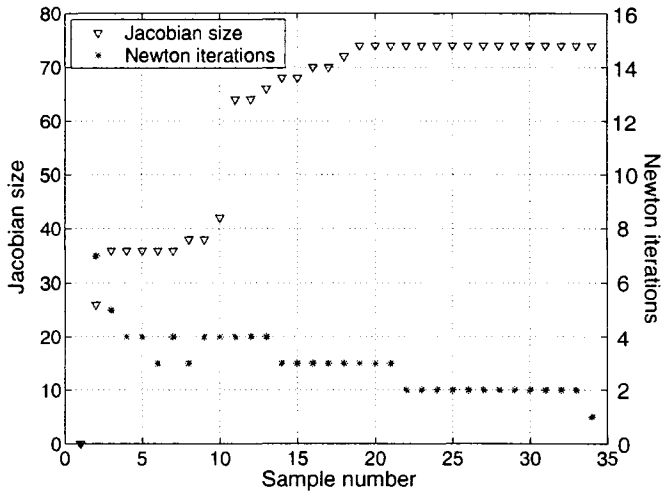

Figure 4.5: Jacobian size and number of Newton iterations.

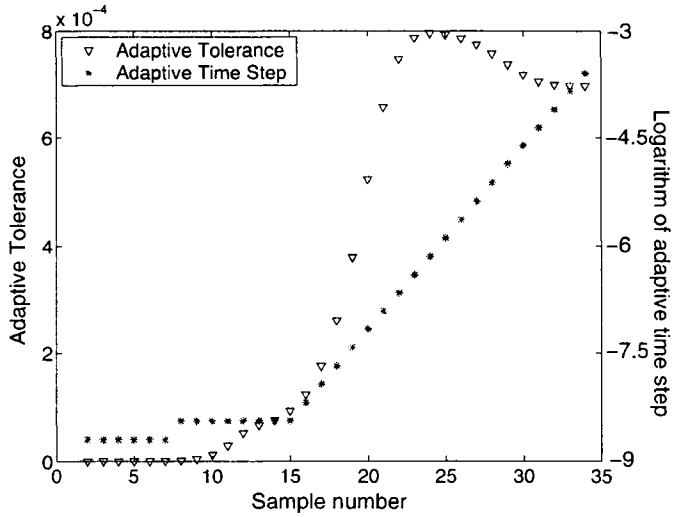

Figure 4.6: Adaptive tolerance and adaptive time step.

Reproduced with permission of the copyright owner. Further reproduction prohibited without permission.

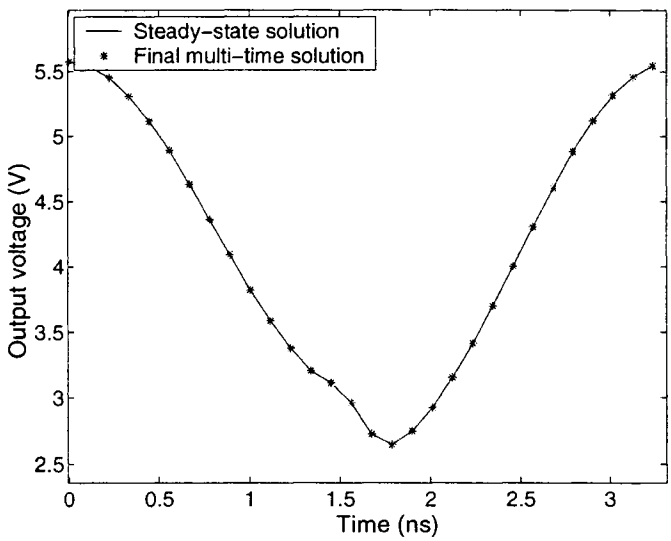

Figure 4.7: Steady-state solution compared to final multi-time solution.

Reproduced with permission of the copyright owner. Further reproduction prohibited without permission.

Chapter 5

Simulation and Experimental Results

5.1 Introduction

The objective of simulations is to show the efficiency and robustness of each proposed method. Two different type of oscillators: Colpitts oscillator and voltage controlled oscillator (VCO) are described and analyzed both in the steady-state and the transient with proposed methods in Chapter 3 and Chapter 4. In each oscillator, we firstly provide the regular time domain simulation, and then present the WaMPDE simulation result. Finally we compare both simulation results and illustrate the huge advantage of proposed methods. The softwares used in this chapter are Matlab and SPICE.

In the experiment part, we details the physical setup and testing of a VCO circuit which is constructed on a printed circuit board. The objective of the experiment is to verify the WaMPDE simulation results. The key performances for a VCO are its tuning range and output. The performance data for tuning range is presented followed by experimental results of the output voltage. Comparison with simulation results is also provided at the end of this chapter.

5.2 Circuit 1: Colpitts Oscillator

The analysis of a Colpitts oscillator which is taken from [22], is provided in this section. This oscillator uses a capacitive voltage divider in the LC tank circuit. In this circuit shown in Fig. 5.1: $C_1 = C_2 = 2$ pF, $C_c = 400$ pF, $C_e = 100$ pF, $L_1 = 1$ μH, $R_1 = 8$ kΩ, $R_2 = 2$ kΩ, $R_c = 2.4$ kΩ, $R_e = 1.3$ kΩ, $V_{cc} = 11$ V, $BF = 100$, and $BR = 1$. The voltage applying to C_2 is the feedback voltage. C_c and C_E are large bypass capacitors. R_1, R_2, R_C and R_E set the DC bias current in the transistor.

Reproduced with permission of the copyright owner. Further reproduction prohibited without permission.

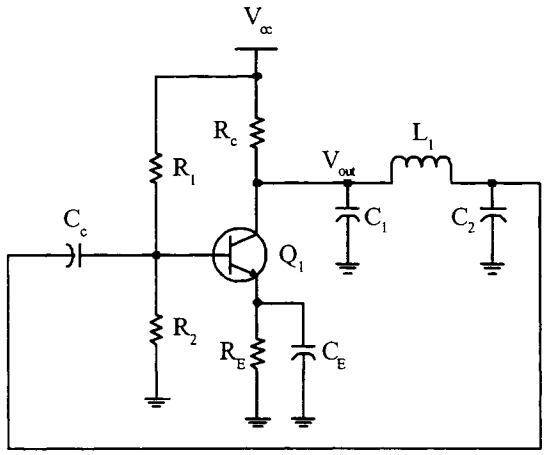

Figure 5.1: The schematic of the Colpitts oscillator.

We consider the Ebers-Moll transistor model shown in Fig. 5.2 to model the saturation.

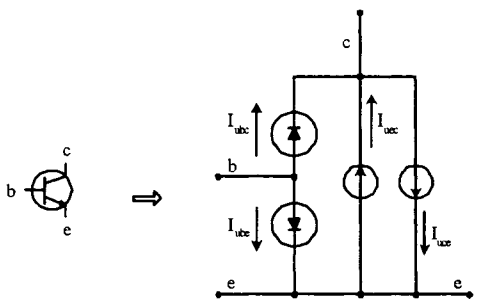

Figure 5.2: The Ebers-Moll model of the bipolar transistor.

The Ebers-Moll model contains two diodes and two current sources which can be used in the forward active mode of operation, reverse active mode, saturation and cut-off. The diode currents and the source currents are represented by

$$\begin{cases} I_{ubc} = \frac{I_s}{BR}(e^{\frac{V_{BC}}{V_T}} - 1) \\ I_{ube} = \frac{I_s}{BF}(e^{\frac{V_{BE}}{V_T}} - 1) \\ I_{uec} = BR \times I_{ubc} \\ I_{uce} = BF \times I_{ube} \end{cases}$$

with saturation current $I_s = 0.01$ pA and thermal voltage $V_T = 26$ mA. Then we substitute those models in Fig. 5.1 and define the node numbers in Fig. 5.3.

Reproduced with permission of the copyright owner. Further reproduction prohibited without permission.

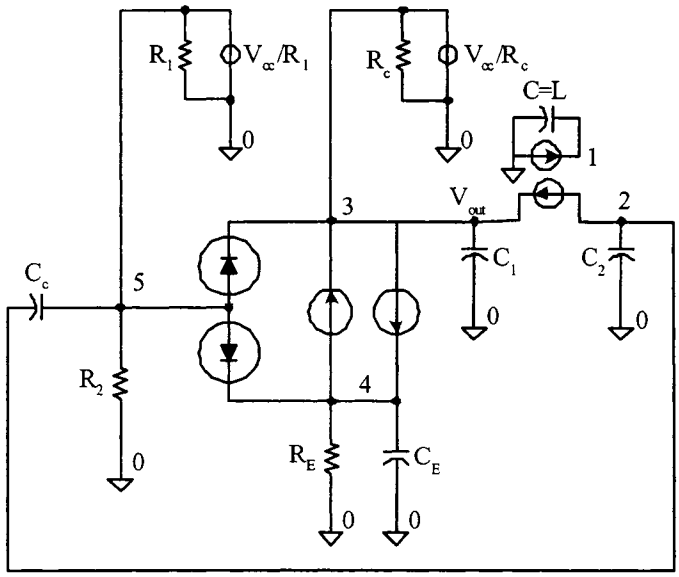

Figure 5.3: The equivalent circuit of the Colpitts bipolar oscillator.

The DC bias points are calculated as:

$$\begin{cases} U_1 = 0V \\ U_2 = 8.4V \\ U_3 = 8.47V \\ U_4 = 1.4V \\ U_5 = 2.2V \end{cases}.$$

5.2.1 Steady-state Analysis

Compared with the LC-tuned bipolar oscillator in the previous chapters, this Colpitts oscillator exhibits an extremely long initial transient (about 0.07 s) compared with the oscillation period to enter the steady-state stage (see in Fig. 5.4). The computational time is 57 seconds in a simulation interval of 0.1ms. Furthermore, some nodes in the circuit, such as the emitter port, present very strong nonlinear behavior, resulting in a large number of harmonics in regular oscillator HB analysis (see in Fig. 5.5).

Adaptive HB in WaMPDE is employed to adaptively control the number of harmonics of each node to achieve the desired tolerance, providing a fast and robust way to analyze this circuit. The adaptive time step control algorithm used in the τ_2 time axis gives another possibility to speed

Reproduced with permission of the copyright owner. Further reproduction prohibited without permission.

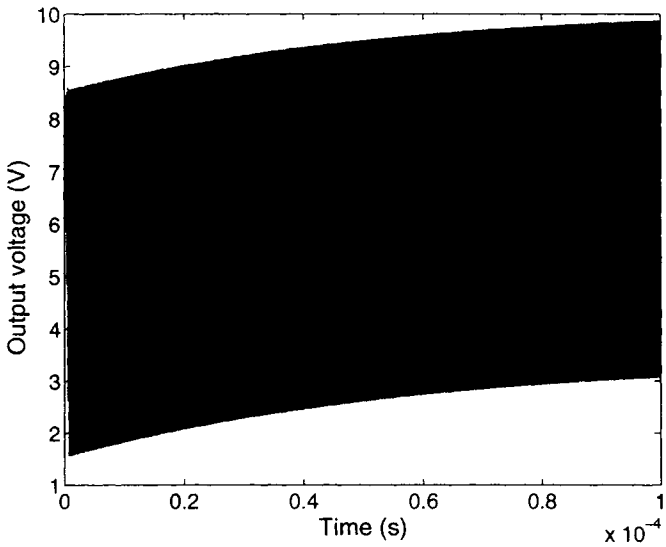

Figure 5.4: Transient response.

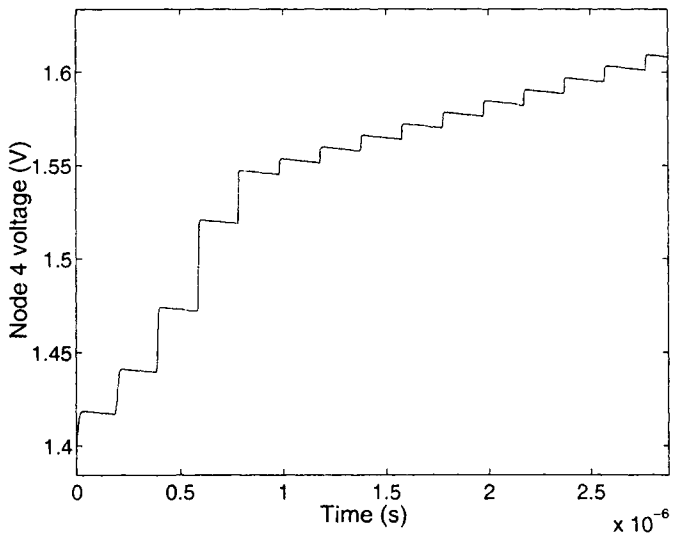

Figure 5.5: The transient of a strong nonlinear node.

Reproduced with permission of the copyright owner. Further reproduction prohibited without permission.

up the simulation. As a result only a few points are needed to cover the entire simulation interval though the initial time step is chosen very short. We begin the steady-state simulation with the DC bias point. A small excitation current was injected into the collector port. The oscillation begins with 3 harmonics and the maximum number of harmonics is 30 compared with minimum 6 at the end of the simulation. The bi-dimensional plot of the output voltage as a function of τ_1 and τ_2 is shown in Fig. 5.6. In this case the computational speed is order of magnitude faster by using the variable number of harmonics. In a 1.5 GHz computer the simulation time is 52 s, saving considerable computational effort.

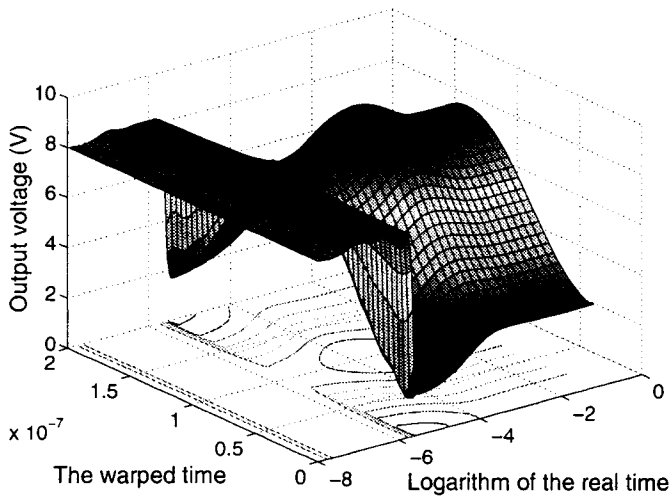

Figure 5.6: Bi-dimensional representation of output voltage.

The local frequency f determined by the warped function $\omega_0(\tau_2)$ is 5.04 MHz, part of which was shown in Fig. 5.7. f represents the local frequency of the oscillator. Like the previous case, the result of oscillator frequency also demonstrates the robustness of the proposed method. Different initial frequencies quickly converge to the correct value and become constant in the asymptotic steady-state stage.

In Fig. 5.8 the steady state is shown together with the final multi-time result. The result is quite good, which demonstrates the efficiency of the proposed steady-state method. Fig. 5.9 shows the Jacobian matrix size and the number of Newton iterations at each time step (line number). It can be observed that few iterations are necessary at each time step. The Jacobian

Reproduced with permission of the copyright owner. Further reproduction prohibited without permission.

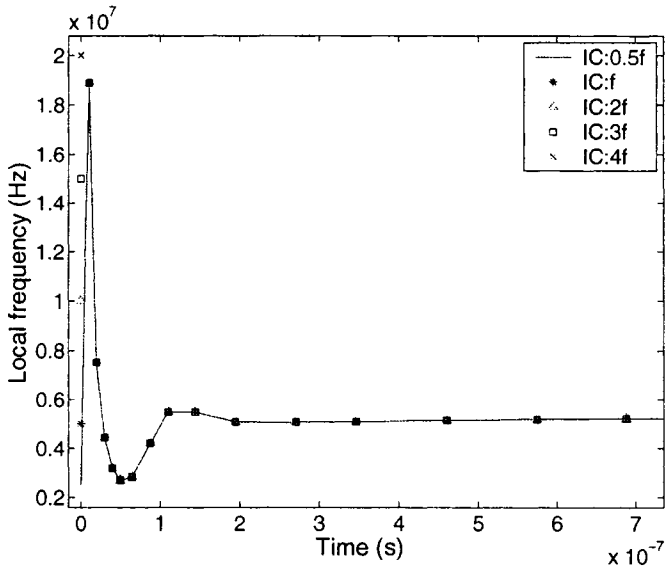

Figure 5.7: Fundamental frequency as a function of τ_2.

matrix size increases just as the number of harmonics increases.

5.2.2 Transient Analysis

The initial conditions comes from the boundary condition system to improve the accuracy of the transient analysis. Adaptive techniques are applied to both time axes τ_1 and τ_2: adaptive HB in τ_1 and adaptive time step in τ_2. The WaMPDE simulation simply starts from the specified initial conditions and the stop time along τ_2 is set to be 0.07 seconds. Fig. 5.10 shows the multi-time expression of the output voltage. The initial number of harmonics is 11 and the adaptive harmonic balance automatically increases the number to maximum 32 and decreases the number to minimum 6 at the end of the simulation. The adaptive time step algorithm increases the step size (Fig. 5.11) depending on the local truncation error and largely speeds up the simulation time. The oscillator frequency determined by the warped function $\omega_0(\tau_2)$ is also represented in Fig. 5.11.

Very good agreement between WaMPDE simulation and the regular time domain simulation has been achieved at the beginning of the simulation shown in Fig. 5.12. It is mentioned here that there exists a very small phase error accumulation in the WaMPDE analysis compared with ODE result after a certain long time interval (also shown in Fig. 5.12). The relative amplitude

Reproduced with permission of the copyright owner. Further reproduction prohibited without permission.

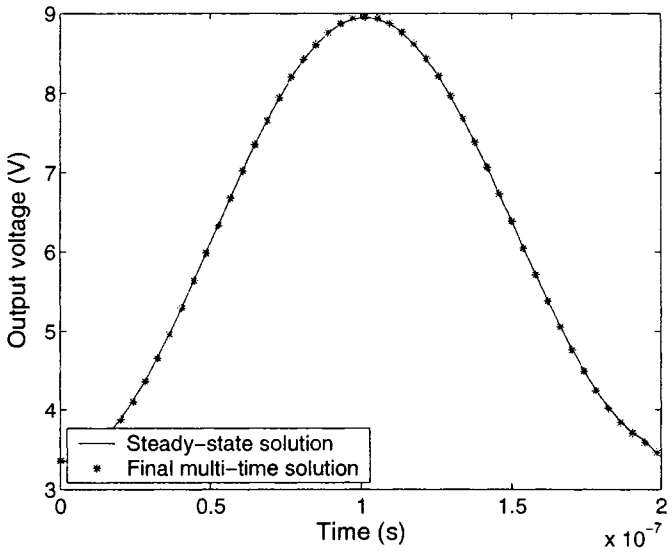

Figure 5.8: Steady-state solution compared to final multi-time solution.

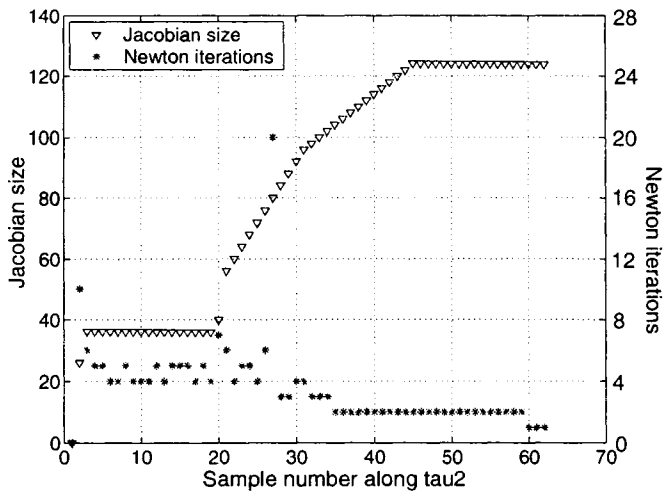

Figure 5.9: Jacobian size and number of Newton iterations.

Reproduced with permission of the copyright owner. Further reproduction prohibited without permission.

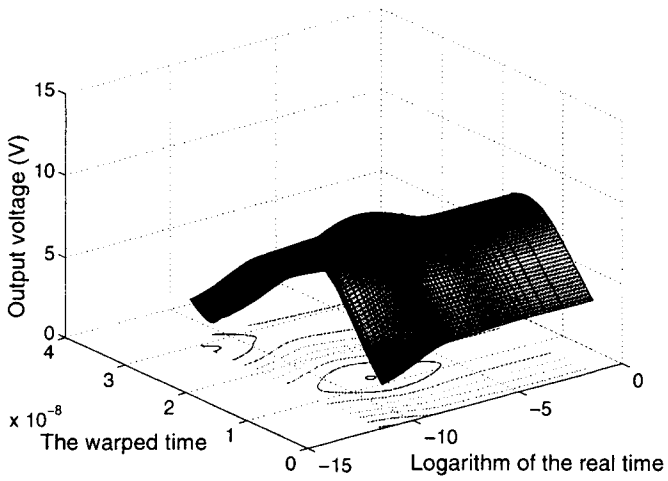

Figure 5.10: Bi-dimensional representation of output voltage.

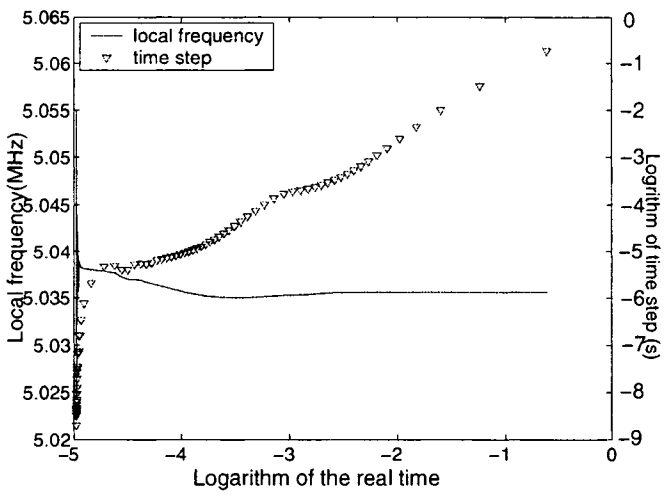

Figure 5.11: Adaptive time step and the fundamental frequency.

Reproduced with permission of the copyright owner. Further reproduction prohibited without permission.

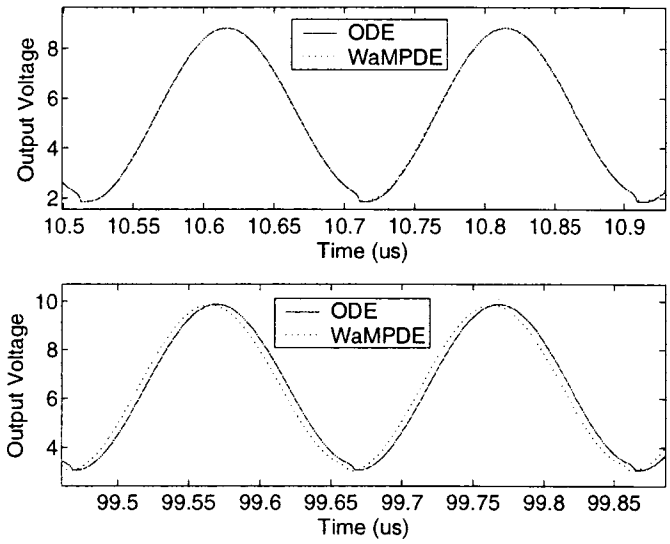

Figure 5.12: WaMPDE solution compared to ODE solution.

error and absolute phase error of the first harmonic in WaMPDE and ODE simulations are presented in Fig. 5.13. The amplitude error is very small, but the phase error may be important in some cases. The phase error in the WaMPDE simulation can be reduced if the acceptable local truncation error in the WaMPDE simulation is reduced as the results of Fig. 5.14 indicate. However, the reduction in the acceptable local truncation error increases the number of time steps along τ_2 and this results in a significantly longer simulation time.

5.3 Circuit 2: BJT Voltage Controlled Oscillator

Tuned oscillators are a very important class in the oscillator family. If a reactive component is a varactor diode then the oscillator may be frequency controlled by the varactor voltage. This kind of oscillator is called Voltage Controlled Oscillator (VCO). A simple VCO circuit was analyzed with WaMPDE in Chapter 2. In this section, we will present a practical BJT VCO circuit which is based on the Clapp-Gouriet configuration from [8] with WaMPDE analysis.

Fig. 5.15 shows the electrical schematic of a BJT VCO. In this circuit $C_1 = 82$ pF, $C_2 = 220$ pF, $C_3 = 47$ pF, $C_4 = 0.46$ μF, $L_1 = 102.55\mu H$, $R_1 = 220$ kΩ, $R_2 = 22$ kΩ, $R_3 = 47$ Ω, $R_c = 2.2$ kΩ, $R_e = 220$ Ω, $R_l = 100$ Ω, $V_{cc} = 12$ V, $BF = 70$, and $BR = 5$. The oscillator frequency is tuned by a diode connected to a control voltage V_{dc} which is either a DC value

Reproduced with permission of the copyright owner. Further reproduction prohibited without permission.

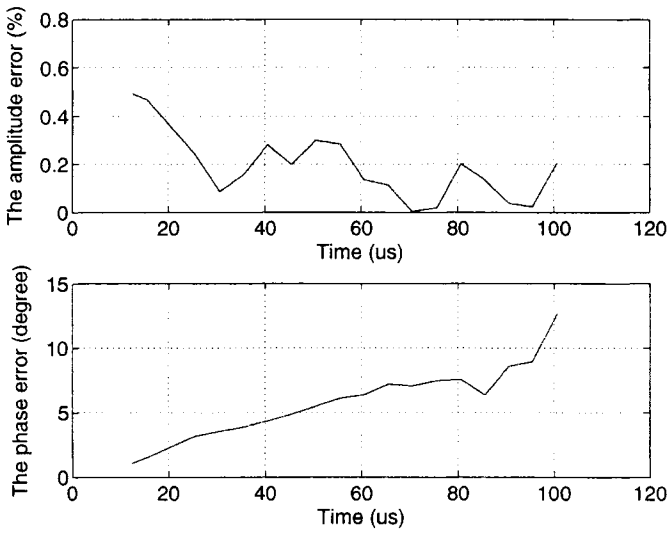

Figure 5.13: Relative error in the magnitude of the first harmonic.

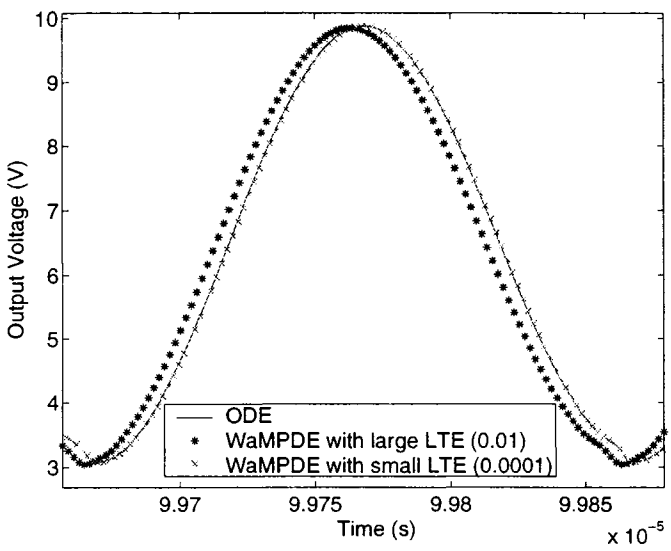

Figure 5.14: Comparison of ODE and WaMPDE with a smaller maximum local truncation error.

Reproduced with permission of the copyright owner. Further reproduction prohibited without permission.

or a sinusoidal function in this VCO circuit. VCOs are used in many applications, such as in frequency modulators, phase-locked loops, and frequency synthesizers.

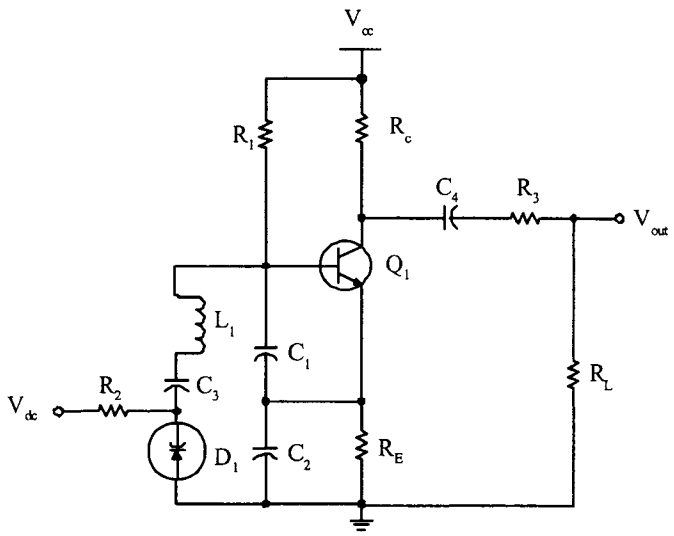

Figure 5.15: A voltage-controlled oscillator using Clapp-Gouriet configuration.

The diode is replaced by the model shown in Fig. 5.16 with:

$$\begin{cases} C_j = \frac{CJ0}{(1-\frac{V_d}{VJ})^{\mu_j}} \\ I_D = I_s(e^{(\frac{V_d}{N \times V_T})} - 1) \end{cases} \tag{5.1}$$

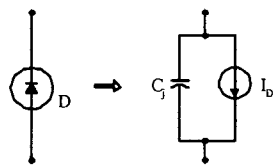

Figure 5.16: The model of the varicap.

Eq. 5.1 express the junction capacitance C_j and the diode current I_D. C_j is modeled by the model parameters $CJ0$, VJ, and μ_j [23]. $CJ0$ is the zero-biased junction capacitance which is the measured capacitance with no voltage applied to the diode. VJ represents the built-in potential of the diode, and μ_j represents the grading coefficient of the device. I_D is calculated by the model parameters I_s, N, and V_T. N represents the emission coefficient factor. The calculation

Reproduced with permission of the copyright owner. Further reproduction prohibited without permission.

of those parameters are in Appendix B.

Then we substitute Fig. 5.15 with all the models and define the node numbers in Fig. 5.17.

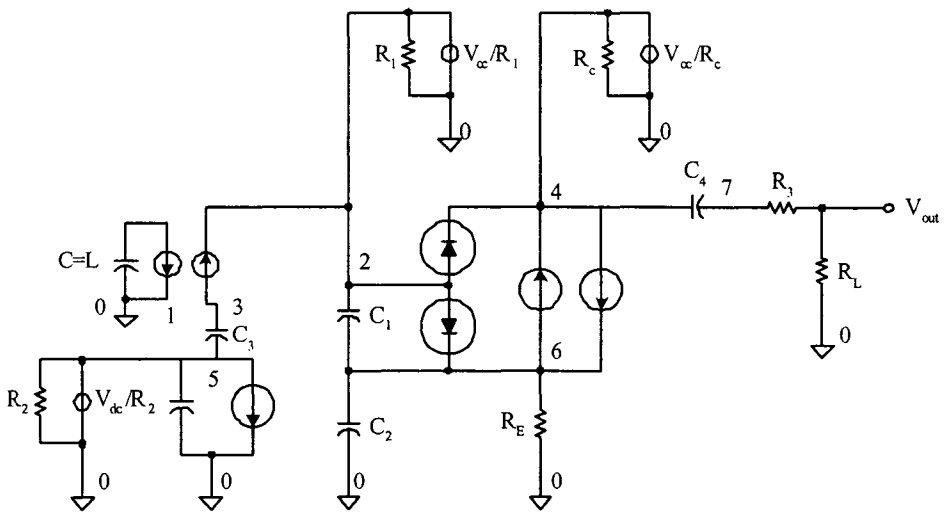

Figure 5.17: The equivalent circuit of the VCO circuit.

The DC bias point is calculated with $V_{dc} = 1.5$ V.

$$\begin{cases} U_1 = 0V \\ U_2 = 1.44V \\ U_3 = 1.44V \\ U_4 = 4.61V \\ U_5 = 1.5V \\ U_6 = 0.75V \\ U_7 = 0V \end{cases}$$

We will analyze this circuit in two different control voltages: a constant DC control voltage V_{dc1} and a sinusoidal control voltage V_{dc2}:

$$\begin{cases} V_{dc1} = 1.5V \\ V_{dc2} = 3 + sin(2\pi \times 10^4 t)V \end{cases}$$

The practical system on the printed circuit board is shown in Fig. 5.18.

The experiment equipment is presented in the follows and a detailed description of the test setup is provided in Appendix B.

Reproduced with permission of the copyright owner. Further reproduction prohibited without permission.

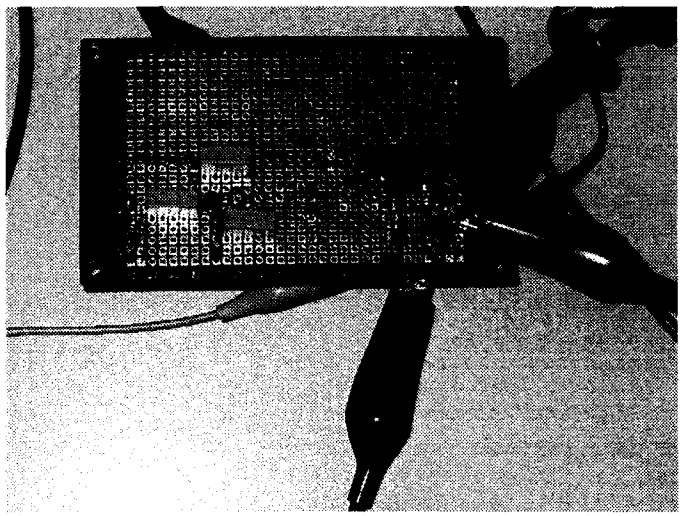

Figure 5.18: The VCO circuit on the actual printed circuit board.

1. Bipolar transistor (MPS918)
2. Oscilloscope (TEK 2445A)
3. Selection of resistors, inductors, capacitors
4. Varactor diode (SK3323RCA)
5. 0-5V power supply and 0-20V power supply

5.3.1 Steady-state Analysis

In steady state analysis, we consider a constant control voltage applied to the diode. The regular Spice time domain simulation is shown in Fig. 5.19.

In this circuit, the output voltage also presents strong nonlinear behavior similar to the Colpitts oscillator. It is suitable to use the proposed WaMPDE method to analyze the steady-state stage under this condition. Fig. 5.20 shows the WaMPDE simulation result. Compared with the regular time domain simulation, the multi-time representation contains less undulation and is easy and clear to analyze.

In Fig. 5.21 the steady state is shown together with the final multi-time result. The steady state result is calculated using the final multi-time solution as the initial condition. The number of Newton iterations in regular oscillator HB is only 2, which means the final periodic solution is

Reproduced with permission of the copyright owner. Further reproduction prohibited without permission.

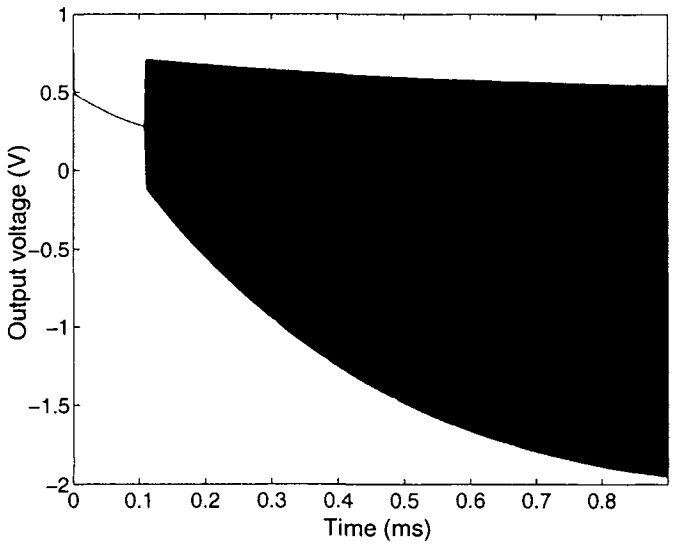

Figure 5.19: Transient response with a constant control voltage (1.5V).

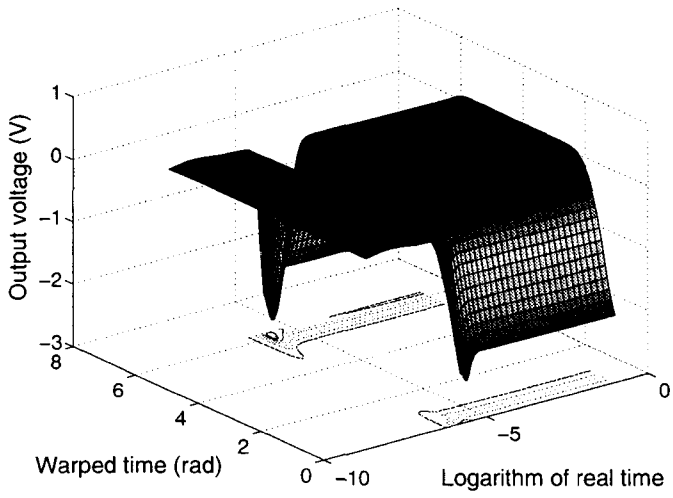

Figure 5.20: Bi-dimensional representation of output voltage.

Reproduced with permission of the copyright owner. Further reproduction prohibited without permission.

very close to the steady-state response. The local frequency determined by the warped function $\omega_0(\tau_2)$ is 6.03 MHz shown in Fig. 5.22.

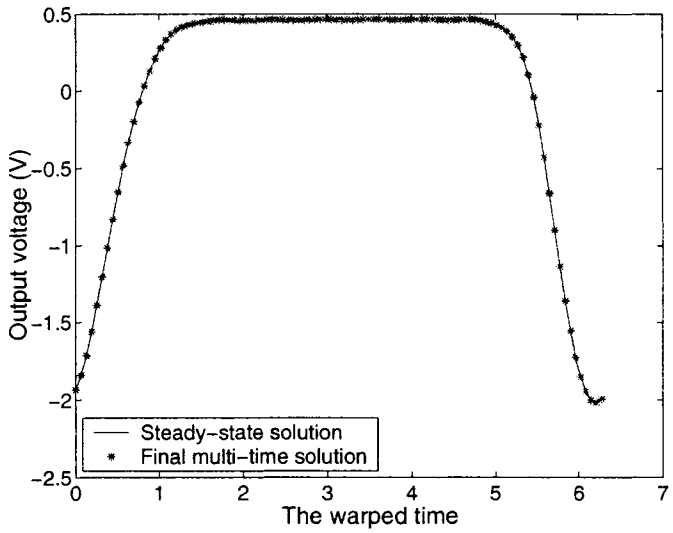

Figure 5.21: Steady-state solution compared to final multi-time solution.

The adaptive tolerance and the adaptive time step control algorithm keep the number of Newton iterations small for each value of τ_2. Fig. 5.23 shows the Jacobian matrix size and the number of Newton iterations at each time step (line number).

5.3.2 Transient Analysis

In transient analysis, we consider a sinusoidal control voltage applied to the diode. The value of C_4 is changed to 330 pF to reduce the oscillation starting time. The regular Spice time domain simulation is shown in Fig. 5.24. It was shown that this VCO circuit exhibits a very slow initial transient under the time varying control voltage. The initial number of harmonics is set to be 8 and the adaptive HB algorithm will automatically reduce or increase the harmonics in each specific node for each value of τ_2. At the end of the simulation, the maximum number of harmonics is 11 and the minimum is 5. The bi-dimensional plot of the output voltage is shown in Fig. 5.25.

The oscillator frequency in Fig. 5.26 follows the time varying control voltage. Adaptive time steps are also shown in the same figure. It is interesting that adaptive time steps also change with the control voltage. Good agreement between WaMPDE simulation and traditional time

Reproduced with permission of the copyright owner. Further reproduction prohibited without permission.

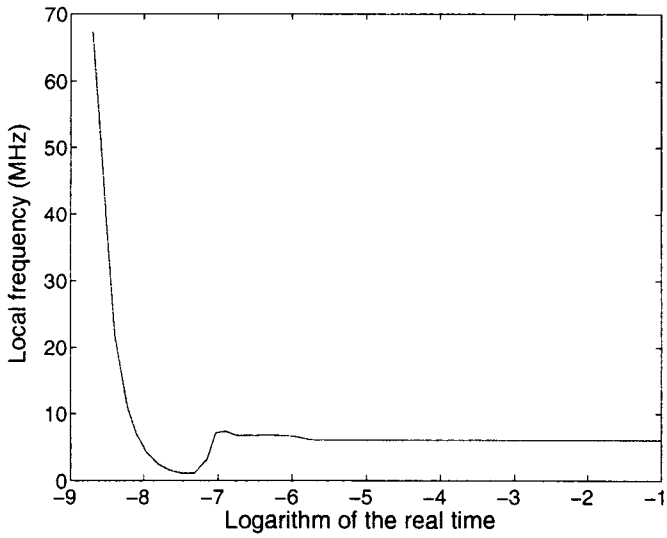

Figure 5.22: Fundamental frequency as a function of τ_2.

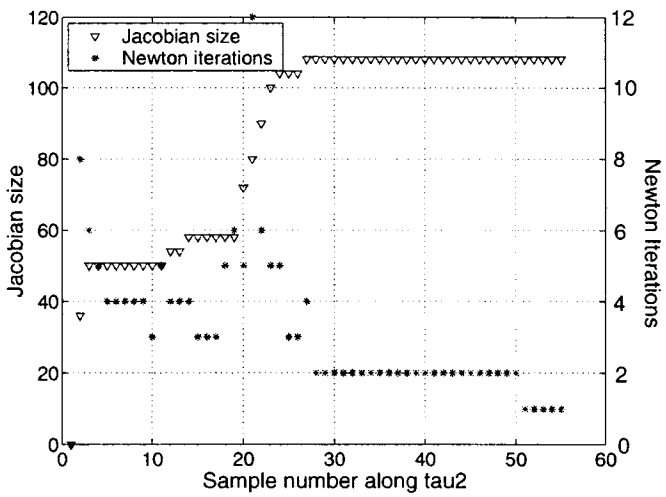

Figure 5.23: Jacobian size and number of Newton iterations.

Reproduced with permission of the copyright owner. Further reproduction prohibited without permission.

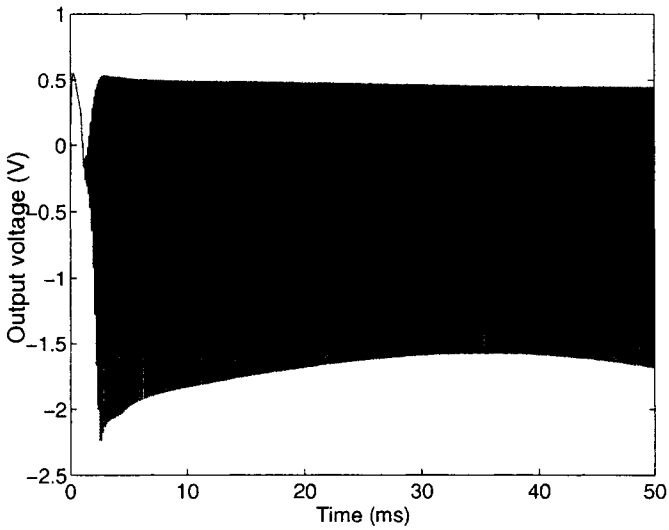

Figure 5.24: Transient response with a sinusoidal control voltage ($V_{dc} = 3 + \sin 10^4 t$.)

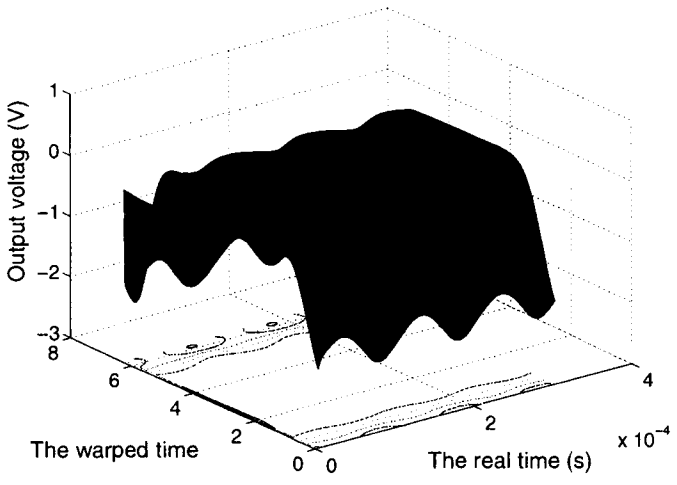

Figure 5.25: Bi-dimensional representation of output voltage.

Reproduced with permission of the copyright owner. Further reproduction prohibited without permission.

domain simulation has been achieved as shown in Fig. 5.27.

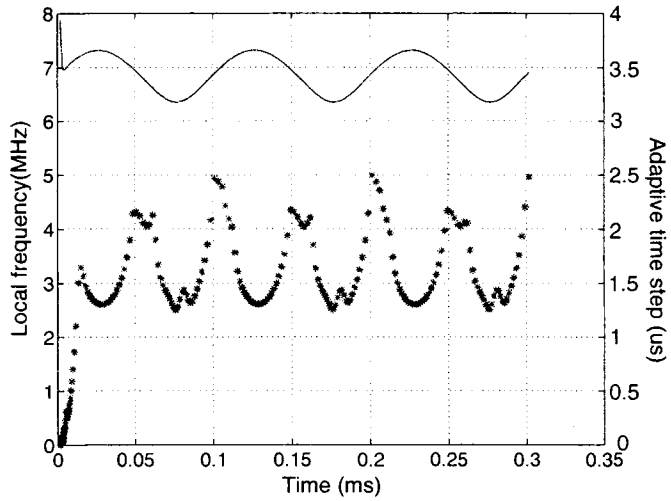

Figure 5.26: Adaptive time step and the local frequency.

A plot showing the first harmonic magnitude and phase difference between the time-marching and WaMPDE analysis is shown in Fig. 5.28. As with the previous case study, there is some phase error that can be reduced by reducing the tolerance of the local truncation error shown in Fig. 5.29.

5.3.3 Experiment Result

To explore the efficiency of proposed methods, the voltage-controlled oscillator was tested. During the test, the control voltage is manually set, and the output is monitored by an oscilloscope. Comparison of experiment results with the simulations is shown in the following sections.

Comparison of Experiment and Simulation Result

A comparison between the simulation and the measurement at the output port of the oscillator is presented in this part.

1. Constant control voltage (1.5 V)

   First, we connect a constant control voltage equal to 1.5V to the diode. The experiment results are shown in Fig. 5.30. An inspection of the output voltage shows that it exhibits very similar performance as presented in the simulation part shown in Fig. 5.31.

Reproduced with permission of the copyright owner. Further reproduction prohibited without permission.

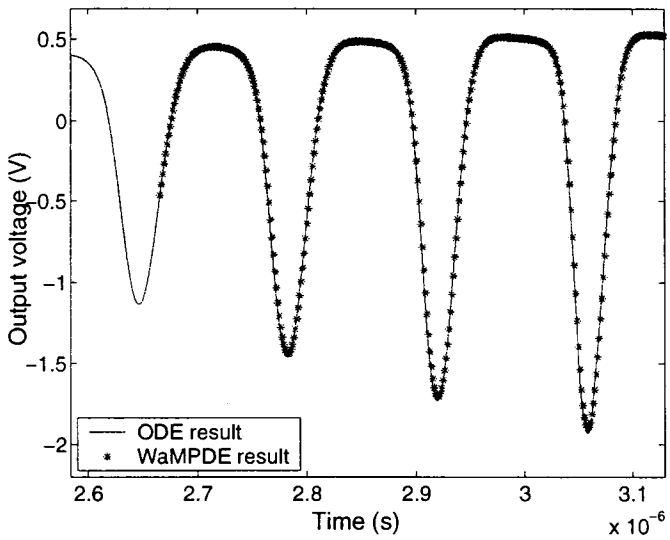

Figure 5.27: Proposed WaMPDE solution compared to ODE solution.

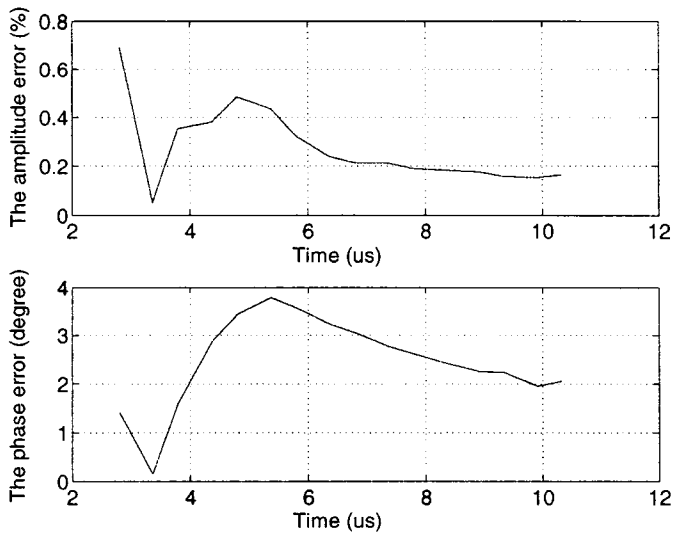

Figure 5.28: Comparison of ODE and Warped MPDE in First harmonic.

Reproduced with permission of the copyright owner. Further reproduction prohibited without permission.

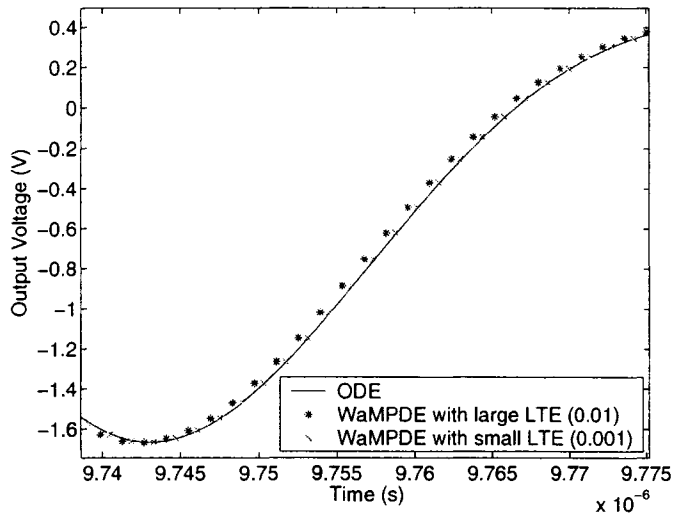

Figure 5.29: Comparison of ODE and WaMPDE with a smaller maximum local truncation error.

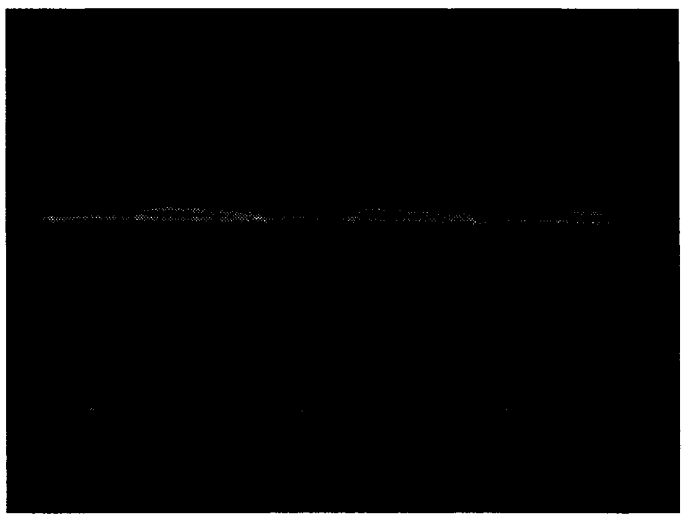

Figure 5.30: The experiment steady-state when control voltage equal 1.5 V.

Reproduced with permission of the copyright owner. Further reproduction prohibited without permission.

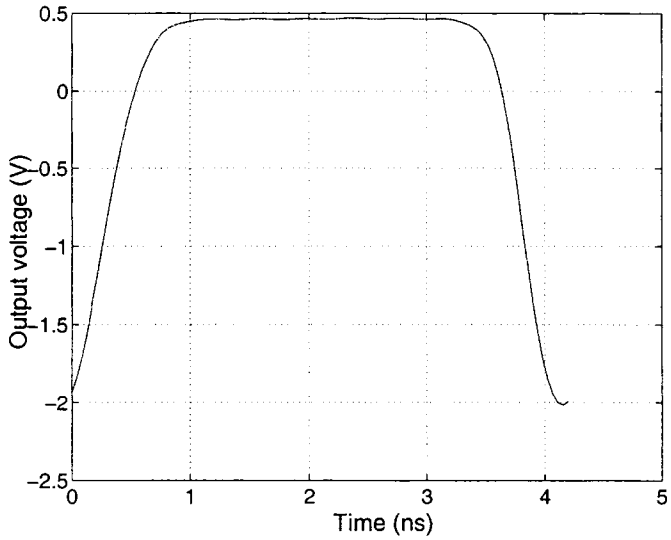

Figure 5.31: simulation result of the output voltage.

From Fig. 5.30, it is observed that the measured oscillation period is approximately 5.41 MHz while the simulated oscillation period is 6.03 MHz. The difference could be attributed to a number of factors:

(a) The internal resistor of the inductor and the error from the predicted diode model.

(b) The SPICE models of the diode and transistor also play a role in the discrepancy.

The main components determining the oscillation frequency are C_1, C_2, C_3, the diode C_D, and the inductor L. Given that there are many uncertainties, the simulated oscillation frequency is considered close to the measured oscillation frequency. Another form of visualization is shown in Fig. 5.32. Here we set a square power supply (see Appendix B), so the transient behavior of this oscillator can be observed. Fig. 5.33 enlarges the beginning part of Fig. 5.32, which is similar to the simulation result (see Fig. 5.19).

2. Sinusoidal control voltage

Since it is usually difficult to get the result from regular time domain simulation such as SPICE when the control voltage is time-varying, the experiment is again processed using a sinusoidal control voltage. Fig. 5.34 shows the result when the voltage across the diode is

Reproduced with permission of the copyright owner. Further reproduction prohibited without permission.

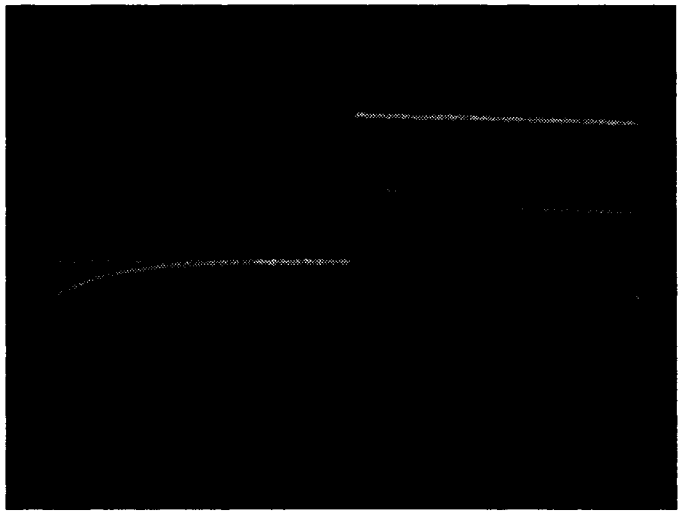

Figure 5.32: The experiment transient when control voltage equal 1.5 V.

Figure 5.33: The beginning part.

Reproduced with permission of the copyright owner. Further reproduction prohibited without permission.

driven by a sinusoidal voltage source with amplitude of 1 V.

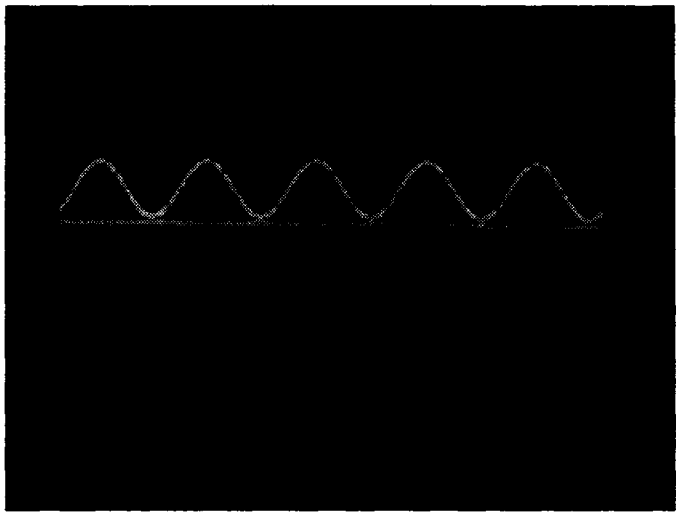

Figure 5.34: The experiment steady-state when sinusoidal control voltage equal $3 + \sin 10^4 t$ V.

The result does not agree very well with the simulations shown in Fig. 5.35. It is noted that the voltage drop in the experiment is 2 V, smaller than 2.5 V in the simulation result. Also there is a very slow rate of oscillations on the top of the simulation result but none is in the experimental result. We use the Hybrid-π model (constant C_μ and C_π) to represent the transistor (see Appendix B). C_μ and C_π are not constant any more when the transistor is in saturation. In this case sometimes the transistor is in saturated stage. We tried different combinations in Spice simulation: one with the separate C_μ and C_π and the other with particular parameters of the transistor. The results are almost the same. So the measurements of the current elements (inductor, capacitor, and transistor) are needed to improved to get a closer fit with measurements.

Optimizing the Tuning Range

The oscillation frequency of the circuit is given by Eq. 2.9. We rewrite it in the following form:

$$\omega L - \frac{1}{\omega C_T} - \frac{1}{\omega C_b} = 0,$$

Reproduced with permission of the copyright owner. Further reproduction prohibited without permission.

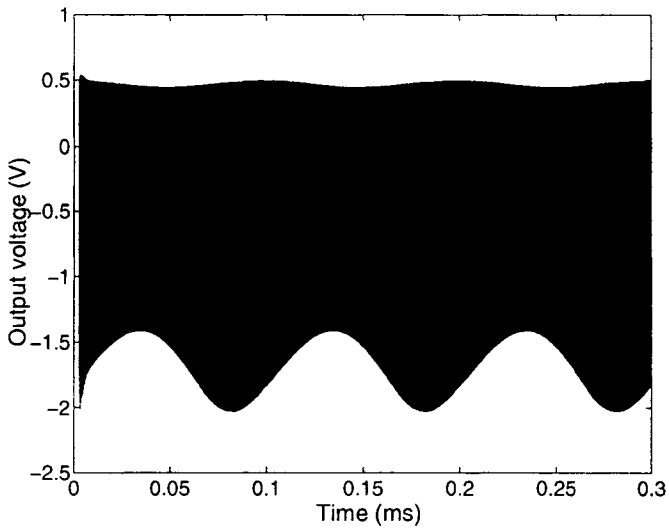

Figure 5.35: Simulation result of the output voltage.

Where $C_T = \frac{C_1 C_2}{C_1 + C_2}$ and C_b is the total capacitance in the tuning network, including the diode junction capacitance. The oscillation frequency of the final steady-state value is:

$$f_{osc} = \frac{1}{2\pi\sqrt{L\frac{C_T C_b}{C_T + C_b}}}.$$

Let C_{b1} and C_{b2} be the minimum and maximum capacitance of the tuning passive network. Then the range of frequency is:

$$\Delta f = \frac{1}{2\pi}\left(\frac{1}{\sqrt{L_b\frac{C_T C_{b1}}{C_T + C_{b1}}}} - \frac{1}{\sqrt{L_b\frac{C_T C_{b2}}{C_T + C_{b2}}}}\right)$$

In this case, the VCO accepts a DC control voltage between -4 V–0 V and is capable of generating an output signal with a frequency between 4.42 MHz and 6.16 MHz. The illustration seen in Fig. 5.36 shows the voltage across the diode being driven voltage source from an initial value of 0 V to -4 V. The tuning range of the VCO was characterized by incrementally sweeping the control voltage in steps of 0.2 V with the output frequency at each step being measured by the oscilloscope. The frequency of the output signal is regulated by the control voltage. Any changes in the control voltage produce a proportional change in the output frequency.

Reproduced with permission of the copyright owner. Further reproduction prohibited without permission.

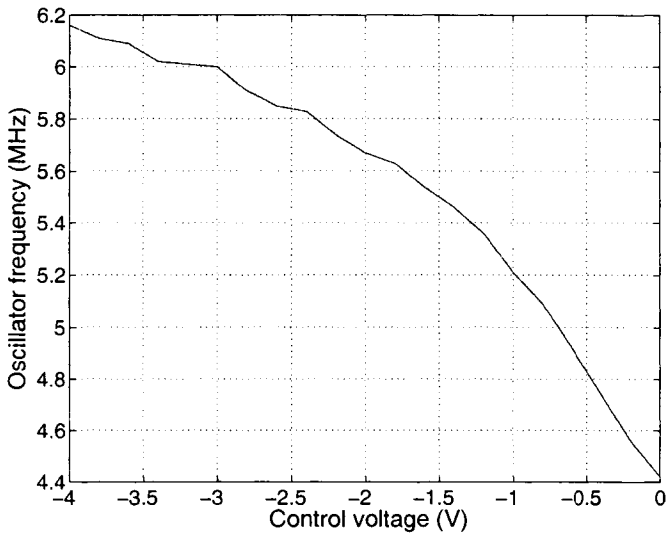

Figure 5.36: Output frequency vs. control voltage of the VCO.

Reproduced with permission of the copyright owner. Further reproduction prohibited without permission.

Chapter 6

Conclusions and Future Work

6.1 Conclusions

WaMPDE is extremely useful and effective for oscillator analysis. In this thesis two novel and fast approaches to capture the transient and steady-state response of oscillators in frequency domain derived from WaMPDE were presented. The following are the main conclusion items based on the simulation and experimental results:

1. For transient analysis the accuracy of the WaMPDE method depends on the accuracy of the boundary conditions. It was also the first time to show how to obtain precise initial boundary conditions in both the oscillation frequency and the transient solution of each state variable to improve the accuracy of the WaMPDE simulation. It also provides a robust route to switch between multiple time domain and traditional time domain simulations. An adaptive time step control algorithm depending on the local truncation error is employed and the computational time is orders of magnitude faster than traditional transient analysis.

2. For steady-state analysis the new method does not require a good initial guess of the oscillation frequency and incorporates several ideas to improve robustness and reduce the computational cost. The method uses the WaMPDE approach to naturally bring the circuit state to the region of convergence of the HB analysis. It was shown for the first time that the transient evolution along the slow time axis provide the optimum conditions to determine the minimum number of harmonics required at each node in the circuit. It also uses adaptive techniques to reduce the computational effort: adaptive HB determines the

Reproduced with permission of the copyright owner. Further reproduction prohibited without permission.

minimum number of harmonics required at each variable and the number of harmonics does not need to be known in advance; adaptive time step decides the optimum size along the real time; adaptive tolerance reduces Newton iterations. As a result of this adaptive scheme the Jacobian matrix in the Newton method is reduced and a significant reduction in the computational effort is achieved. Both the oscillation frequency and the steady-state solution of each state variable are obtained in a fast and accurate way.

The simulation of different types of oscillators and the experiment of the VCO circuit demonstrate the excellent performance of both proposed methods.

6.2 Future Work

Following the investigations described in this thesis, some topics could be taken up in the future research work:

1. Development of a general method to write the system nonlinear equations. It is beneficial to deal with some large circuits with hundreds of nodes.

2. If R_f in the circuit of Fig. 3.24 is reduced to 200 Ω, the oscillation period eventually doubles and this originates a subharmonic component as shown in Fig. 6.1. The proposed method is not able to detect this condition. The detection of subharmonic generation and chaos in a WaMPDE simulation is a topic for the future research.

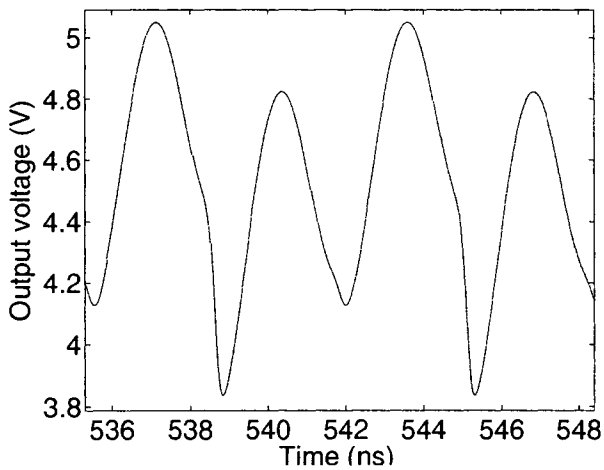

Figure 6.1: Transient simulation with $R_f = 200\ \Omega$ showing subharmonic generation.

Reproduced with permission of the copyright owner. Further reproduction prohibited without permission.

3. Improvement of the phase error in transient analysis. Now we need to sacrifice the simulation time to reduce the phase error.

4. WaMPDE study in Phase-Locked-Loops (PLLs). Now we use two time scales to analyze oscillators. In PLLs the voltage-controlled oscillator can be represented in two time axes: warped time and slow time, since the slow varying control voltage from the low pass filter and the comparatively much faster oscillations. Simultaneously the external signal which is one of the inputs of the phase detector can be also represented in multiple time domain. So PLLs can be analyzed in three time axes: warped time, fast time and slow time.

5. Improve circuit modeling to get a closer fit with measurements.

Reproduced with permission of the copyright owner. Further reproduction prohibited without permission.

Appendix A

Newton-Raphson Method

The Newton-Raphson method uses an iterative process to converge one root of a function [15, 24]. Consider a function

$$f(x) = 0. \tag{A.1}$$

The specific root that the process locates depends on the initial value x_n.

$$x_{n+1} = x_n - \frac{f(x_n)}{f'(x_n)}, \tag{A.2}$$

with $n = 0, 1, 2\cdots$. Here, x_n is the current known value, $f(x_n)$ represents the value of the function at x_n, and $f'(x_n)$ is the derivative at x_n. x_{n+1} represents the next value that converges to the final solution.

If a system consists of n non-linear equations:

$$F(x) = \begin{bmatrix} f_1(x) \\ f_2(x) \\ \vdots \\ f_n(x) \end{bmatrix} = \begin{bmatrix} 0 \\ 0 \\ \vdots \\ 0 \end{bmatrix} \tag{A.3}$$

with n variables $x = (x_1, x_2, ..., x_n)$. Eq. A.3 can be solved iteratively as:

$$x^{j+1} = x^j - J^{-1}F(x^j) \tag{A.4}$$

where J is the Jacobian Matrix presented by:

Reproduced with permission of the copyright owner. Further reproduction prohibited without permission.

$$J = \frac{\partial F}{\partial x} = \begin{bmatrix} \frac{\partial f_1}{\partial x_1} & \frac{\partial f_1}{\partial x_2} & \cdots & \frac{\partial f_1}{\partial x_n} \\ \frac{\partial f_2}{\partial x_1} & \frac{\partial f_2}{\partial x_2} & \cdots & \frac{\partial f_2}{\partial x_n} \\ \vdots & \vdots & \vdots & \vdots \\ \frac{\partial f_n}{\partial x_1} & \frac{\partial f_n}{\partial x_2} & \cdots & \frac{\partial f_n}{\partial x_n} \end{bmatrix} \tag{A.5}$$

Eq. A.5 can be formulated numerically in the following equation when the nonlinearities are not very strong:

$$\frac{\partial f_j}{\partial x_k} = \frac{f_j(x_k^{i+1}) - f_j(x_k^i)}{x_k^{i+1} - x_k^i}. \tag{A.6}$$

Reproduced with permission of the copyright owner. Further reproduction prohibited without permission.

Appendix B

Experiment Parameter Validation

B.1 DC analysis

The BJT employed in the oscillator is $MPS918$, a wide-band 800 MHz NPN transistor in $TO-92$ plastic package (Motorola Semiconductors 1996). The datasheet and the Spice model of $MPS918$ are in [25] and [26] respectively supplied by the manufacturers. The transition frequency f_T(800 MHz) is more than sufficient for this job. The forward beta BF is equal to 70. The circuit for DC bias simulation is shown in Fig. B.1.

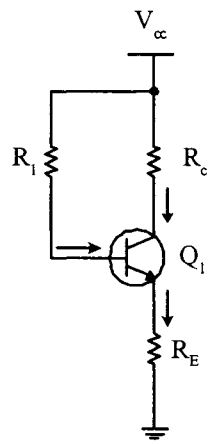

Figure B.1: DC bias analysis of the VCO circuit.

The result of DC simulation for this VCO circuit in the calculations below:

$$I_b = \frac{V_{cc} - V_{be}}{R_1 + (BF + 1) \times R_e} = 48\mu A$$

Reproduced with permission of the copyright owner. Further reproduction prohibited without permission.

$$I_c = BF \times I_b = 3.36mA$$

$$I_e = (BF + 1) \times I_b = 3.41mA$$

$$U_c = V_{cc} - I_c \times R_c = 4.61V$$

$$U_b = V_{cc} - I_b \times R_1 = 1.44V$$

$$U_e = I_E \times R_E = 0.75V$$

$$g_m = \frac{I_c}{V_T} = 0.129$$

B.2 Diode

The diode in the VCO circuit is the tuning element. It plays an important role: varying the frequency of oscillation by the control voltage V_{dc}. Because the varactor diodes directly affect the tuning range and the gain of the VCO, their specifications are critical to achieving adequate performance. The diode in this experiment is the $SK3323RCA$. We use the circuit in Fig. B.2 to determine its capacitance.

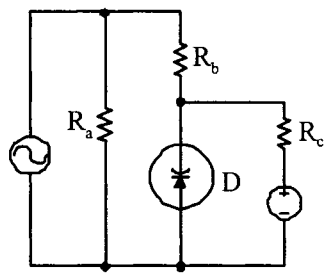

Figure B.2: The circuit used to check the capacitance of the diode.

In Fig. B.2, $R_a = 47\Omega$, $R_b = 10$ kΩ, and $R_c = 100$ kΩ. The total resistor seen from the diode is

$$\frac{1}{R} = \frac{1}{(R_a + R_b)} + \frac{1}{R_c}$$

Reproduced with permission of the copyright owner. Further reproduction prohibited without permission.

Then we can measure τ and calculate the capacitance of the diode by:

$$C = \frac{\tau}{R}$$

In SPICE, the junction capacitance is modeled by the model parameters $CJ0$, VJ, and μ_j [23]. $CJ0$ is the zero-biased junction capacitance which is the measured capacitance with no voltage applied to the diode. VJ represents the built-in potential of the diode, and μ_j represents the grading coefficient of the device. They all influence the capacitance characteristic of the diode. The junction capacitance C_j related to voltage V_d is expressed in Eq. B.1:

$$C_j = \frac{CJ0}{(1 - \frac{V_d}{VJ})^{\mu_j}} \tag{B.1}$$

Fig. B.3 illustrates the effect of the diode capacitance variation for reverse voltage. A similar curve from the calculation of Eq. B.1 is also inserted for comparison. $CJ0$ is easily obtained from the intersection of the curve onto the y -axis as shown in Fig. B.3. The $CJ0$ value is 15.29 pF.

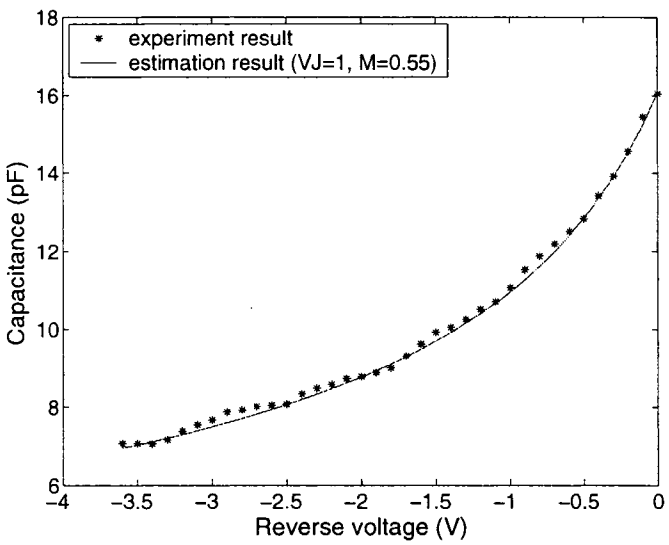

Figure B.3: Diode capacitance variation for reverse voltage.

Fig. B.4 gives the plot of the optimum value of VJ and M where C is the measured capacitance and DC is the diode voltage. This figure also provides some insight of the diode characteristic. If the value of VJ used for the x -axis variable is equal to the value of VJ needed

Reproduced with permission of the copyright owner. Further reproduction prohibited without permission.

for the model, the plot curve will be close to a straight line. If the value of VJ is too large or too small, the plot will be curved [23]. We choose $VJ = 1$ and $M = 0.55$.

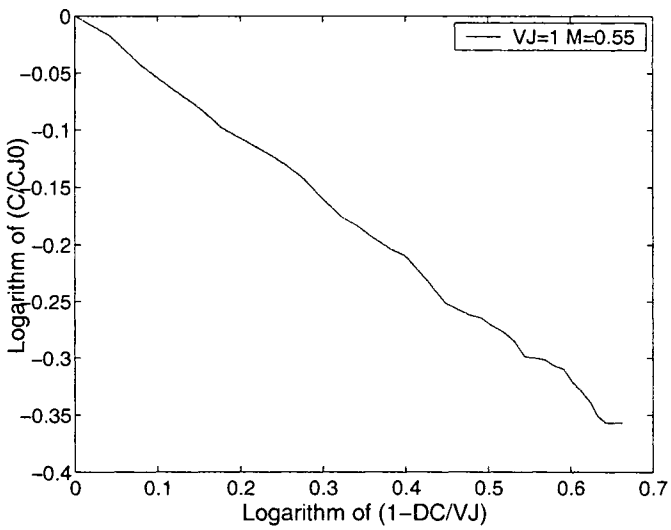

Figure B.4: Graph to determine the model parameters M and VJ.

B.3 Inductor

To measure the precise value of the inductor, a measurement circuit is selected in Fig. B.7 with $R_a = R_b = 100\ \Omega$.

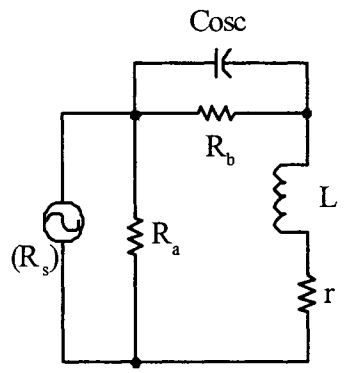

Figure B.5: The circuit used to measure the inductor.

Reproduced with permission of the copyright owner. Further reproduction prohibited without permission.

The total resistor seen from the inductor is:

$$R = \frac{1}{(\frac{1}{R_s} + \frac{1}{R_a})} + R_b + r$$

Then we measure τ and calculate the inductance by using $L = \tau \times R$. The inductance is 102.55μ H with series resistance $r = 8.65\Omega$. It is clear that the internal resistor r satisfies Eq. 2.8 and the oscillation will naturally build up.

B.4 Transistor

This part deals with measuring C_μ and C_π in the Hybrid-π model of the $MPS918$ transistor shown in Fig. B.6. C_μ is the collector-base junction capacitance and C_π is the base-charging or diffusion capacitance plus the base-emitter junction capacitance. They all influence the performance of the experiment.

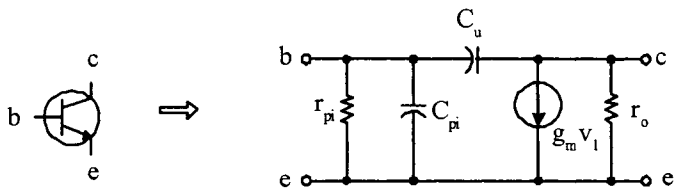

Figure B.6: Hybrid-π model of the transistor.

The test circuit shown in Fig. B.7 is used to check those parameters. Because of two unknowns we need two equations with two different values of R_c: 2.2 kΩ and 687.5 Ω. The procedure of the calculation is shown below.

$$r_\pi = \frac{\beta}{g_m} = \frac{70}{0.129} = 542.15\Omega$$

$$R_{eq} = \frac{1}{\frac{1}{r_\pi} + \frac{1}{R_s}} = 76.8\Omega$$

$$\tau_{total} = C_{pi}R_{eq} + C_\mu[R_{eq}(1 + g_m R_c) + R_c] + C_{osc}R_c$$

$$\begin{cases} C_\mu = 0.73\ pF \\ C_\pi = 59.9\ pF \end{cases}$$

Reproduced with permission of the copyright owner. Further reproduction prohibited without permission.

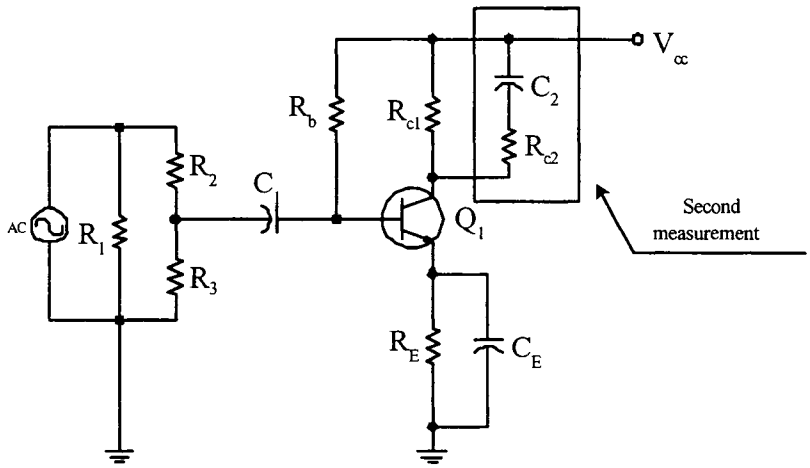

Figure B.7: The circuit used to check the parameters of the transistor.

B.5 Square Power Supply

To observe the transient behavior of experiment results, a square power supply is generated by a *LM*741 operational amplifier. The circuit is shown in Fig. B.8. We can get an amplified square power supply (from 0 v to 12 v) with the input (from 0 v to 1 v) generated by the function generator.

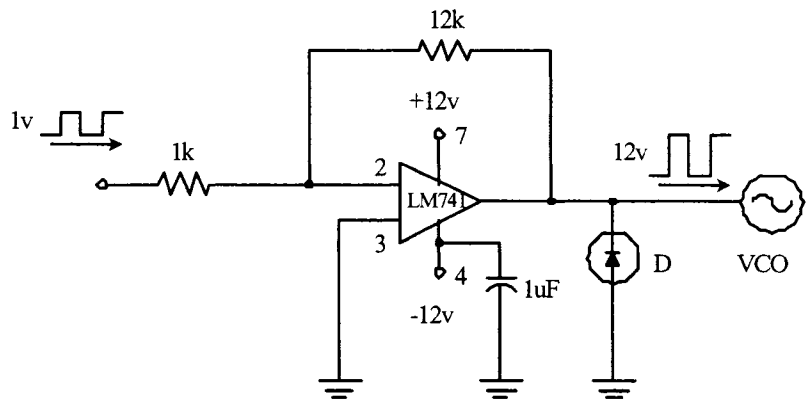

Figure B.8: The circuit used to generate square power supply.

B.6 Summary

We summarized all the parameters in table B.1.

Reproduced with permission of the copyright owner. Further reproduction prohibited without permission.

The experimental parameters		
DC Analysis	I_b	48 μA
	I_c	3.36 mA
	I_e	3.41 mA
	U_b	1.44 V
	U_c	4.61 V
	U_e	0.75 V
	g_m	0.129
Diode	$CJ0$	15.29 pF
	VJ	1
	M	0.55
Inductor	L	102.55 μA
	r	8.65 Ω
Transistor	BF	70
	BR	5
	C_μ	0.73
	C_π	59.9

Table B.1: The experimental parameters.

Reproduced with permission of the copyright owner. Further reproduction prohibited without permission.

Appendix C

Matlab File List

C.1 LC-tuned bipolar oscillator

Steady-state analysis				
oscillatorMain.m	resultlana.m	EXPlana.m	nonlinearone.m	nonlineartwo.m
nonlinearthree.m	nonlinearfour.m	nonlinearfive.m	nonlinearsix.m	amplitudelana.m
lanadiff2.m	nonlinearoneinf.m	nonlineartwoinf.m	nonlinearthreeinf.m	nonlinearfourinf.m
nonlinearfiveinf.m	nonlinearsixinf.m	lanaplot.m		

Transient analysis			
oscillatorMain.m	icfromNewton.m	icfromode.m	lanaIC2.m
PolyInter2.m	oscifilter.m	initialVT.m	EXPlana.m
derilanafirst.m	odelanafirst.m	odelanasecond.m	nonlinearonefirst.m
nonlinearthreefirst.m	nonlinearfourfirst.m	nonlinearfivefirst.m	nonlinearsixfirst.m
ifftlanafirst.m	ifftlanasecond.m	resultlana.m	derilana.m
derivativetau2ub.m	nonlinearone.m	nonlineartwo.m	nonlinearthree.m
nonlinearfive.m	nonlinearsix.m	amplitudelana.m	Aprolana.m
AHB.m	twotooneHB.m	twotooneHuatu1.m	lanaplot.m
lanaIC3.m	bipolar.m	nonlineartwofirst.m	nonlinearsevenfirst.m
derivativetau2ua.m	nonlinearfour.m	parlana1.m	

Reproduced with permission of the copyright owner. Further reproduction prohibited without permission.

C.2 Colpitts oscillator

Steady-state analysis				
oscillatorMain.m	resultlana.m	EXPlana.m	nonlinearone.m	nonlineartwo.m
nonlinearthree.m	nonlinearfour.m	nonlinearfive.m	nonlinearsix.m	amplitudelana.m
lanadiff2.m	nonlinearoneinf.m	nonlineartwoinf.m	nonlinearthreeinf.m	nonlinearfourinf.m
nonlinearfiveinf.m	nonlinearsixinf.m	lanaplot.m		

Transient analysis			
oscillatorMain.m	icfromNewton.m	icfromode.m	lanaIC2.m
PolyInter2.m	oscifilter.m	initialVT.m	EXPlana.m
derilanafirst.m	odelanafirst.m	odelanasecond.m	nonlinearonefirst.m
nonlinearthreefirst.m	nonlinearfourfirst.m	nonlinearfivefirst.m	nonlinearsixfirst.m
ifftlanafirst.m	ifftlanasecond.m	resultlana.m	derilana.m
derivativetau2ua.m	nonlinearone.m	nonlineartwo.m	nonlinearthree.m
nonlinearfive.m	nonlinearsix.m	amplitudelana.m	Aprolana1.m
AHB.m	twotooneHB.m	twotooneHuatu1.m	lanaplot.m
lanaIC3.m	bipolar.m	nonlineartwofirst.m	nonlinearsevenfirst.m
derivativetau2ua.m	nonlinearfour.m	parlana1.m	colpitts.m
nonlinearsevenfirst.m	parlana2.m		

C.3 Voltage-controlled oscillator

Reproduced with permission of the copyright owner. Further reproduction prohibited without permission.

Steady-state analysis				
oscillatorMain.m	resultlana.m	EXPlana.m	nonlinearone.m	nonlineartwo.m
nonlinearthree.m	nonlinearfour.m	nonlinearfive.m	nonlinearsix.m	amplitudelana.m
lanadiff2.m	nonlinearseven.m	nonlineareight.m	amplitudelana.m	derivativetau2ua.m
derilanaBE.m	EXPkris.m	EXPsophie1.m	lanaplot.m	

Transient analysis			
oscillatorMain.m	icfromNewton.m	icfromode.m	lanaIC2.m
PolyInter2.m	oscifilter.m	initialVT.m	EXPlana.m
derilanafirst.m	odelanafirst.m	odelanasecond.m	nonlinearonefirst.m
nonlinearthreefirst.m	lanaIC3.m	bipolar.m	nonlinearseven.m
ifftlanafirst.m	ifftlanasecond.m	resultlana.m	derilana.m
derivativetau2ua.m	nonlinearone.m	nonlineartwo.m	nonlinearthree.m
nonlinearfive.m	nonlinearsix.m	amplitudelana.m	Aprolana1.m
AHB.m	twotooneHB.m	twotooneHuatu1.m	lanaplot.m
derivativetau2ua.m	nonlinearfour.m	parlana2.m	onetime.m
nonlinearsevenfirst.m	parlana2.m	derivativetau2ub.m	nonlineareight.m

Reproduced with permission of the copyright owner. Further reproduction prohibited without permission.

Bibliography

[1] O. Narayan and J. Roychowdhury, "Analyzing oscillators using multitime PDEs," *IEEE Transactions on Circuits and Systems-1: Fundamental Theory and Applications,* vol.50, no.7, Jul. 2003, pp. 894–903.

[2] C. Chang, M. B. Steer, S. Martin and E. Reese, "Computer-aided analysis of free-running microwave oscillators," *IEEE Trans. on Microwave Theory and Techniques*, vol. 39, no.10, Oct. 1991, pp. 1735–1745.

[3] E. Ngoya, A. Suarez, R. Sommet and R. Quéré, "Steady state analysis of free or forced oscillators by harmonic balance and stability investigation of periodic and quasi-periodic regimes," *Int. J. of Microwave and Millimiter-Wace CAE*, vol.5, no. 3, 1995, pp. 210–223.

[4] M. Gourary, S. Ulyanov, M. Zharov, and S. Rusakov, "Simulation of high-Q oscillators," *1998 IEEE/ACM ICCAD Digest*, 1998, pp. 162–169.

[5] U. Jorges and G. Jummel,"Finding the steady state of high-Q circuits with proper initial values of the transient analysis," *Circuits and Devices Magazine, IEEE,* vol.13, Nov. 1997, pp. 6–8.

[6] T. Aprille and T. Trick,"A computer algorithm to determine the steady-state response of nonlinear oscillators," *Circuits and Systems, IEEE Transactions on [legacy, pre - 1988],* vol.19, Jul 1972, pp. 354–360.

[7] J. Roychowdhury, "Analyzing circuits with widely separated time scales using numerical PDE methods," *IEEE Transactions on Circuits and Systems-1: Fundamental Theory and Applications,* vol.48, no.5, May 2001, pp. 578–594.

Reproduced with permission of the copyright owner. Further reproduction prohibited without permission.

[8] Jack A. Smith, *Modern Communication Circuits, second edition.* 1997 McGraw-Hill.

[9] A. Collado, F. Ramírez, A. Suarez and J. P. Pascual, "Harmonic balance analysis and synthesis of coupled-oscillator arrays," *IEEE Microwave and Wireless Components Letters*, vol. 14, no. 5, March 2004, pp. 192–194.

[10] A. Brambilla and P. Maffezzoni,"Envelope-following method to compute steady-state solutions of electrical circuits,"*IEEE Transactions on Circuits and Systems-1: Fundamental Theory and Applications,* vol.47, Jul. 2000, pp. 999–1008.

[11] V. Rizzoli, A. Constanzo and A. Neri, "Harmonic balance analysis of microwave oscillators with automatic suppression of degenerate solution," *Electronic Letters*, vol. 28, no. 3, Jan. 1992, pp. 256–257.

[12] H. Asai, H. Makino, "Frequency domain latency and relaxation-based harmonic analysis of nonlinear circuits,"*Proc. of the 34th Midwest Symp. on Circuits and Systems,* vol. 1, May 1991, pp. 202–205.

[13] M. Gourary, S. G. Rusakov, S. L. Ulyanov, M. M. Zharov, K. K. Gullapalli, B. J. Mulvaney, "A new technique to exploit frequency domain latency in harmonic balance simulators,"*Proceedings of the 1999 Design Automation Conference*, vol. 1, Jan. 1999, pp. 65–68.

[14] R. Larchevéque and E. Ngoya, "Compressed transient speeds up the periodic steady state analysis of nonlinear microwave circuits," *1996 IEEE MTT-S Digest*, pp. 1369–1372.

[15] Richard L. Burden, *Numerical Analysis, fifth edition.* 1993, PWS Publishing Company, Boston.

[16] http://www.math.ufl.edu/help/matlab-tutorial/

[17] Stephen A. Maas, *Nonlinear Microwave and RF Circuits, Second edition*, 2003, Artech House Pub.

[18] Axel Wenzler and Ernst Lueder, "Analysis of The Periodic Steady-state in Nonlinear Circuits Using An Adaptive Function Base", IEEE, 1999

[19] http://www.eng.fsu.edu/ dommelen/courses/eml3100/aids/intpol.

Reproduced with permission of the copyright owner. Further reproduction prohibited without permission.

[20] Paulo J. C. Rodrigues, *Computer-aided Analysis of Nonlinear Microwave Circuits.* May 1997, Norwood, MA: Artech House.

[21] J. Roychowdhury, "Making Fourier-envelope simulation robust," *2002 IEEE/ACM ICCAD*, pp. 240–245.

[22] Richard R. Spencer and Mohammed S.Ghausi,*Introduction to Electronic Circuit Design.* 2003, Prentice Hall.

[23] Ron Kielkowskl, *Spice Practical Device Modeling.* 1995 McGraw-Hill.

[24] http://www.shodor.org/UNChem/math/newton.

[25] http://www.duncanamps.com/spice/bjt/npn.mod.

[26] http://www.datasheetcatalog.com/datasheets _ pdf/M/P/S/9/MPS918.shtml.

Reproduced with permission of the copyright owner. Further reproduction prohibited without permission.